# Modelling dynamic topographies of planetary bodies


Bernhard Steinberger

*Deutsches GeoForschungsZentrum, Potsdam*

*and*

*Centre for Earth Evolution and Dynamics, Univ. Oslo*


GFZ
Helmholtz Centre
POTSDAM

UNIVERSITAS OSLOENSIS
MDCCCXI

CEED
The Centre for Earth Evolution and Dynamics

**Outline**

→ What is dynamic topography and why is it important?

→ Numerical models of dynamic topography on Earth and comparison to observations

- Instantaneous flow based on tomography
  - (a) only radial viscosity variations
  - (b) coupling with more realistic lithosphere
- Time-dependent flow
  - (a) backward advection based on tomography
  - (b) forward models based on subduction history
  - (c) adjoint models

→ Implications

→ Other planets: equipotential surface and topography

- Instantaneous models (indirectly based on tomography)
- Forward convection models

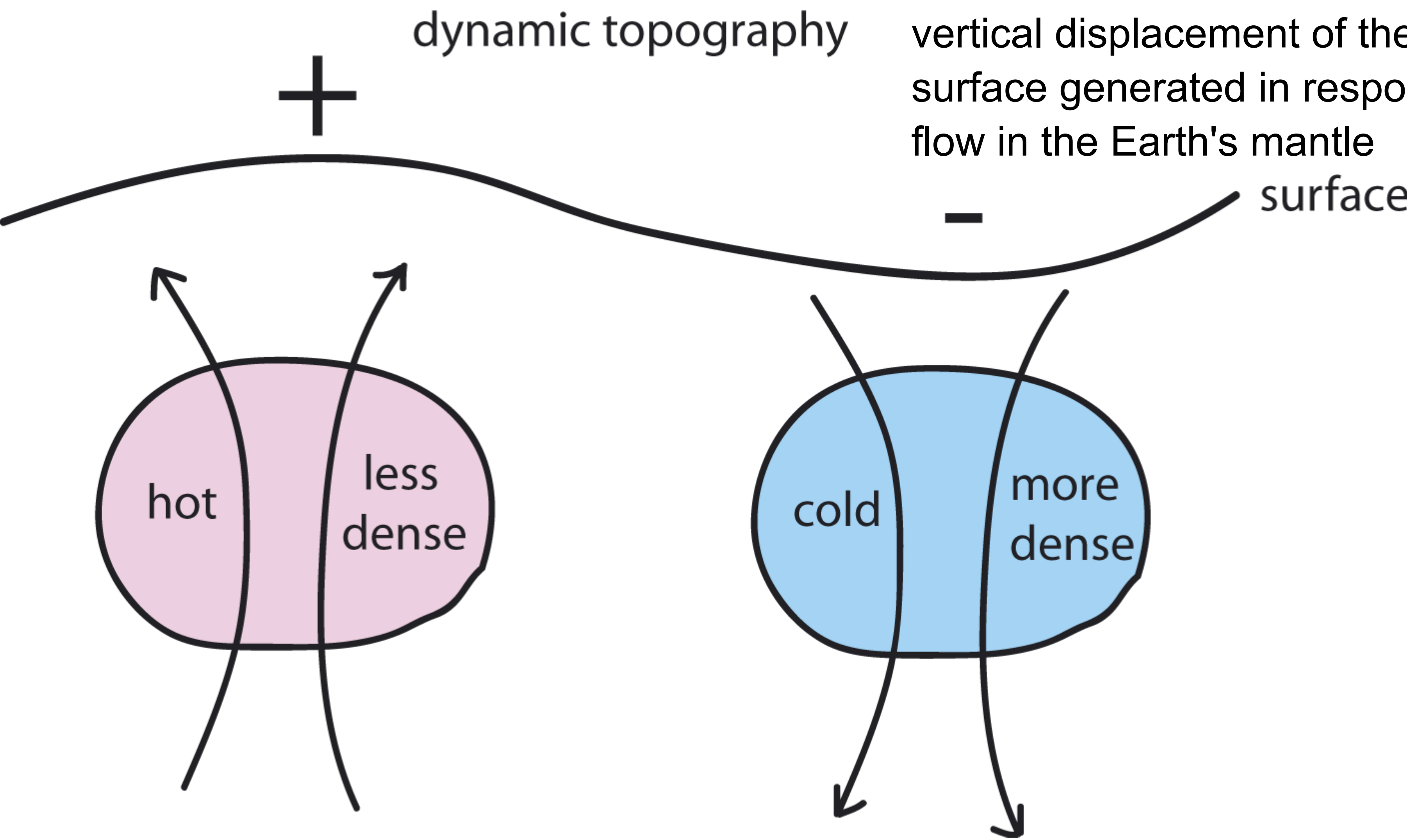


vertical displacement of the Earth's surface generated in response to flow in the Earth's mantle

NATURE VOL. 313 14 FEBRUARY 1985 ARTICLES 541

# Lower mantle heterogeneity, dynamic topography and the geoid

**Bradford H. Hager, Robert W. Clayton, Mark A. Richards, Robert P. Comer* & Adam M. Dziewonski***

Seismological Laboratory, California Institute of Technology, Pasadena, California 91125, USA

**Why is it important to know dynamic topography?**

Many areas on Earth within few hundred meters above or below sea level (bright green / light blue on map)

Dynamic topography expected to reach a few hundred meters and hence may influence when and where sediments and natural resources may form

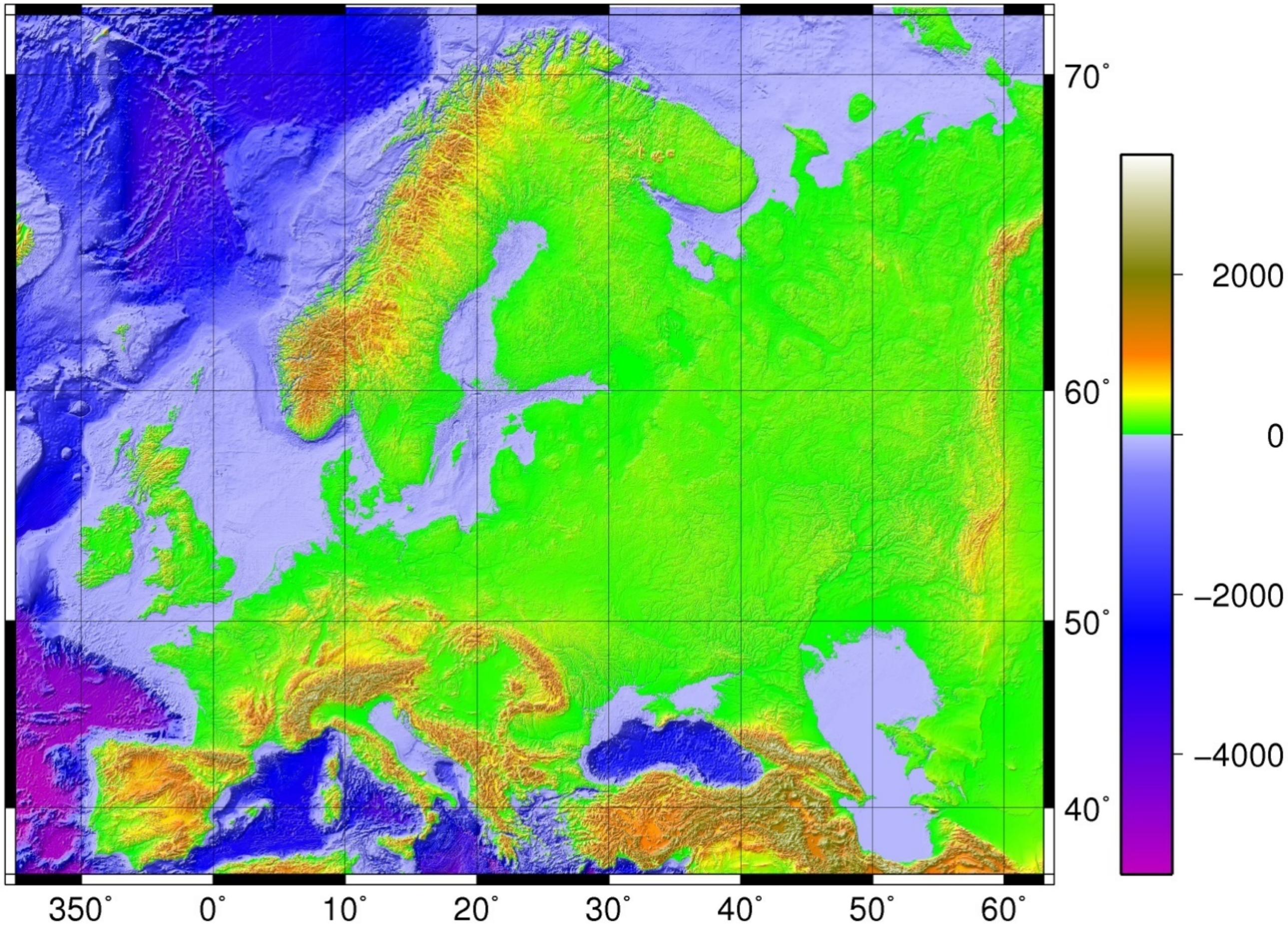


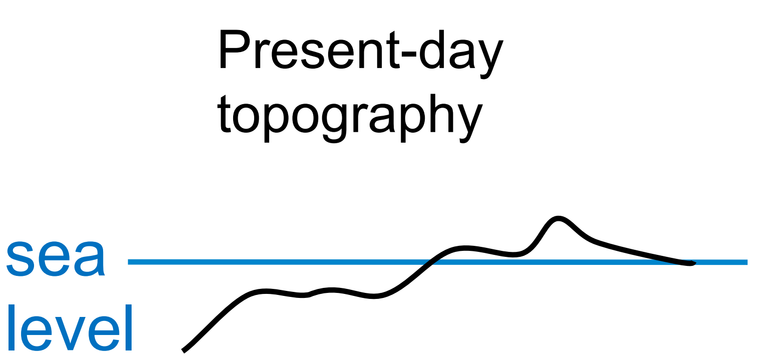

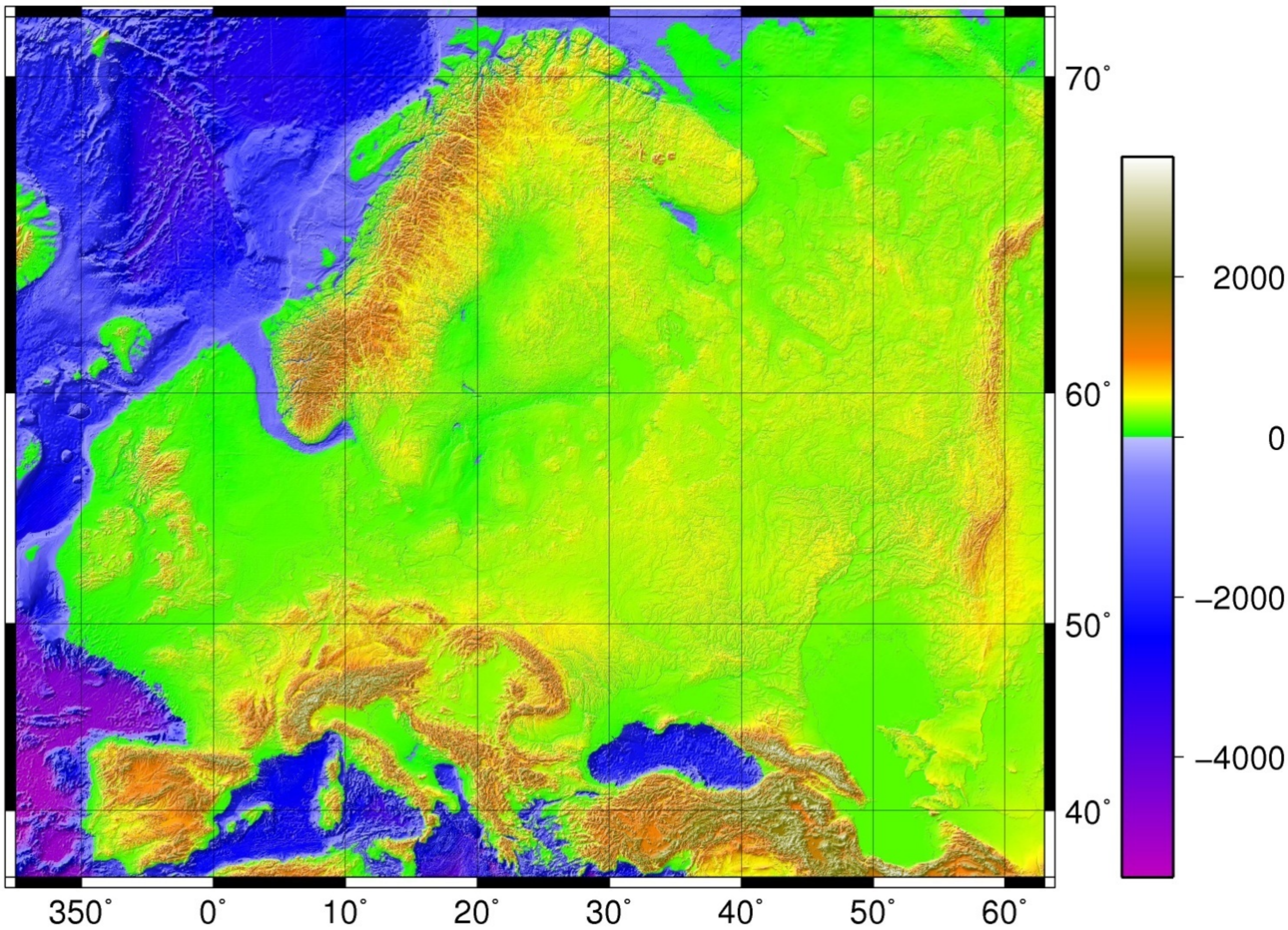

70°
60°
50°
40°
350°
0°
10°
20°
30°
40°
50°
60°
2000
0
−2000
−4000


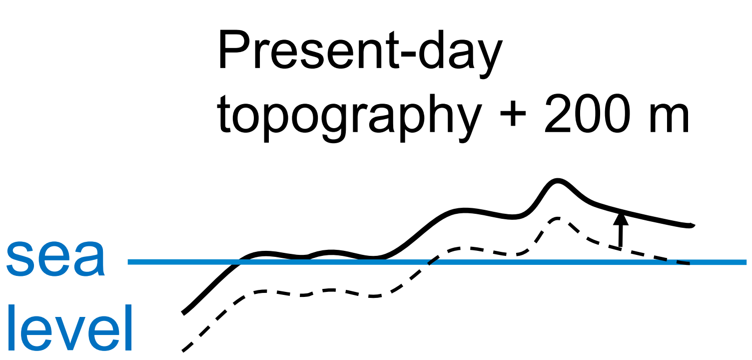

Present-day
topography + 200 m
sea
level

LETTERS TO NATURE VOL 344 · 19 APRIL 1990

# Bounds on global dynamic topography from Phanerozoic flooding of continental platforms

**Michael Gurnis**

Department of Geological Sciences, University of Michigan, Ann Arbor, Michigan 48109-1063, USA

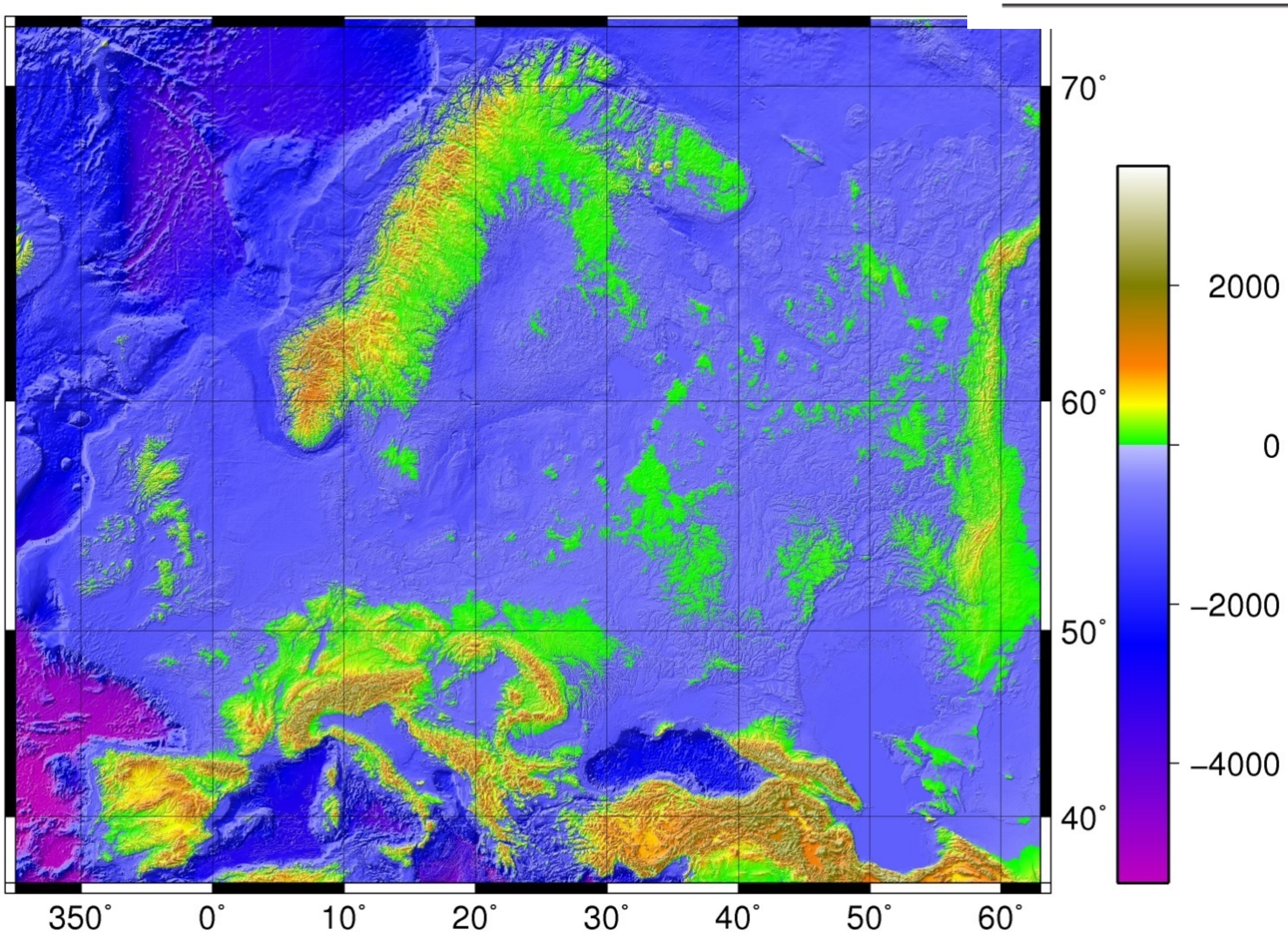


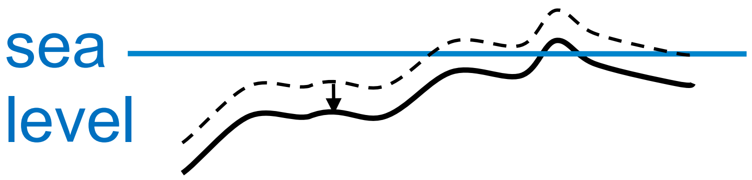

Dynamic topography changes ocean basin volume and hence sea level Figure from Conrad and Husson (Lithosphere, 2009)

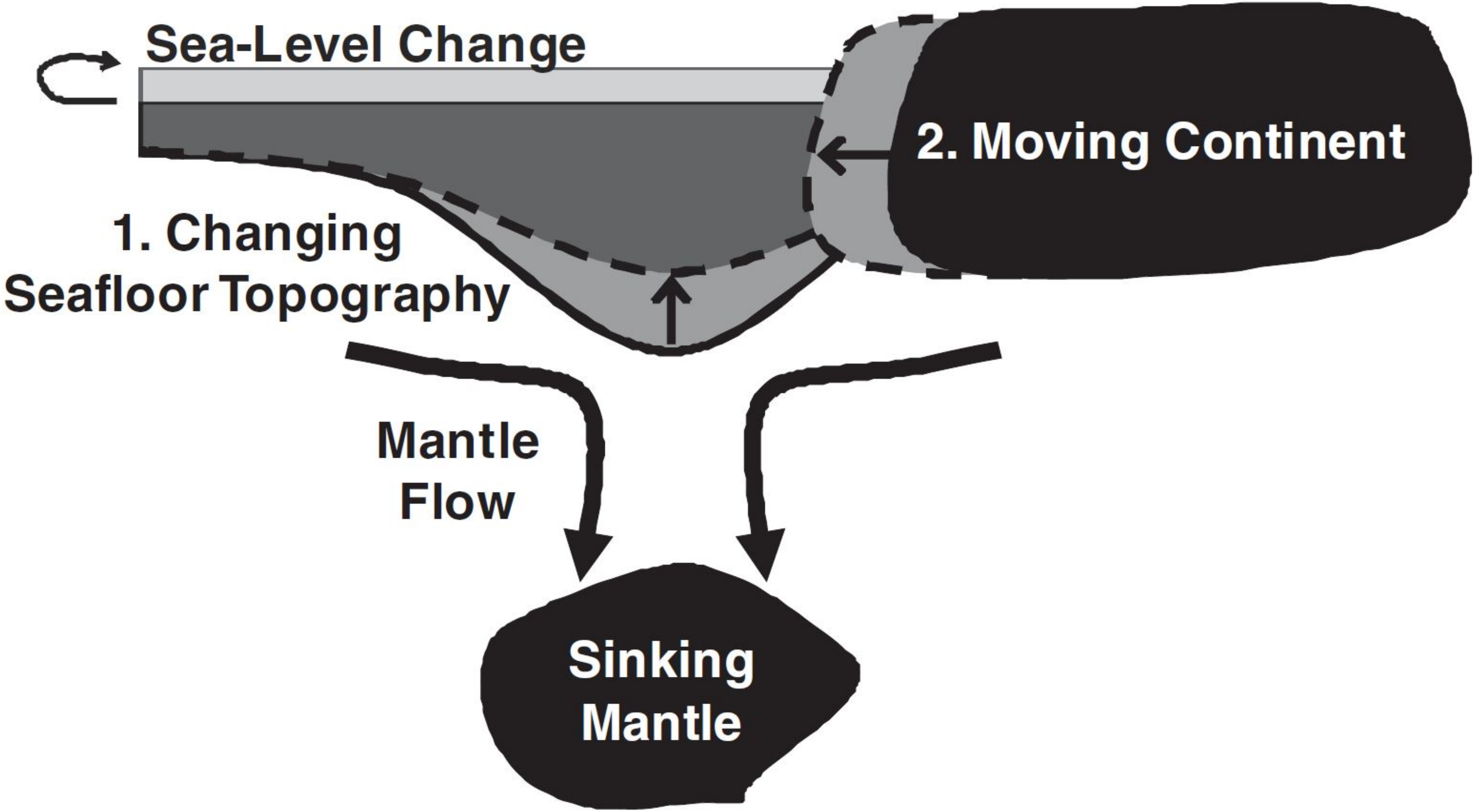

Plate reconstruction and hotspot motion from Doubrovine et al. (2012)

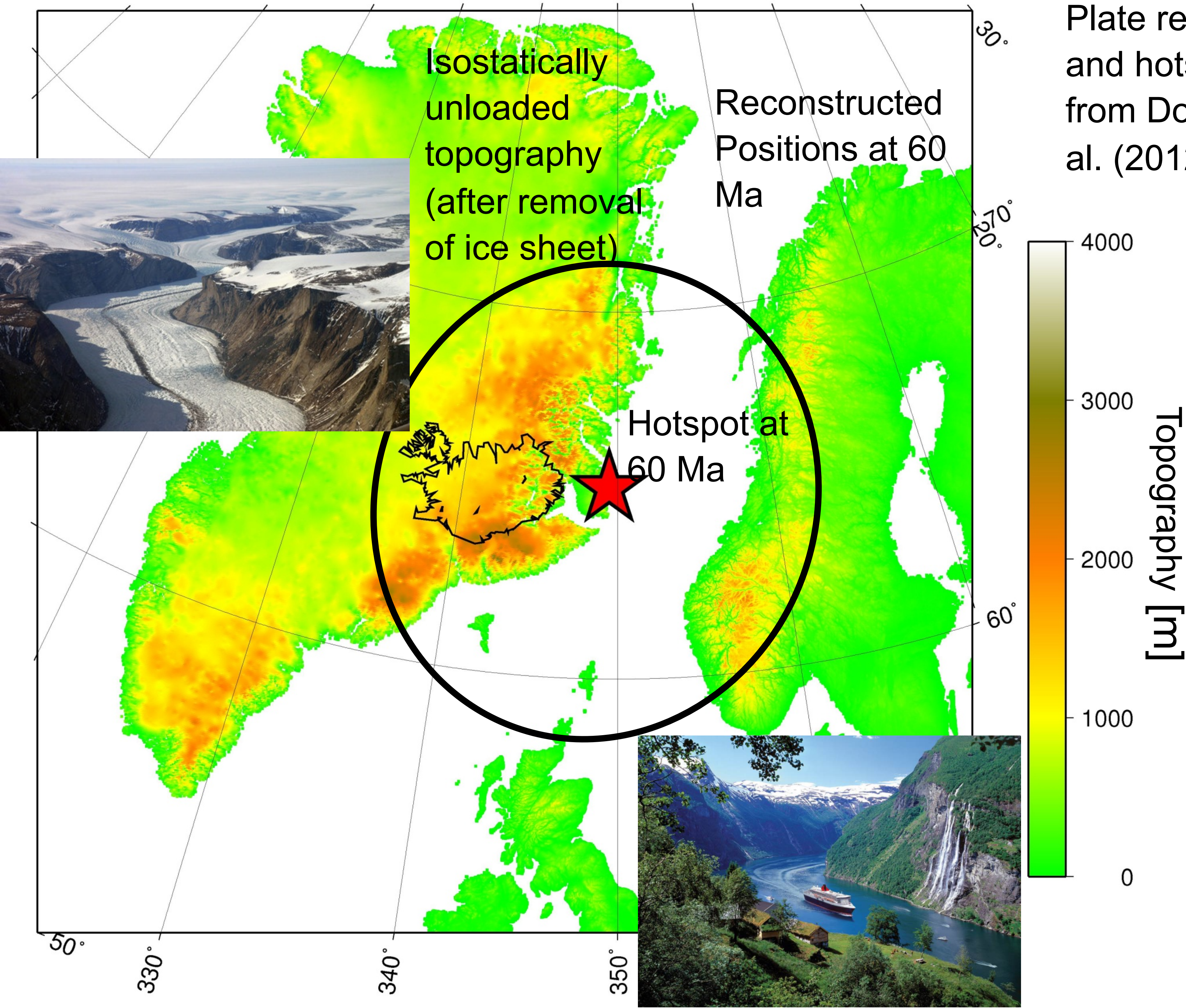

# Computing dynamic topography

Numerical model:
Often fixed computational domain
No boundary displacement
Instead convert computed vertical stresses $T_{rr}$ to topography h:
$h = T_{rr} / (\Delta\rho\, g)$
whereby g is gravity

Reality: Boundary displacement

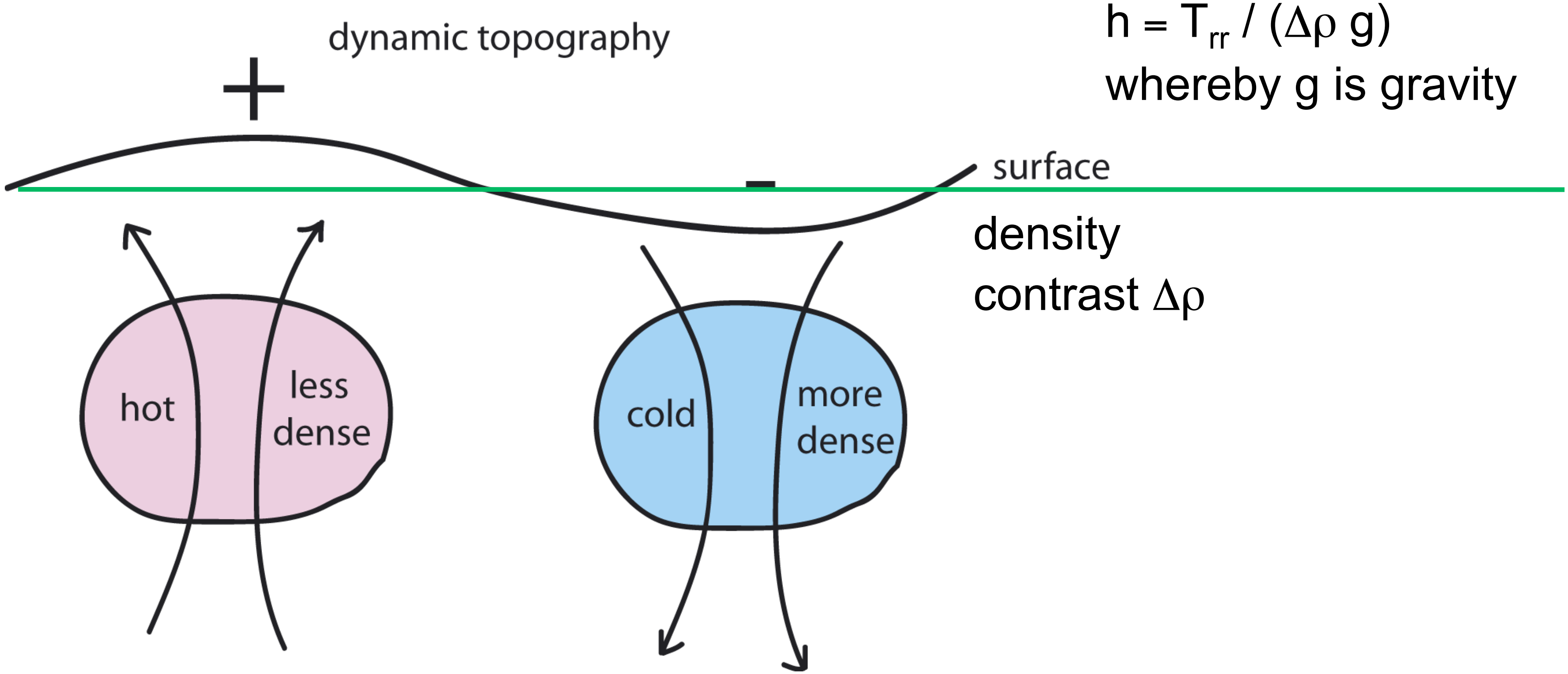

## Instantaneous mantle flow computation

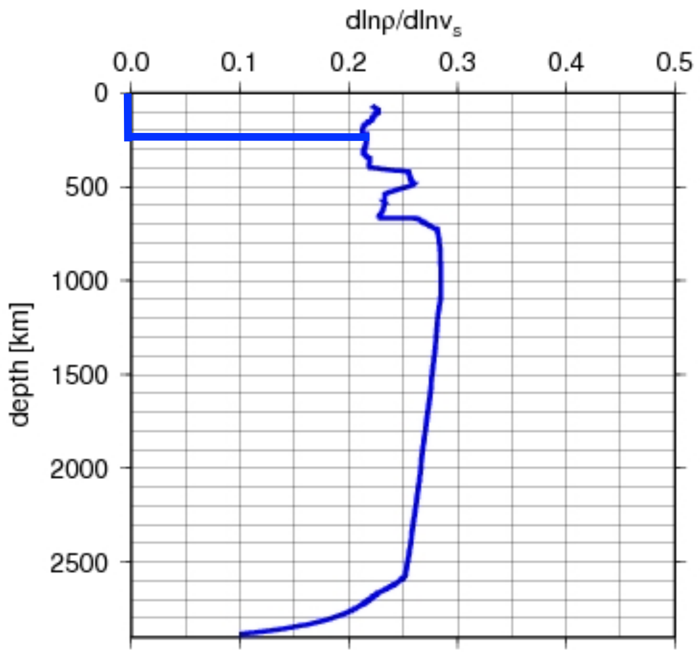


- Density model based on tomography (here: Simmons, Forte, Grand, 2006)
- Here, all density anomalies above 220 km are removed
- thermal velocity-density scaling based on mineral physics
- radial viscosity structure based on mineral physics and optimizing fit to geoid etc. (Steinberger and Calderwood, 2006)
- Spectral method (Hager and O'Connell, 1979, 1981)

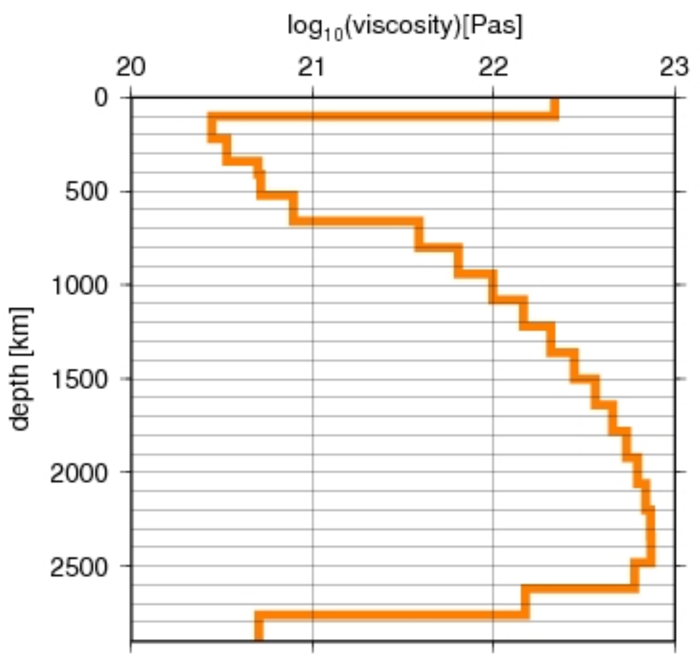


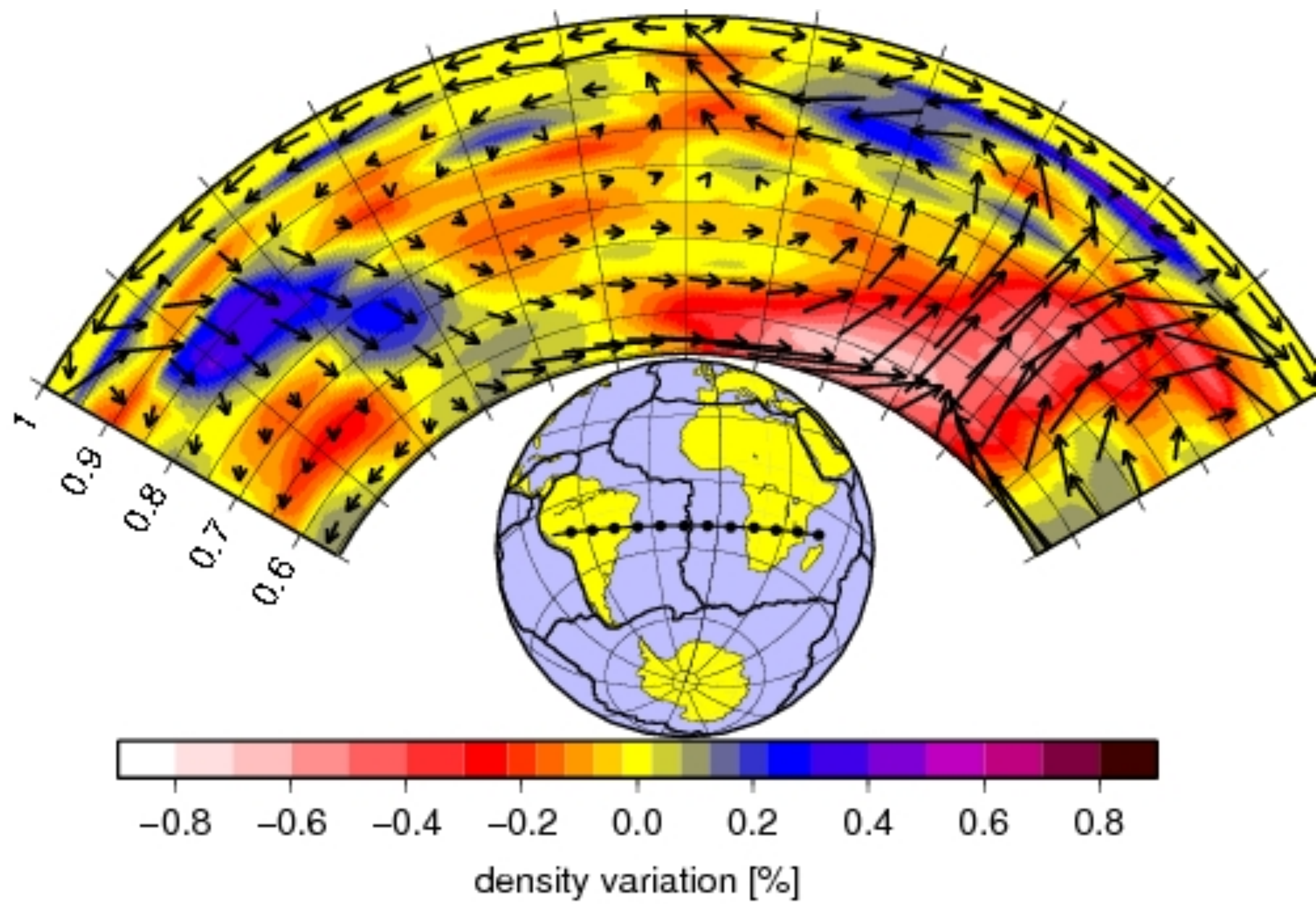

Download flow code «HC» with user interface from http://geodynamics.org/cig/software/hc; courtesy of Thorsten Becker

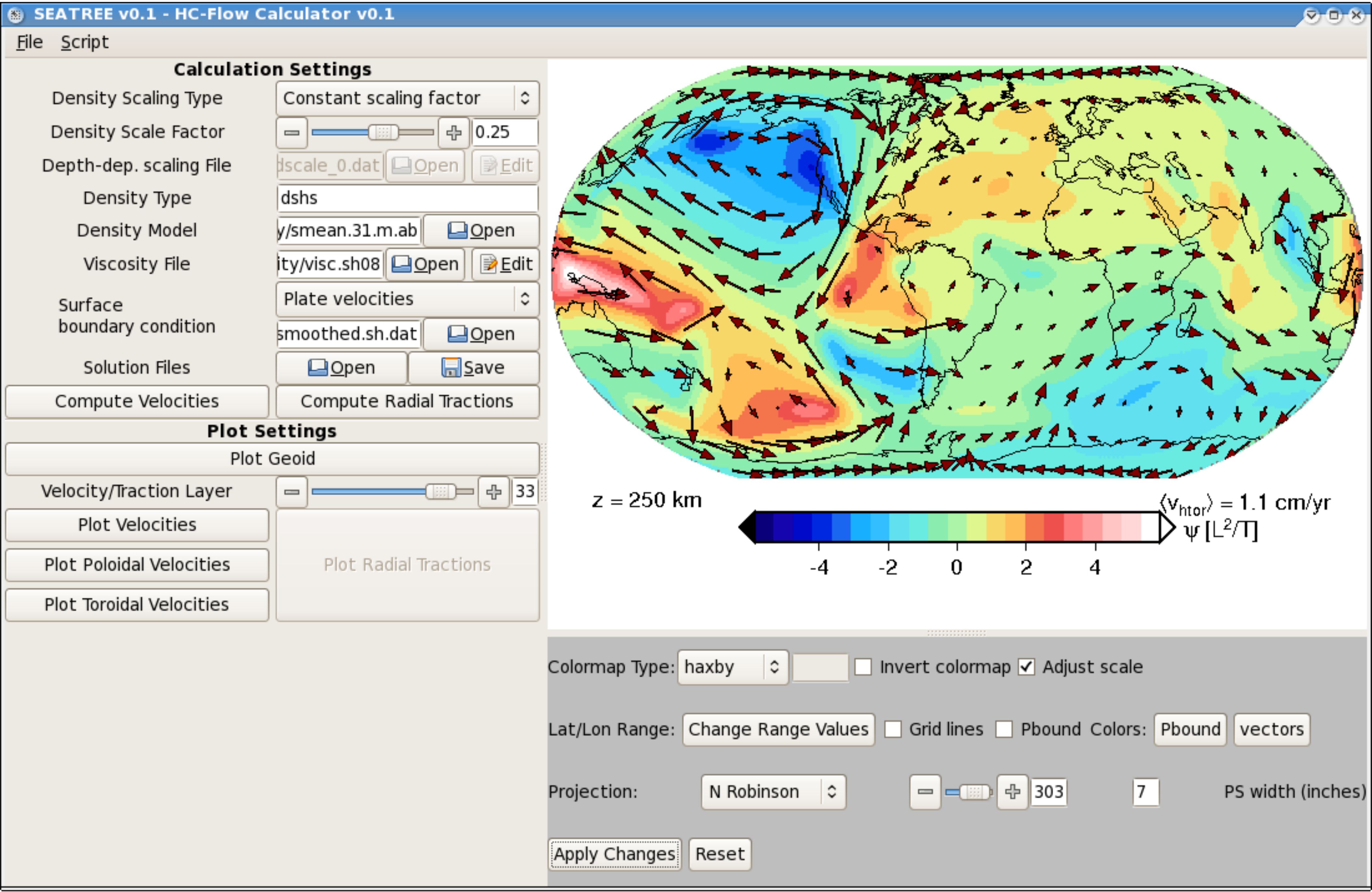

# Computation for instantaneous flow based on seismic tomography

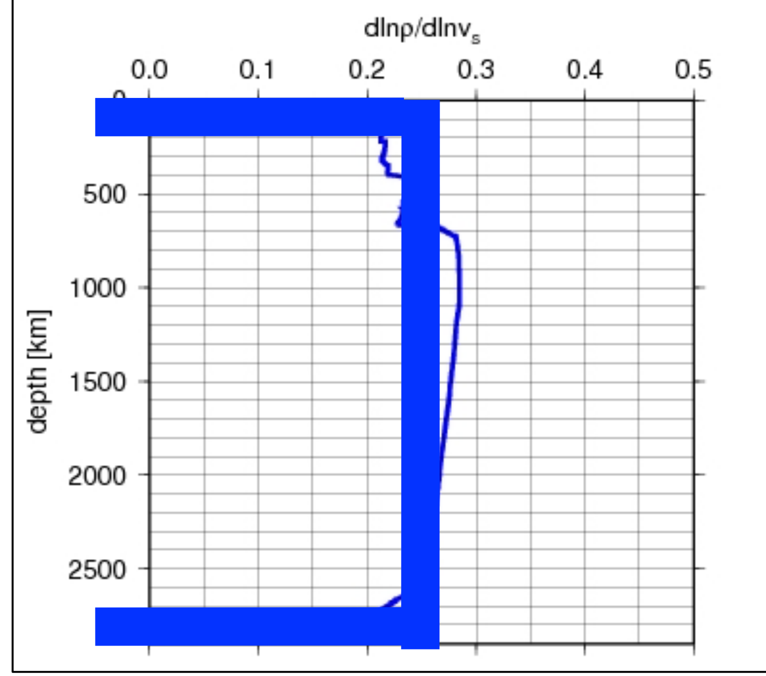


Within continental lithosphere, probably cannot use "thermal" conversion

Convert seismic velocity to density anomalies assuming thermal origin

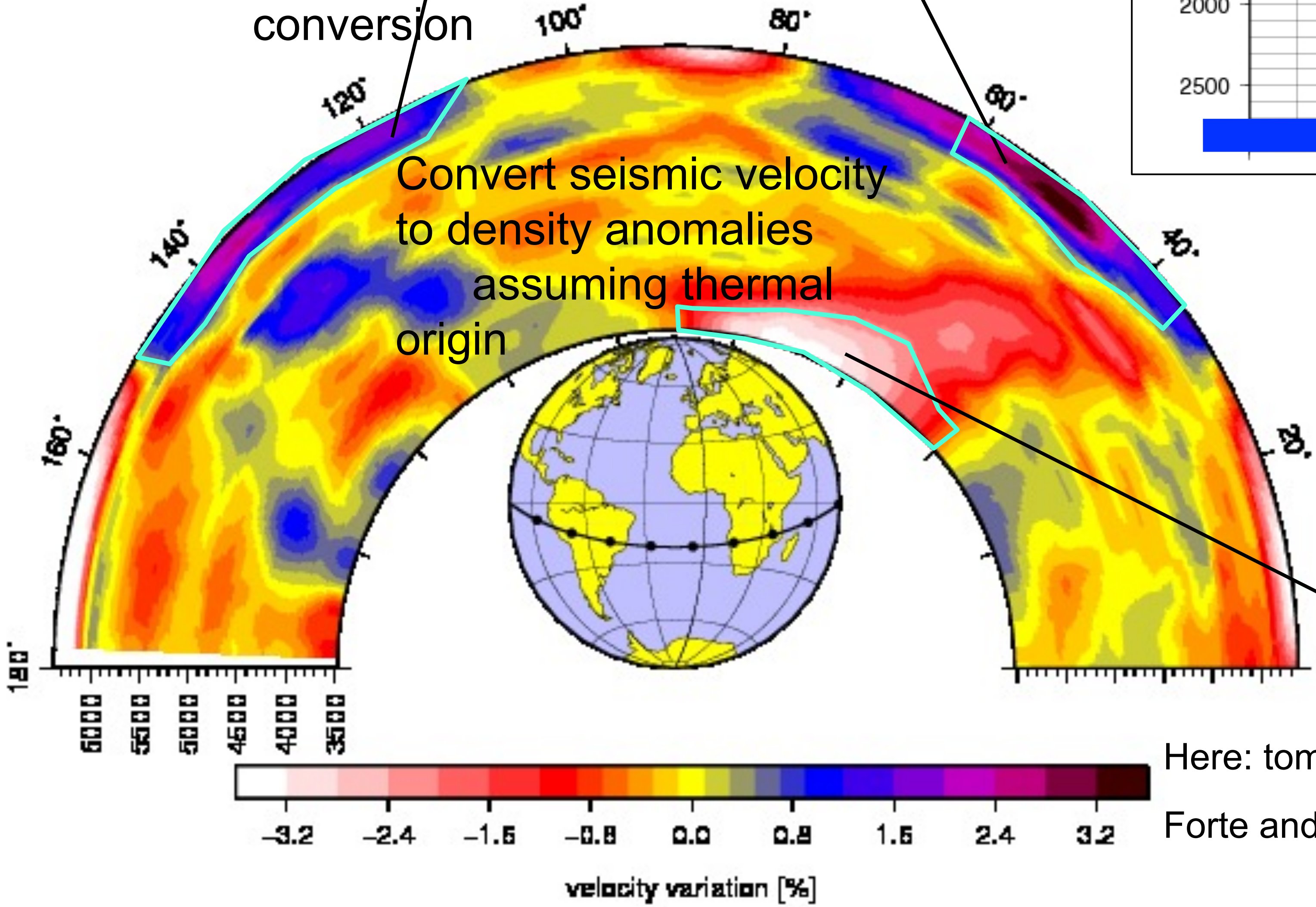


Conversion factor for thermal anomalies inferred from mineral physics (Steinberger and Calderwood, 2006)

Within LLSVPs, probably cannot use "thermal" conversion either

Here: tomography model of Simmons, Forte and Grand (2006)

Attempt to “remove lithosphere” by setting density anomaly to 0.2 % wherever, above 400 km depth and on continents, inferred density anomaly is positive >0.2 % at that depth and everywhere above

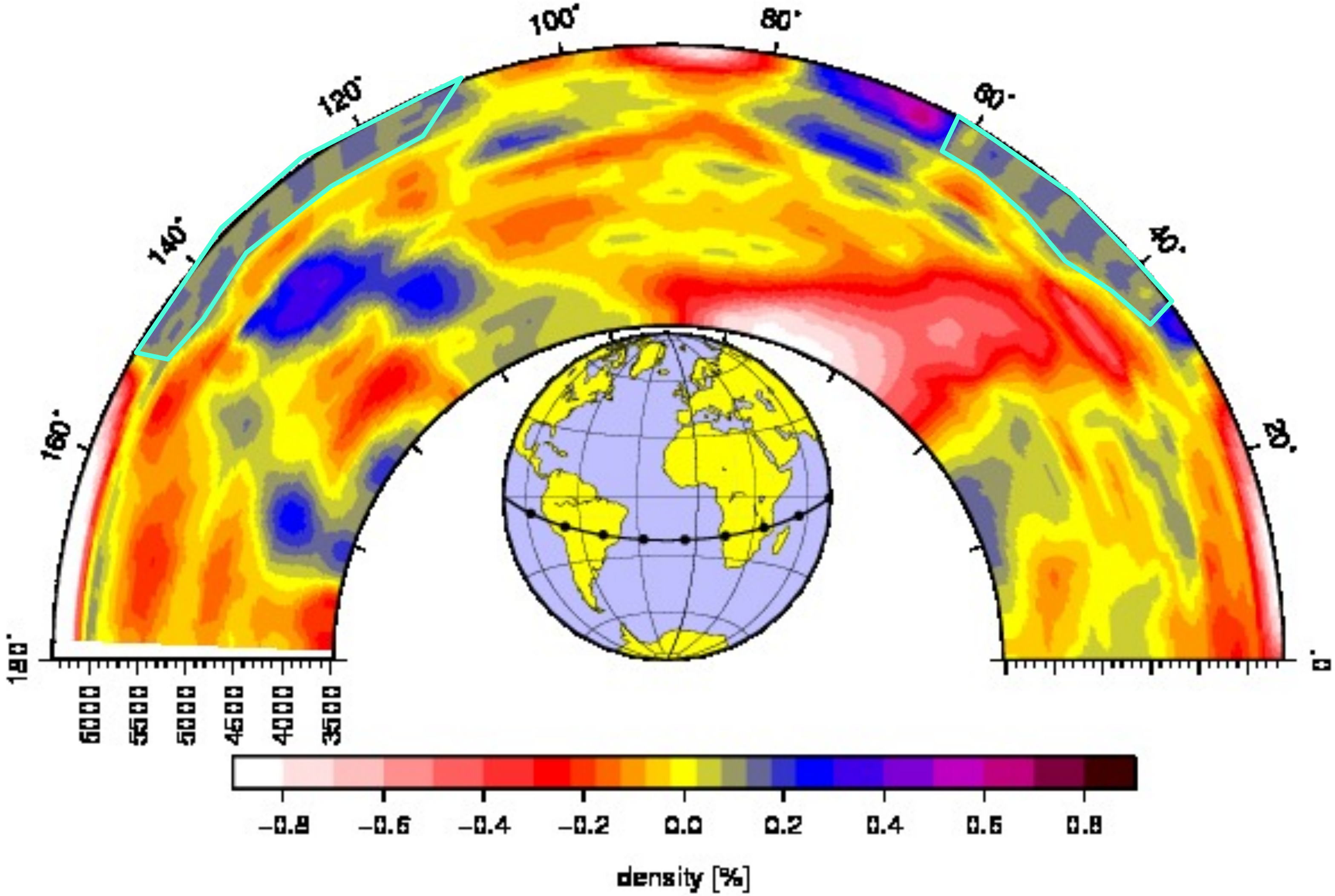

→Lithospheric thickness not well constrained
→models a, d and e based on tomography
→b based on heat flow
→c from receiver functions

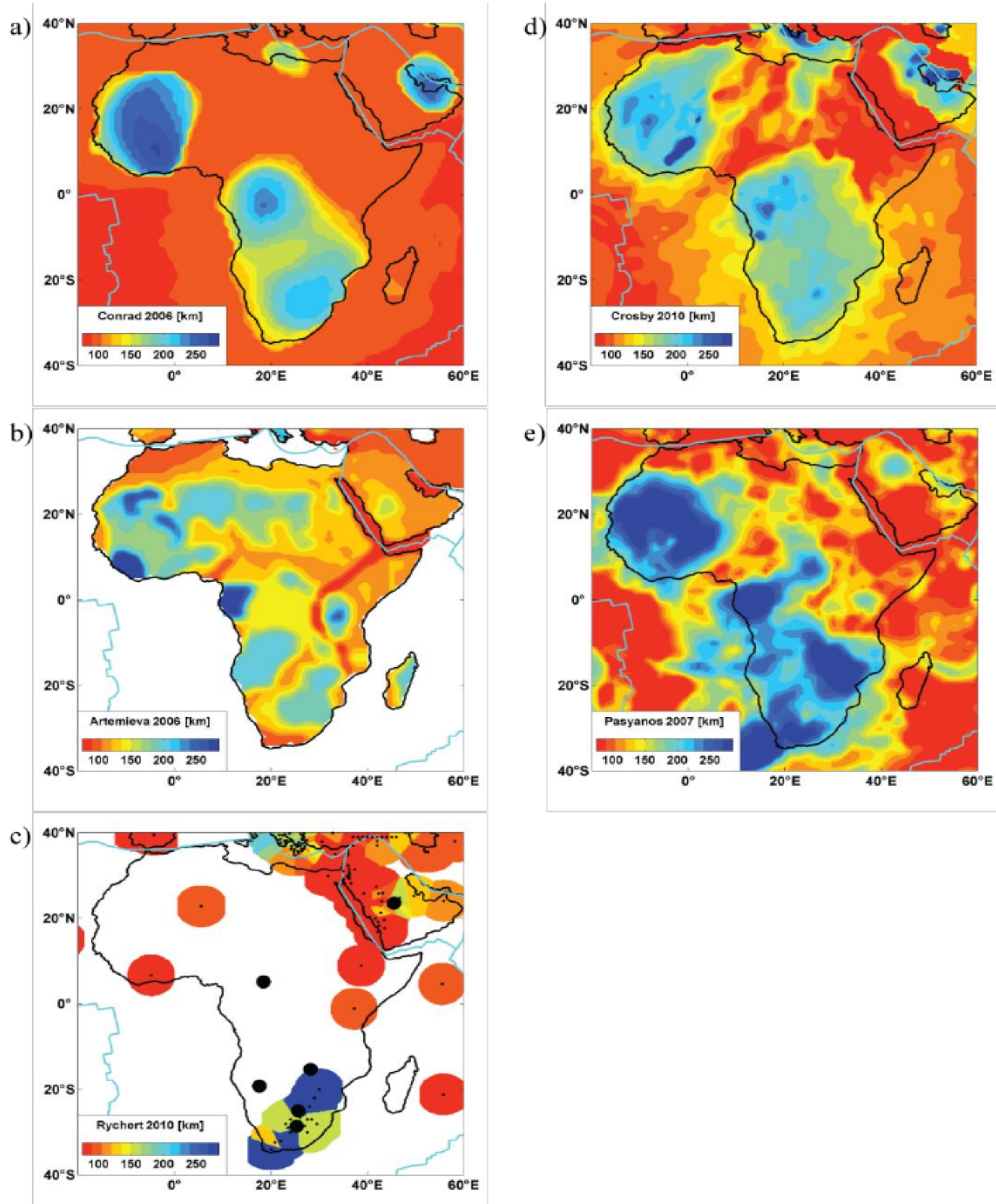

If viscosity only depends on radius:
Effect of density anomalies $\delta\rho_{lm}$ at given depth z and spherical harmonic degree l on topography can be described in terms of topography kernels $K_{r,l}(z)$:
Beneath water : $\Delta\rho_s = 2280$ kg/m$^3$

$$h_{lm} = \int \delta\rho_{lm}(z) K_{r,l}(z) dz / \Delta\rho_s$$

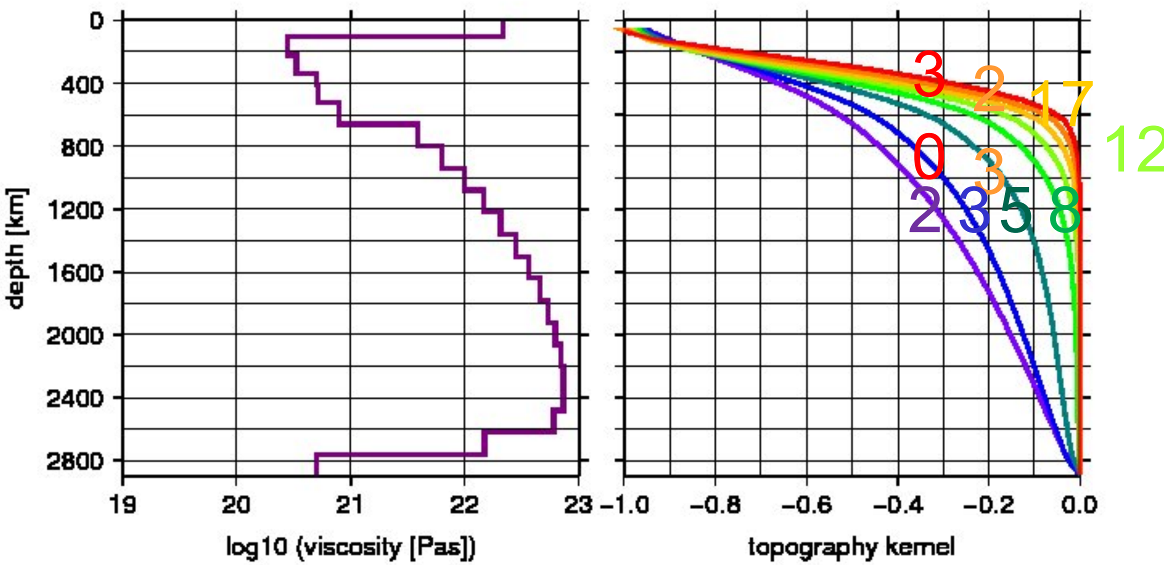


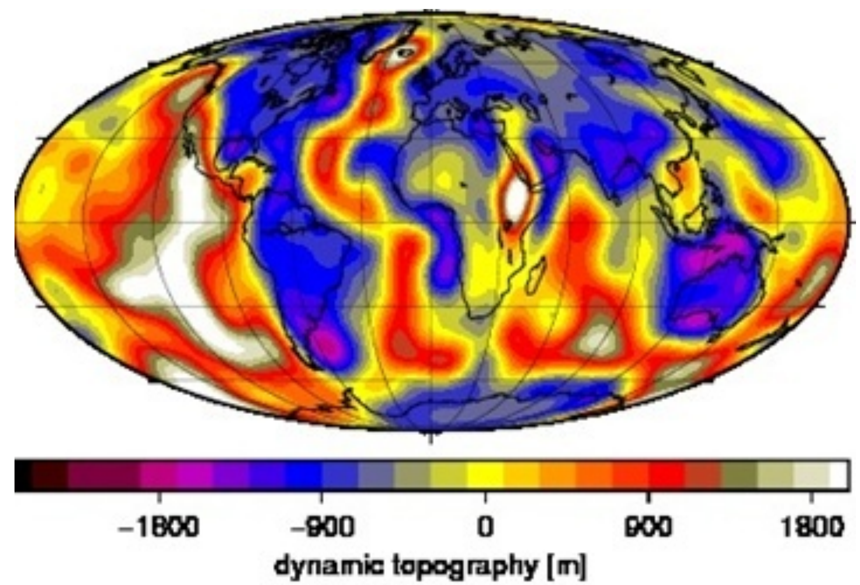


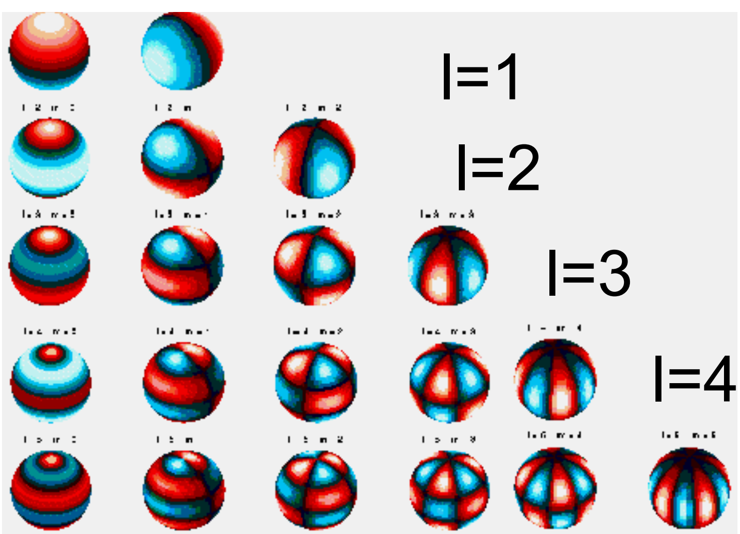

l=1
l=2
l=3
l=4
l=5

spherical harmonics

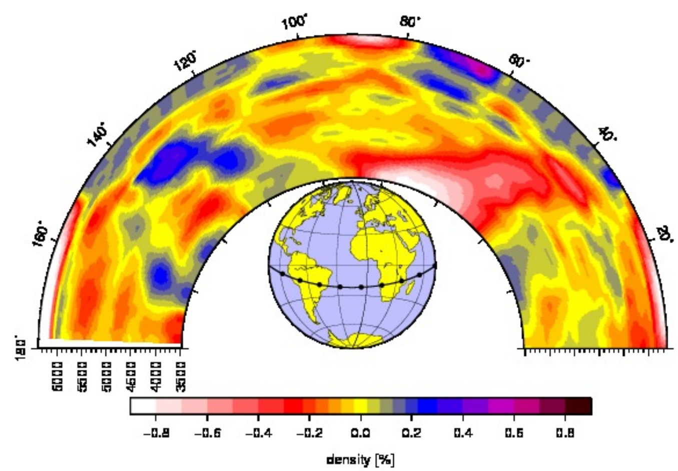

age_3.6 ocean floor age grid (Müller, Sdrolias, Gaina and Roest, G3, 2008)

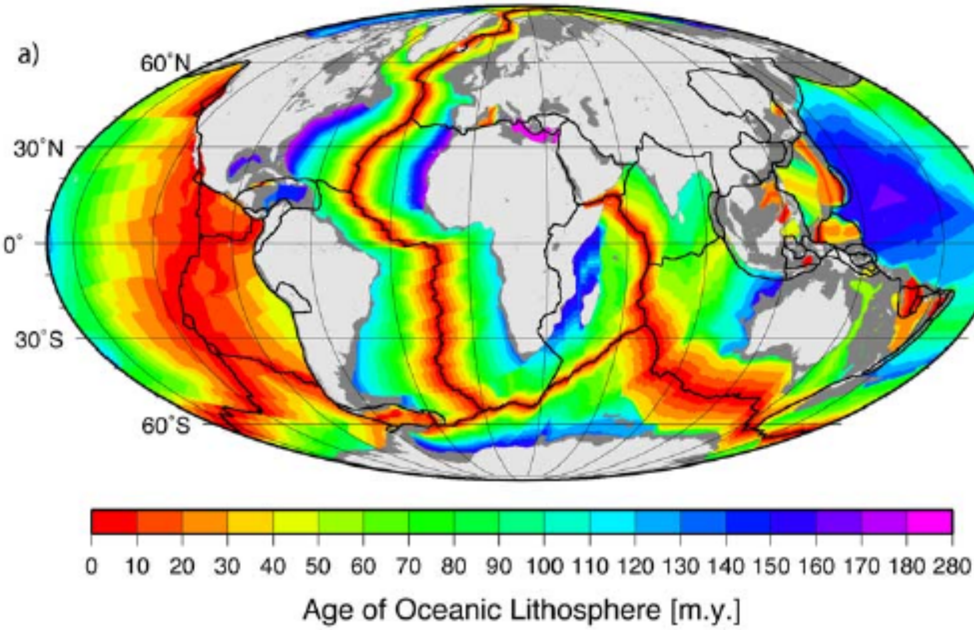


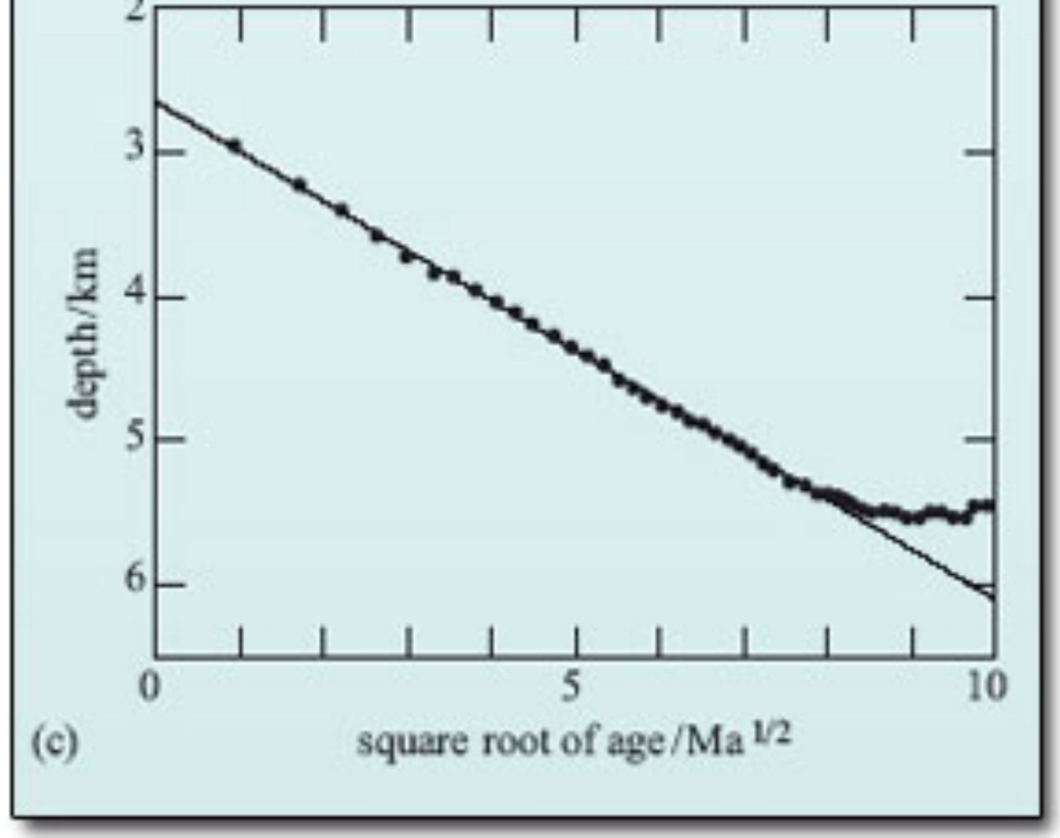


Computed “ridge” topography
(assuming sqrt(age) law for ages < 100 Ma

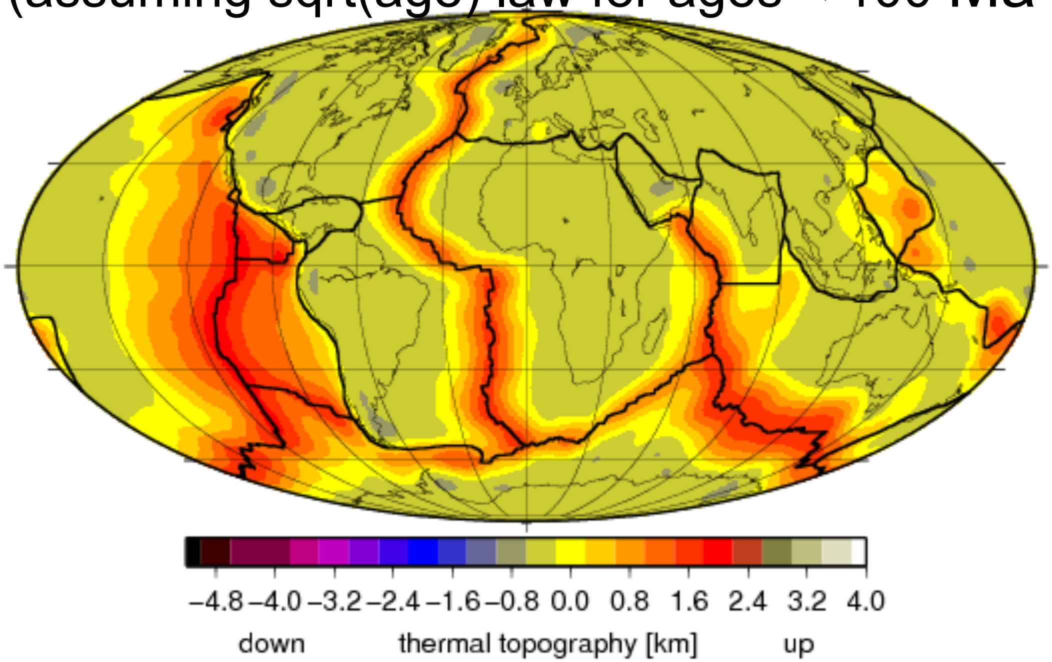


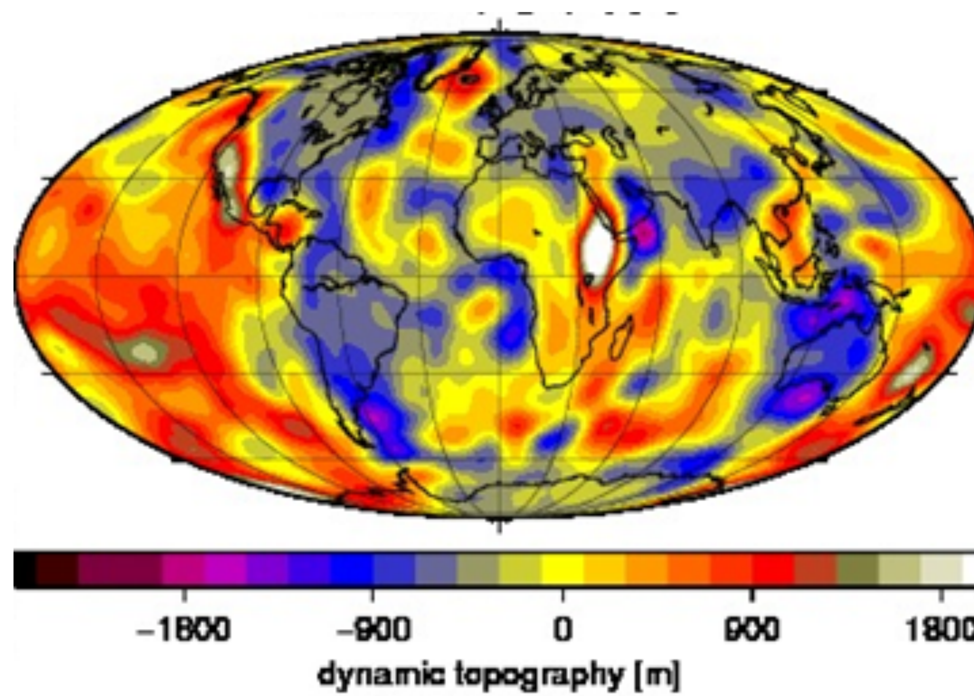

# Dynamic topography – dependence on boundary condition

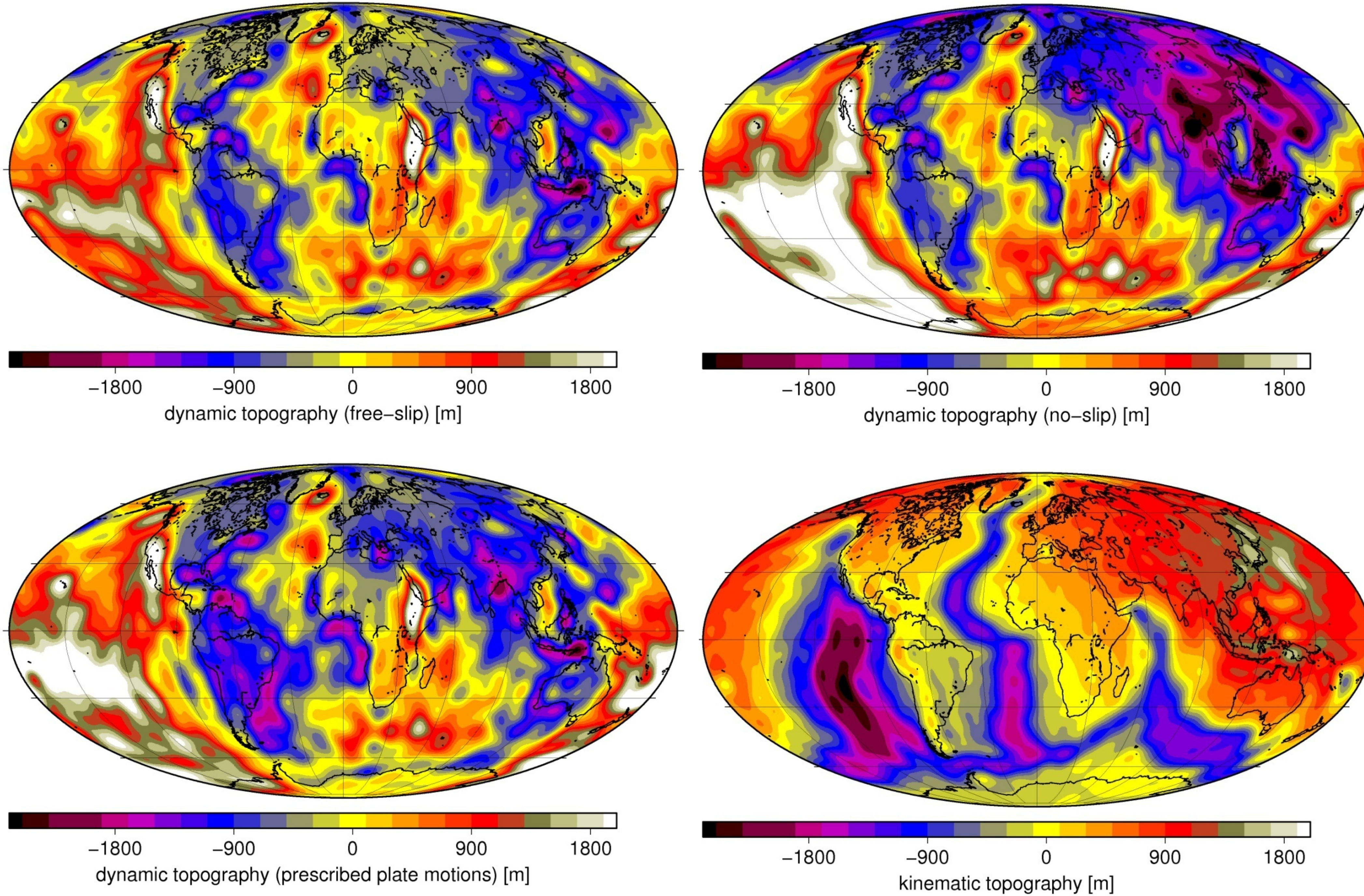

# Inferring dynamic topography from observations

## Actual topography

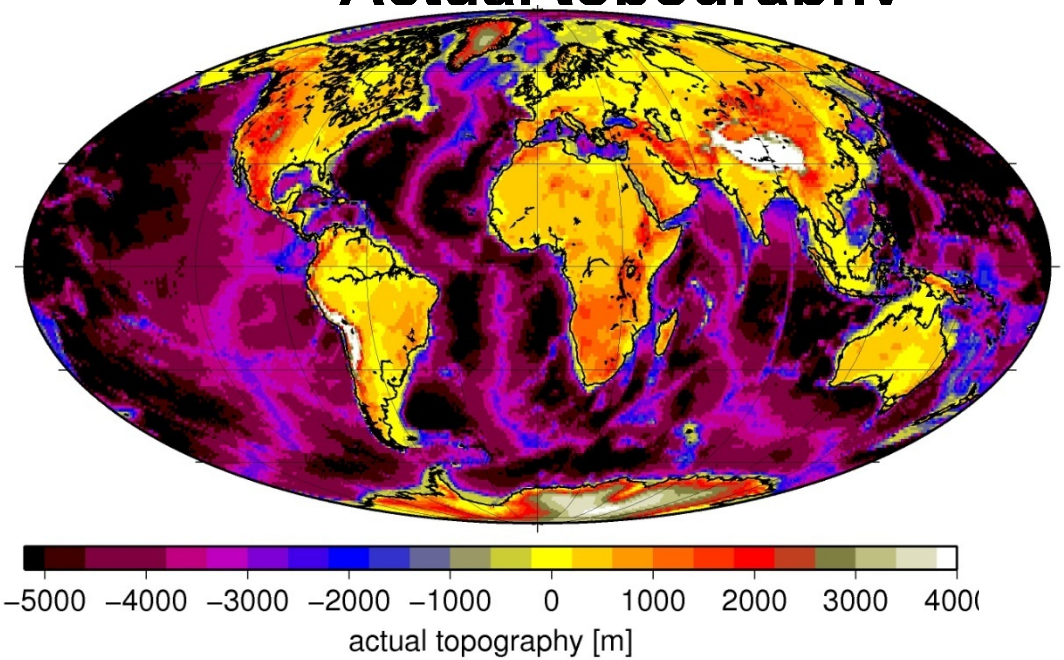


## MINUS
## Isostatic topography

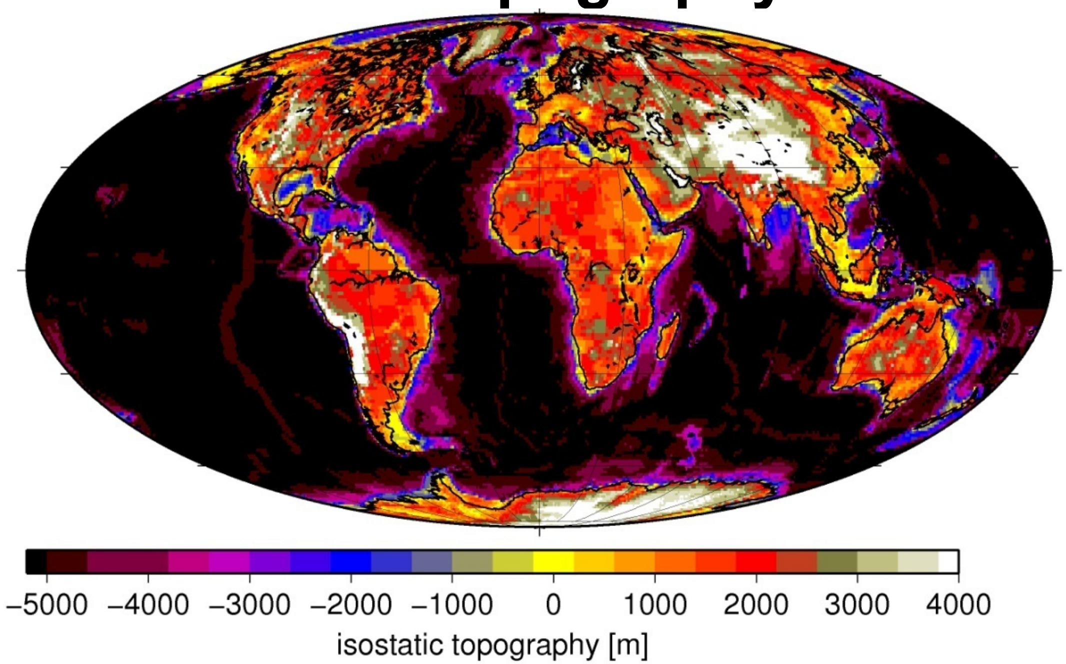



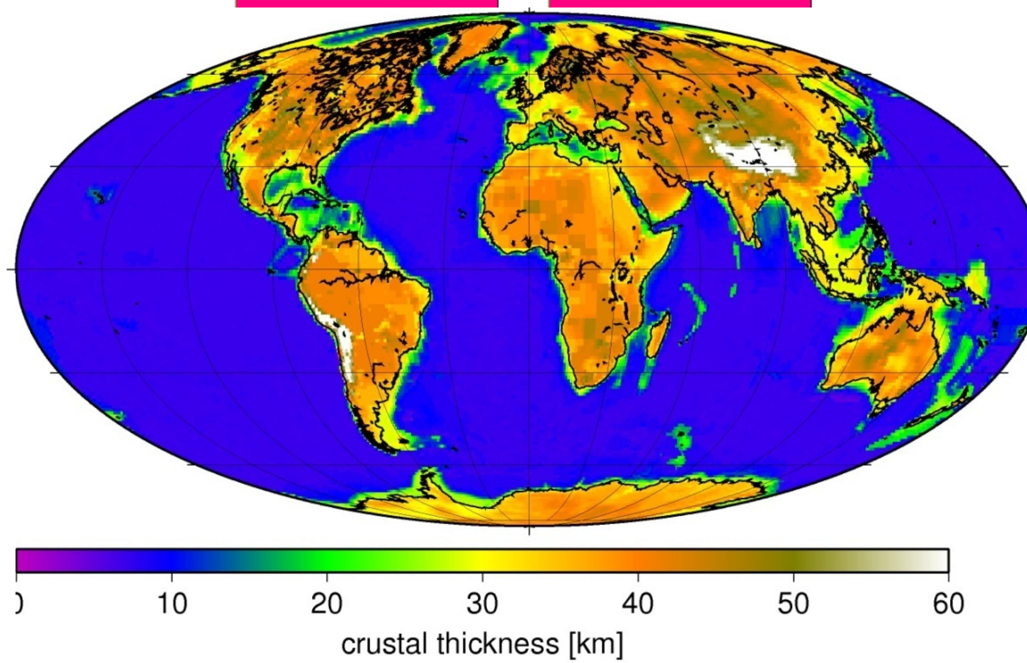


Computed based on densities and thicknesses of crustal layers in CRUST 1.0 model (Laske et al., http://igppweb.ucsd.edu/~gabi/crust1.html

## Actual

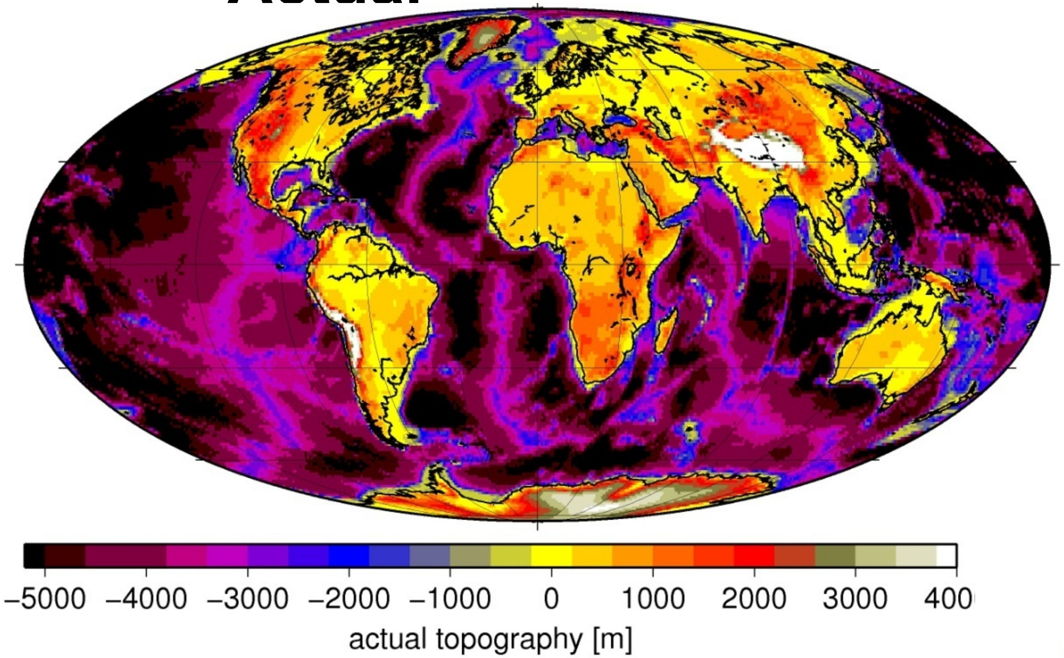


## MINUS
## Isostatic topography

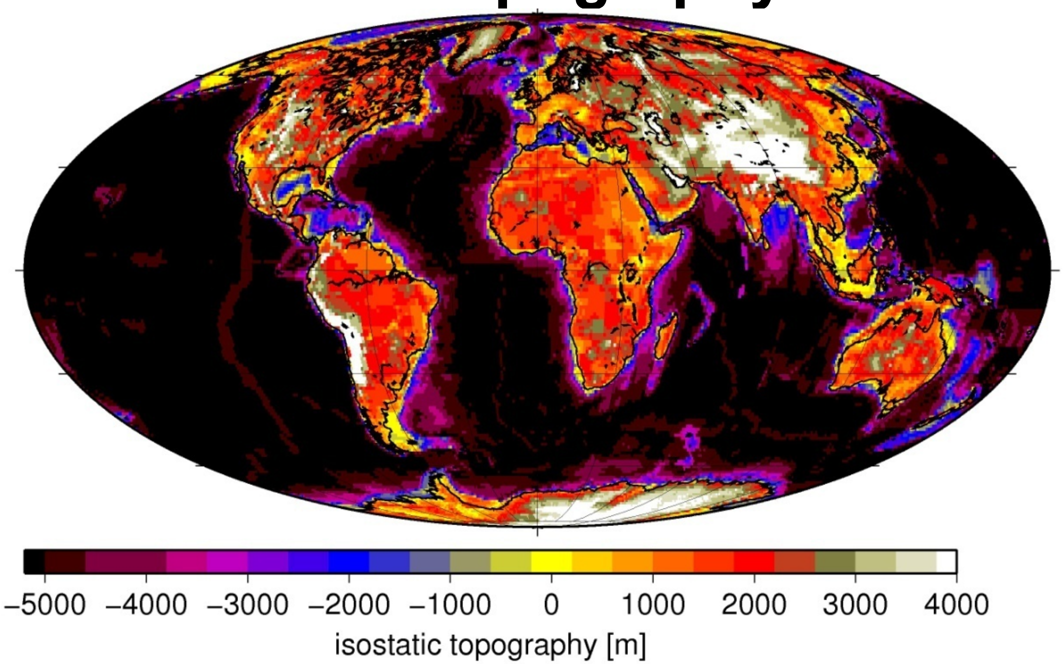


=

## Non-isostatic topography

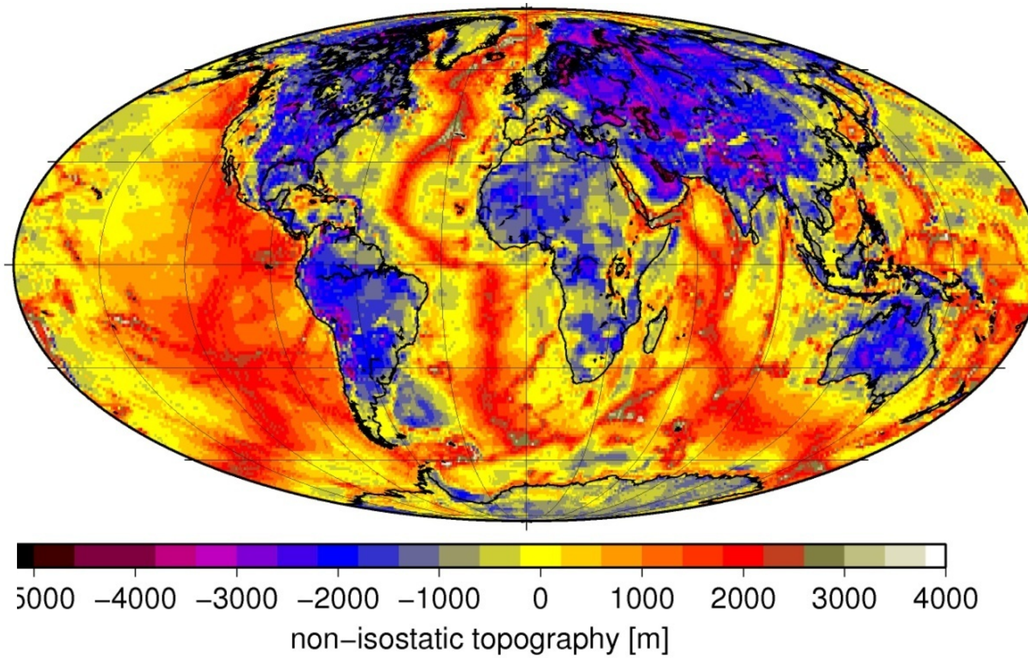

# Non-isostatic

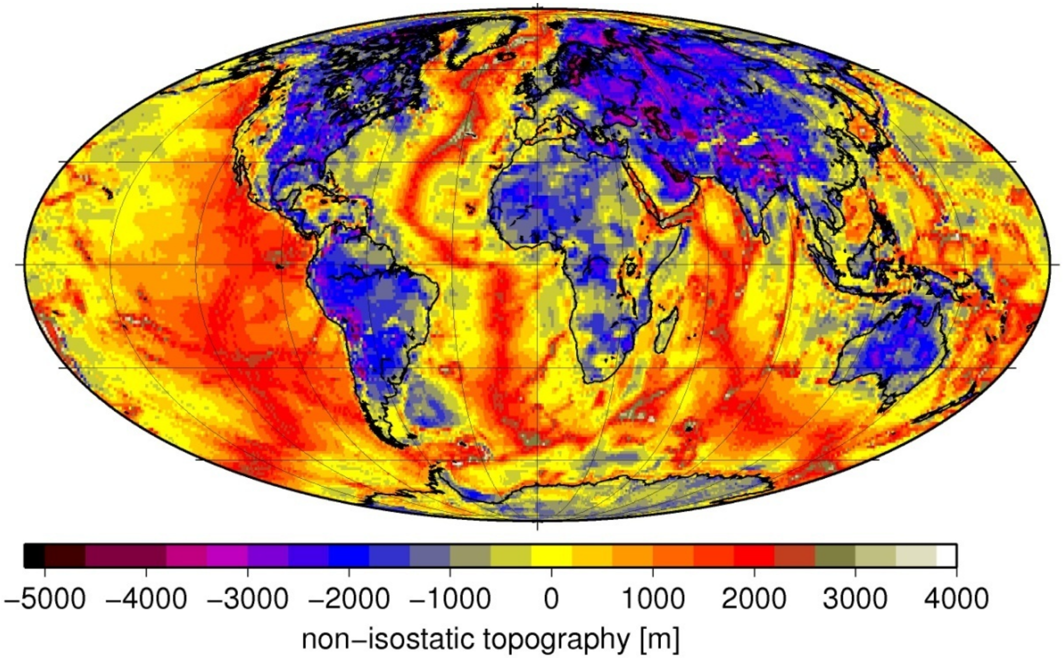


Using Crust 1.0

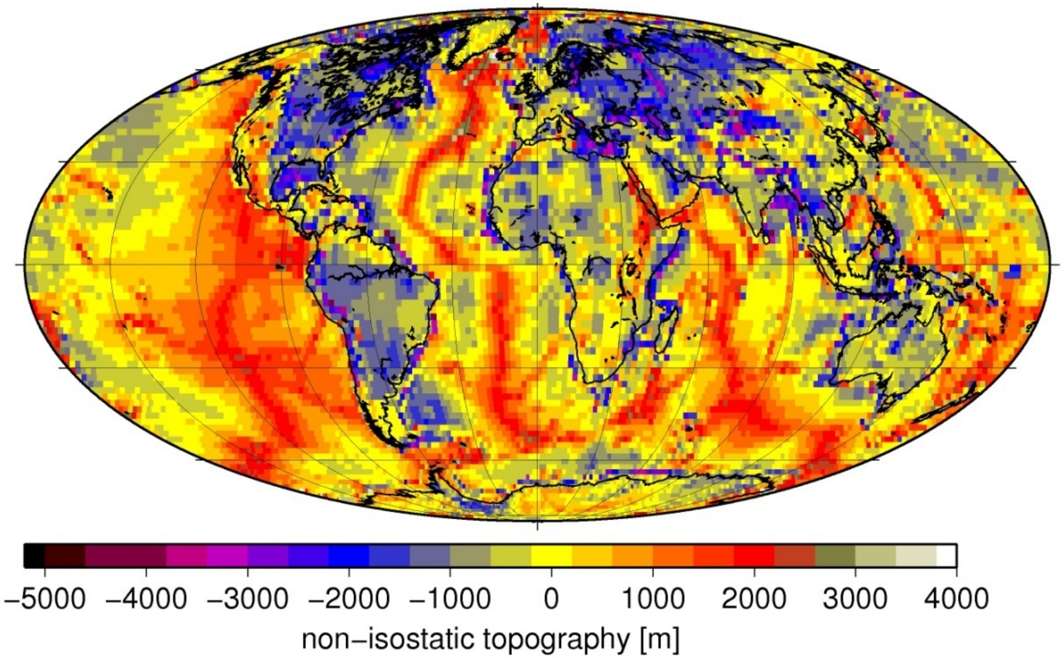


Using Crust 2.0

## Non-isostatic topography

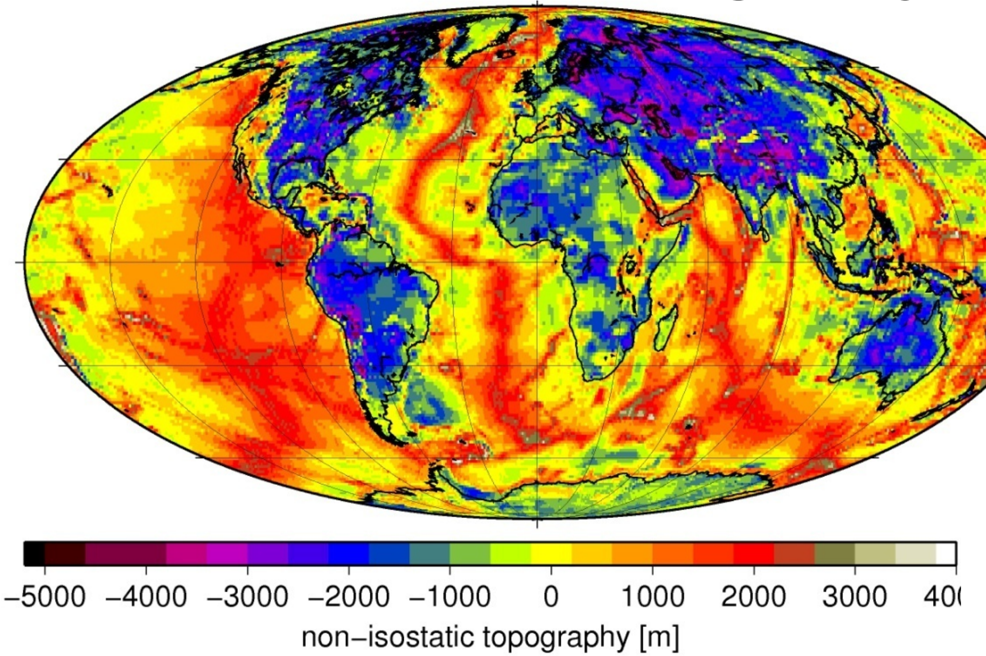


## MINUS ridge topography

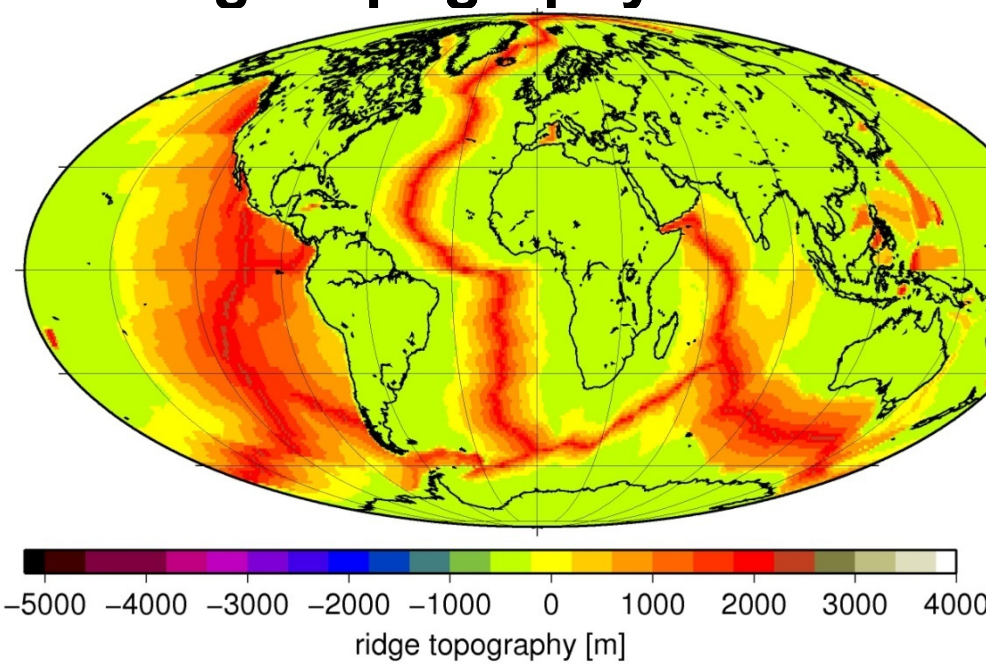


=

## residual topography

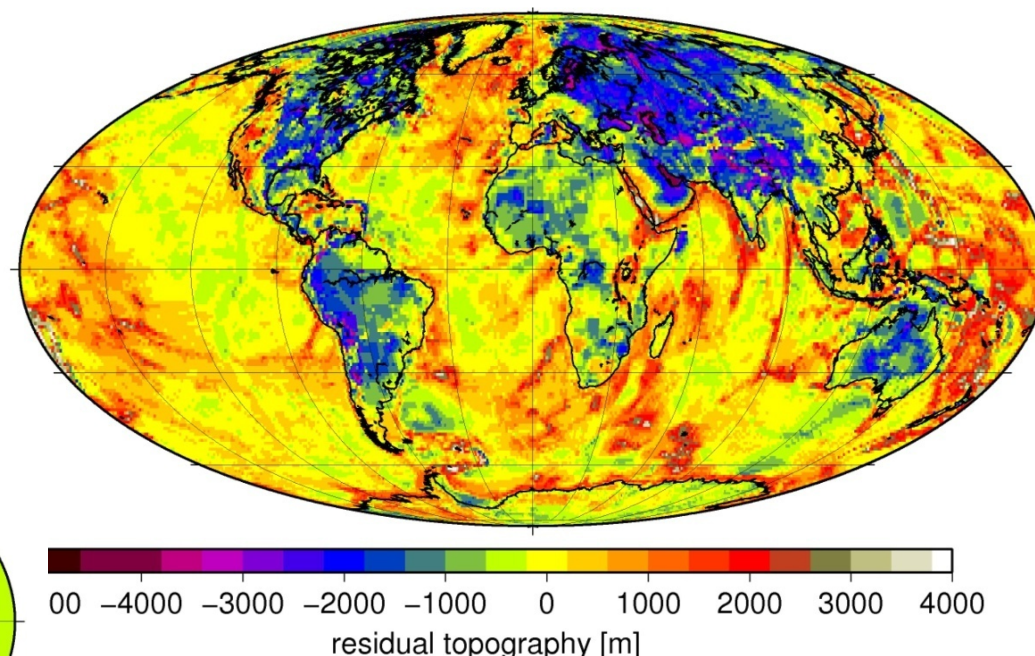


Continents like 100 Ma ocean floor

**Non-isostatic topography**

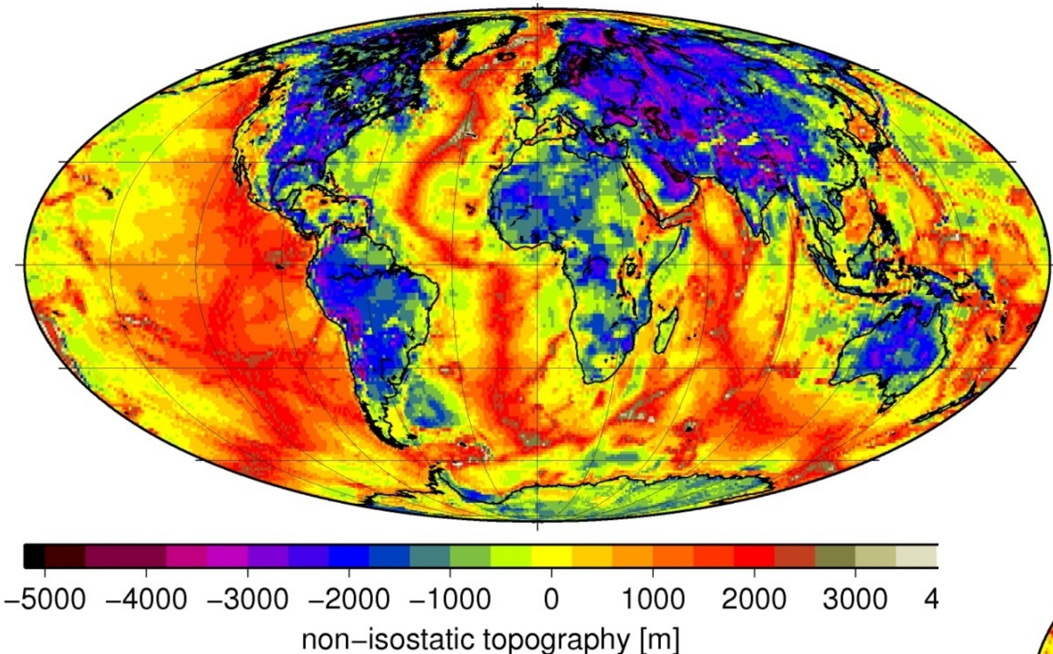


**MINUS**
**ridge topography**

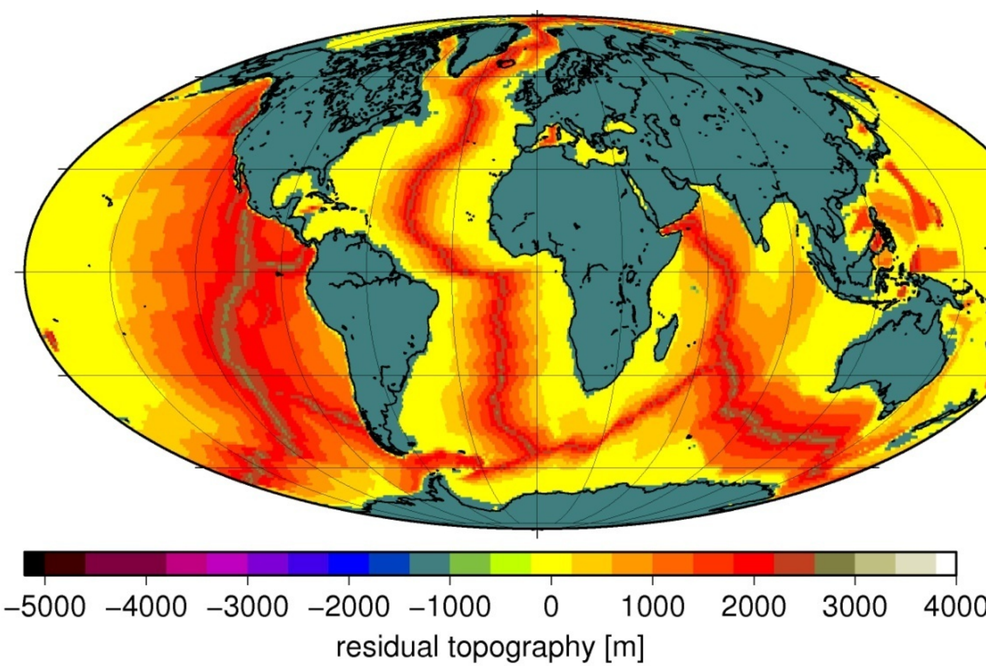


=

**residual topography**

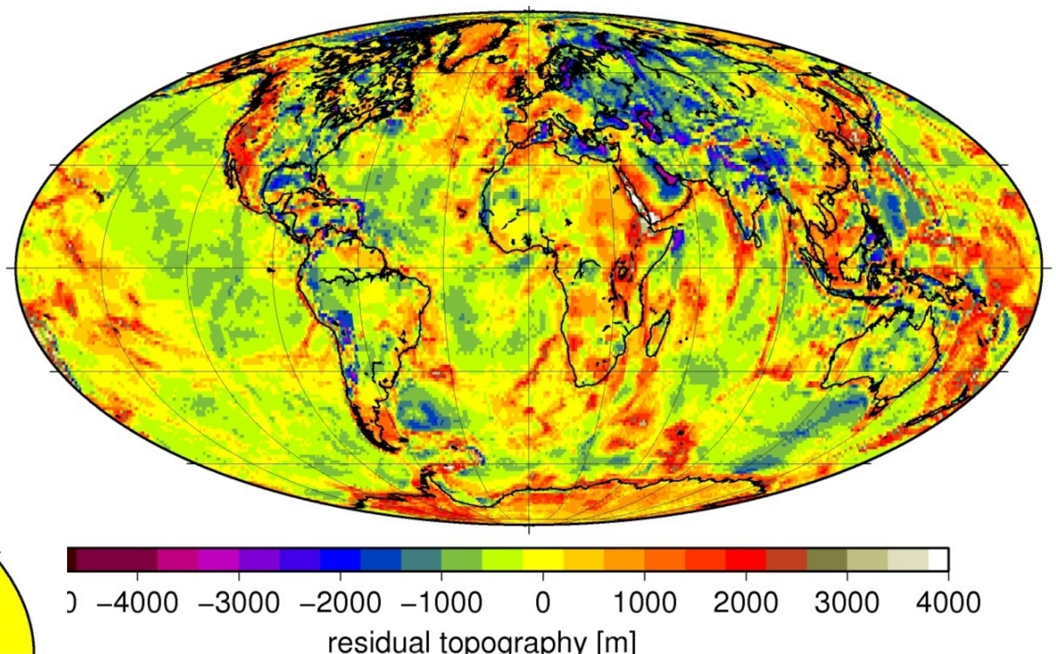


Continents sqrt (200 Ma) topography

## Non-isostatic topography

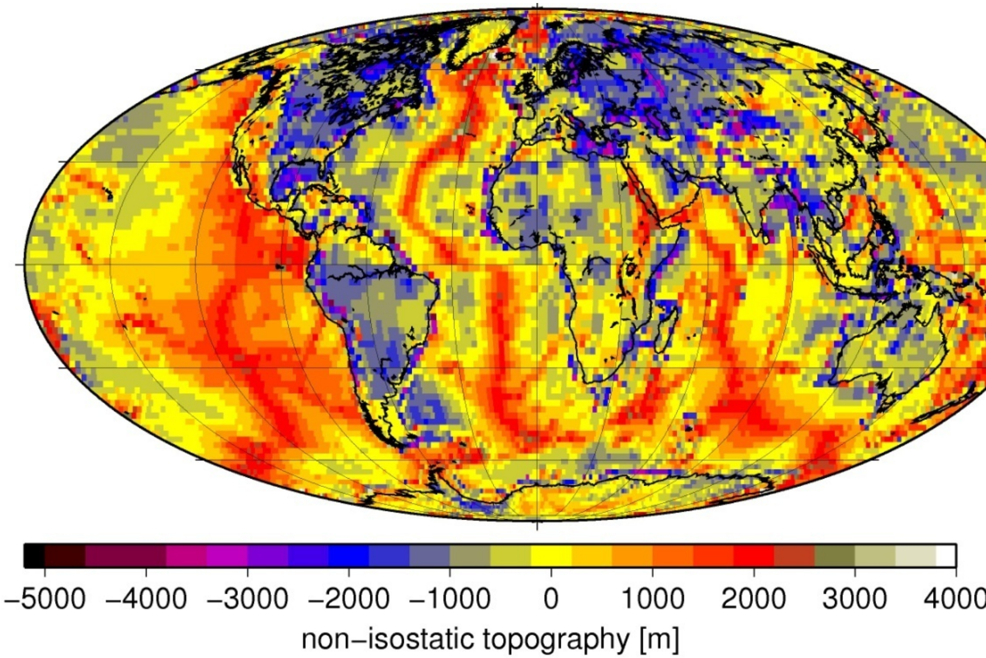


Using Crust 2.0

## MINUS
## ridge topography

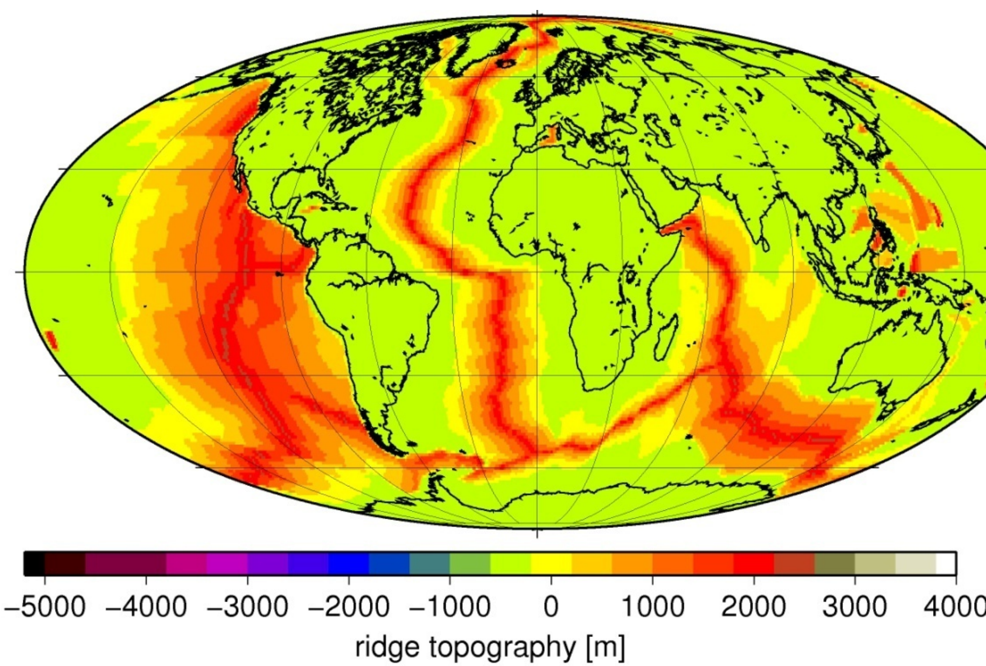


=

## residual topography

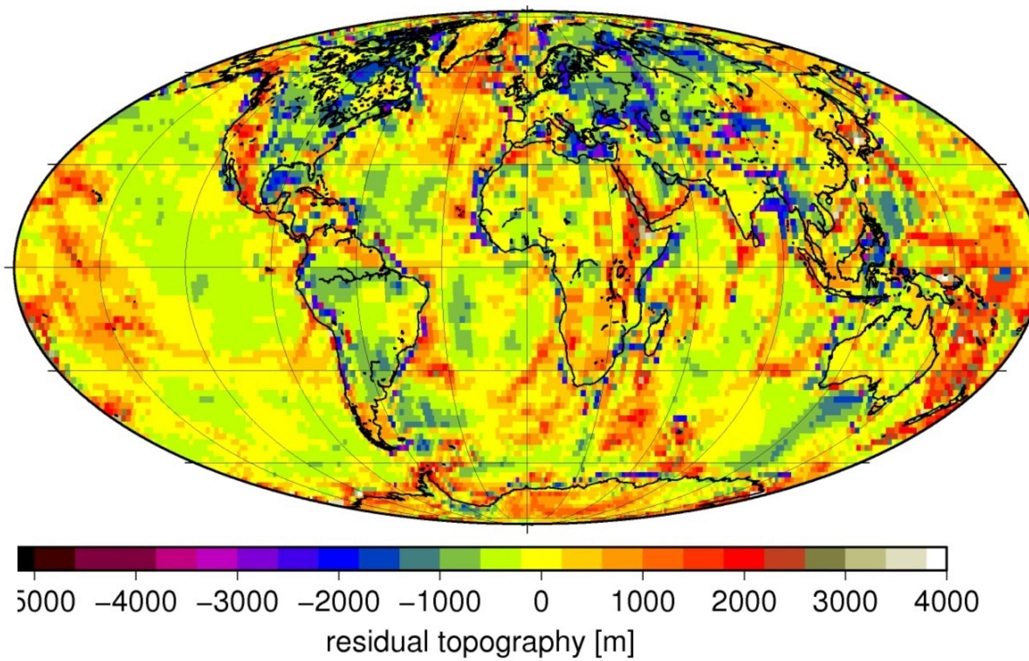


Continents like 100 Ma ocean floor

# residual topography, l=1-31

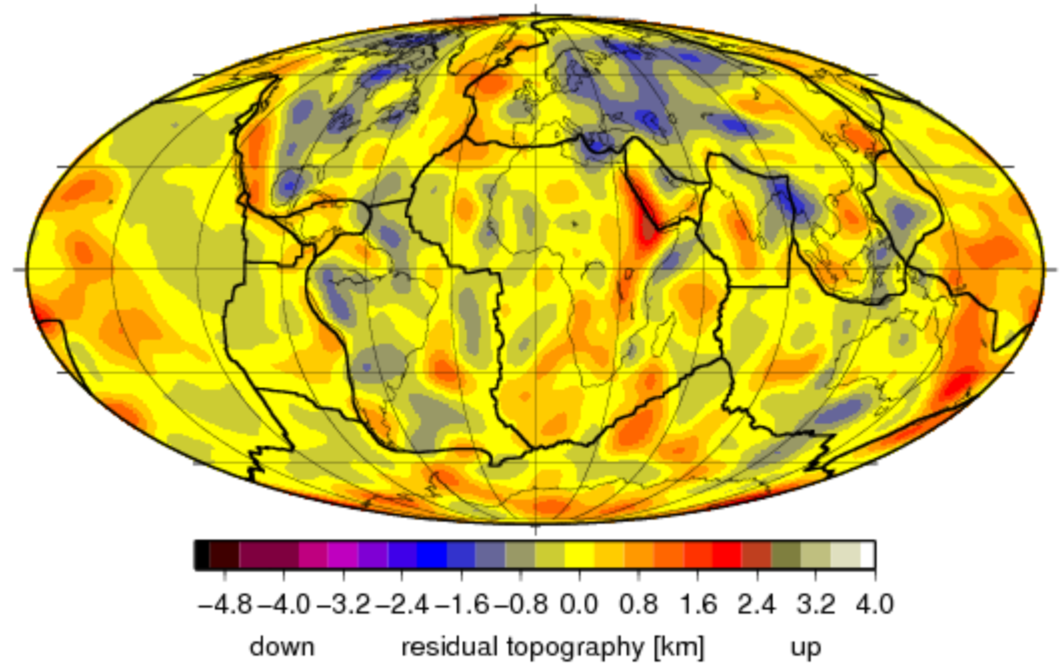

Residual topography is the observation-based quantity to which dynamic topography computed from mantle flow can be compared

**residual topography, l=1-31**

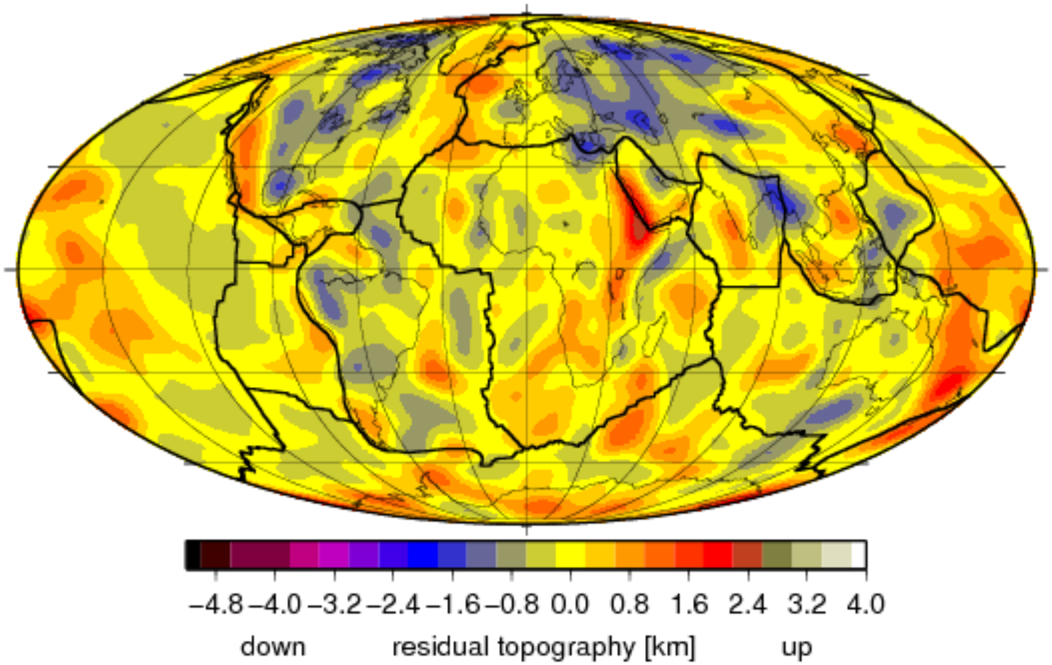


**residual topography, l=1-31**

Values above sea level multiplied with factor 1.45, because dynami topography is computed for globa seawater coverage

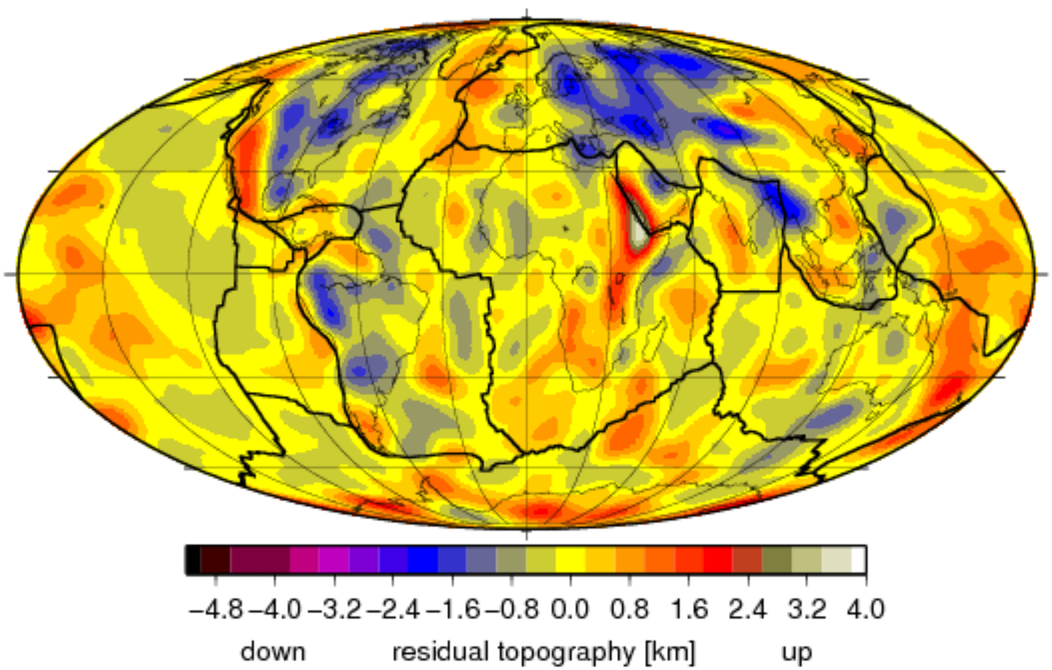

**residual topography, l=1-12,** above sea level mulitiplied with 1.45

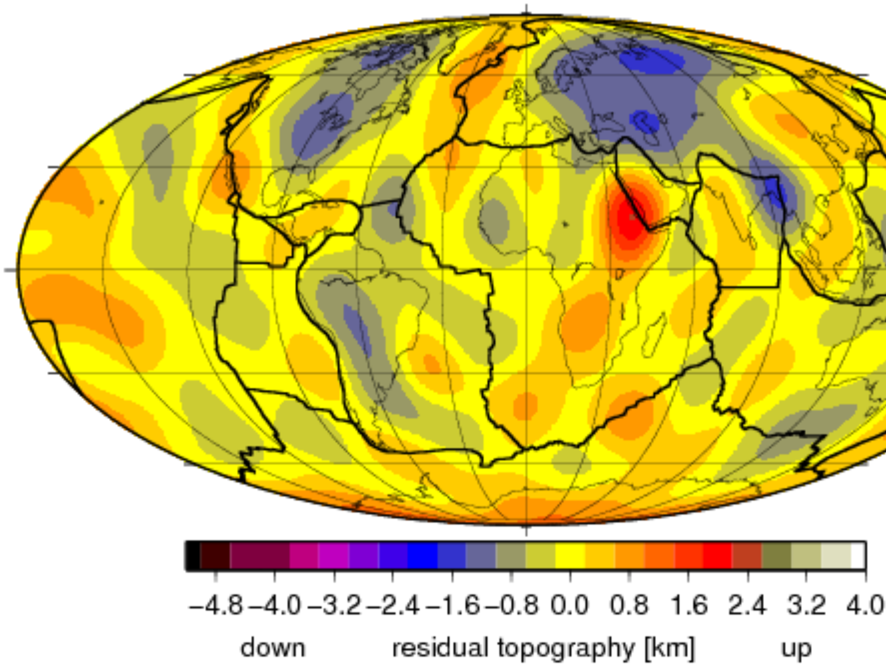


**residual topography, l=1-31**

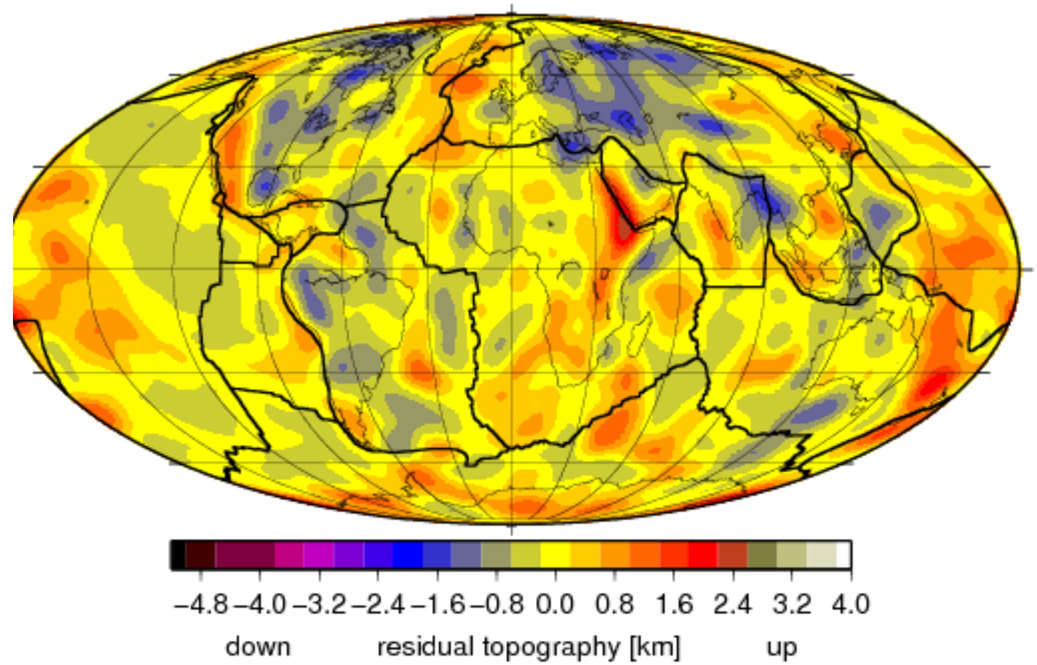


**residual topography, l=1-31**
Above sea level multiplied with 1.45

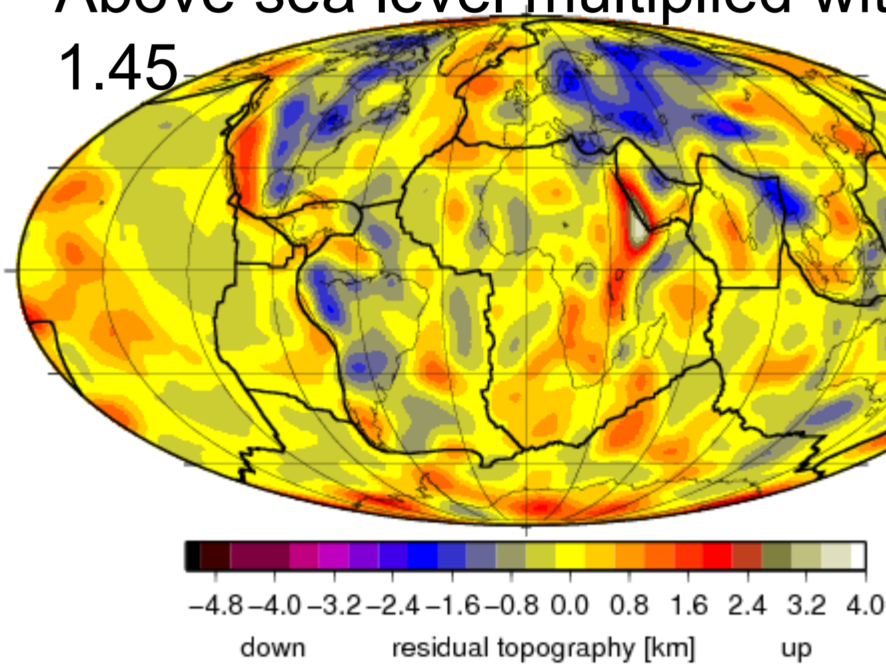

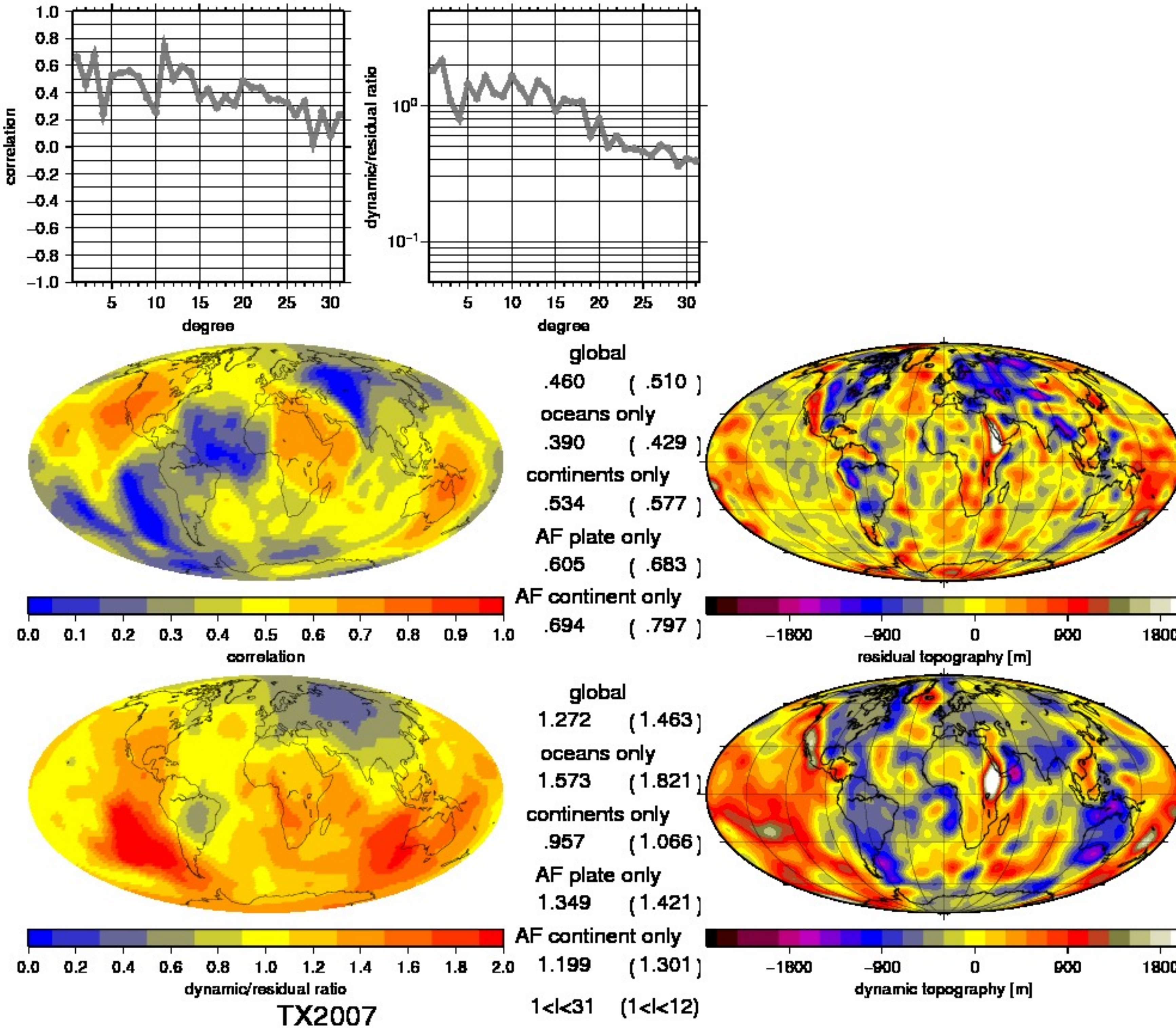
correlation
degree
dynamic/residual ratio
degree
global
.460 ( .510 )
oceans only
.390 ( .429 )
continents only
.534 ( .577 )
AF plate only
.605 ( .683 )
AF continent only
.694 ( .797 )
correlation
residual topography [m]
global
1.272 (1.463)
oceans only
1.573 (1.821)
continents only
.957 (1.066)
AF plate only
1.349 (1.421)
AF continent only
1.199 (1.301)
dynamic/residual ratio
dynamic topography [m]
1<l<31 (1<l<12)
TX2007

Results without subtracting ridge topography

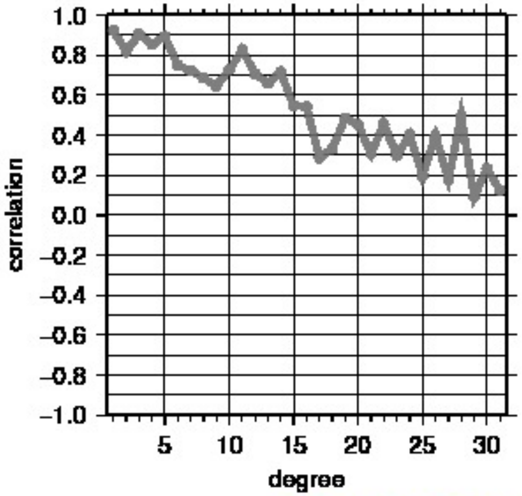


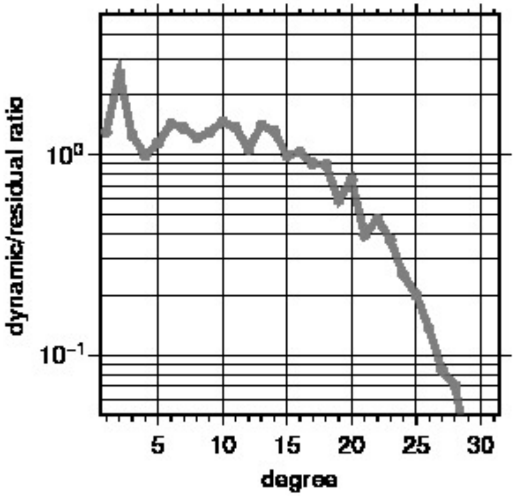


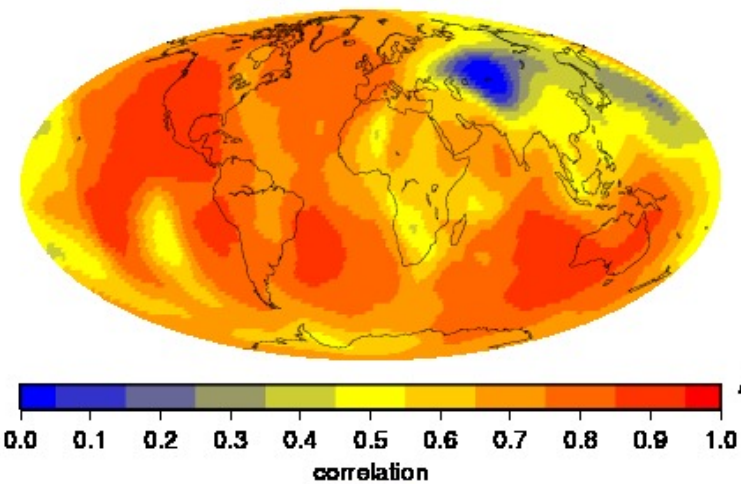


global
.754 ( .816 )
oceans only
.748 ( .817 )
continents only
.574 ( .657 )
AF plate only
.705 ( .774 )
AF continent only
.686 ( .798 )

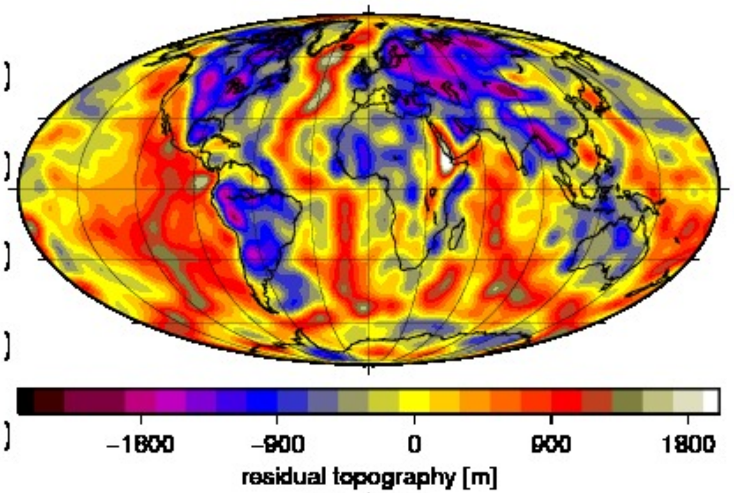


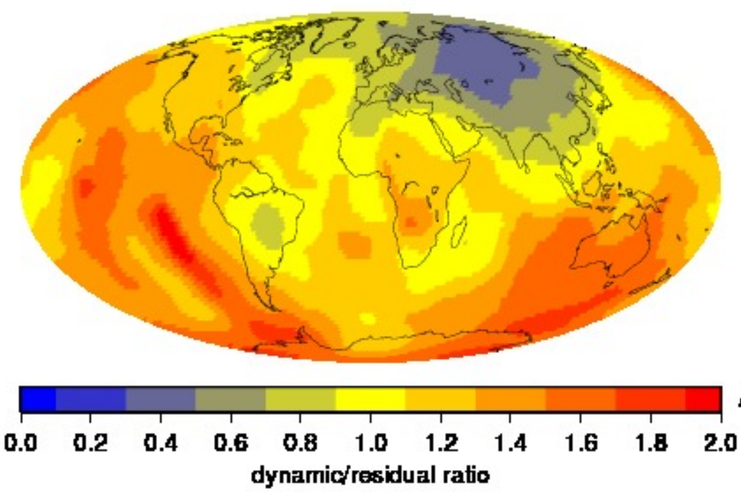


TX2007

global
1.245 (1.330)
oceans only
1.519 (1.670)
continents only
.950 (1.040)
AF plate only
1.135 (1.130)
AF continent only
1.213 (1.292)

1<l<31 (1<l<12)

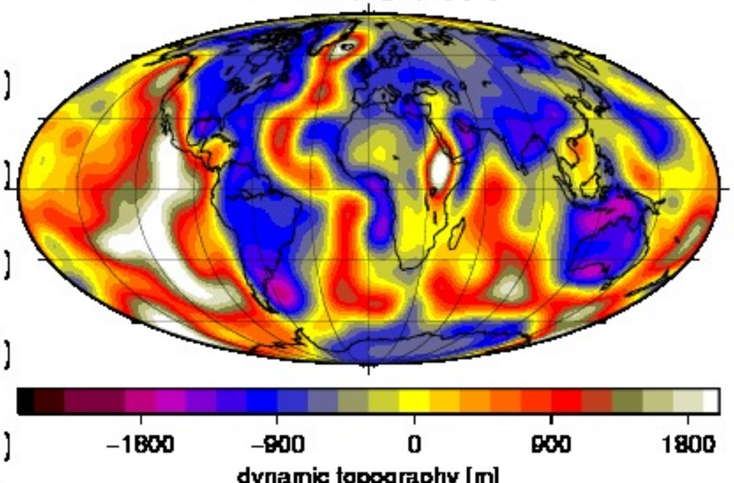

Results with thermal scaling from s-wavespeed to density also within continental lithosphere

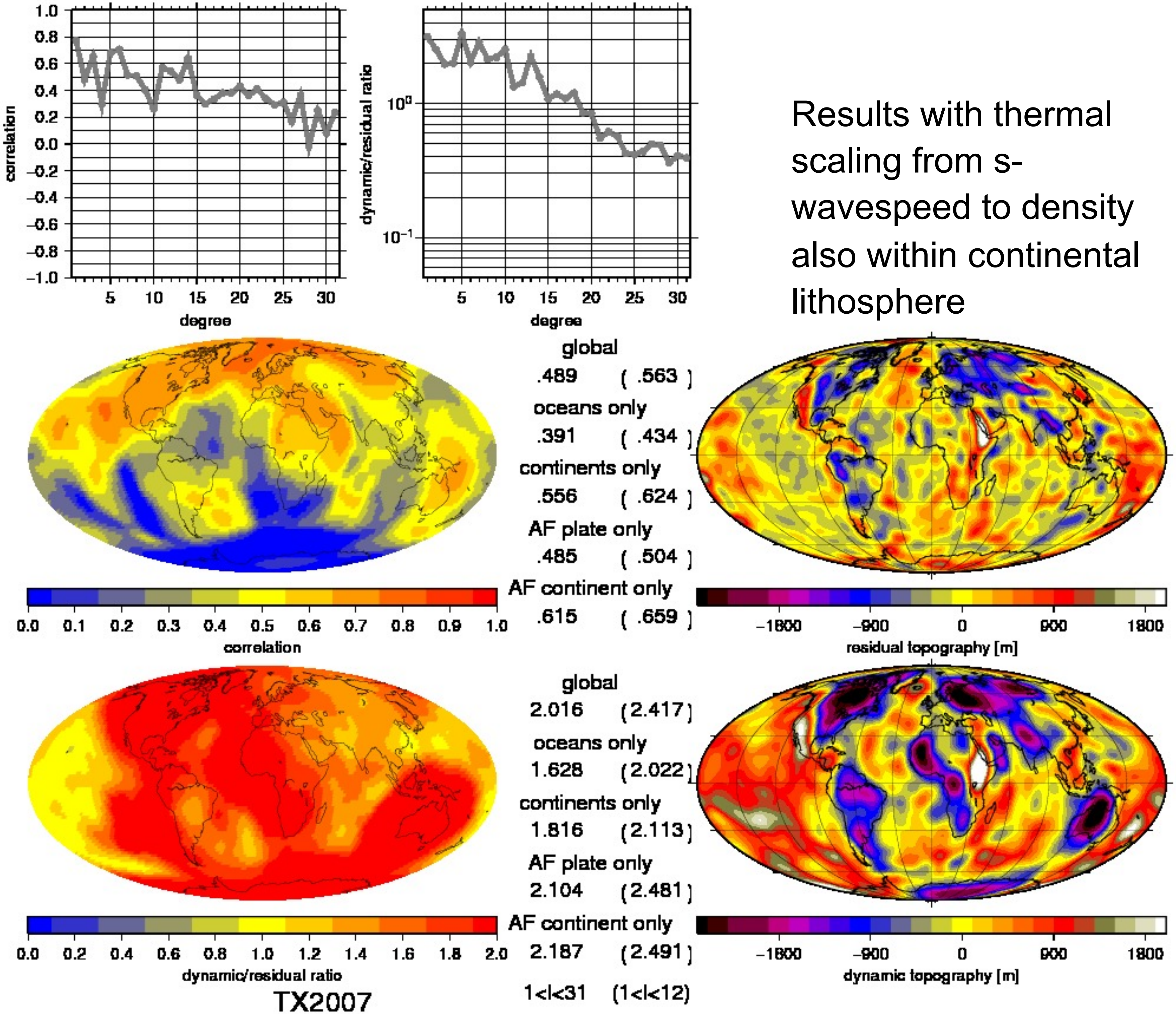

# With self-generated plate boundaries

Lithospheric code (Finite Elements)

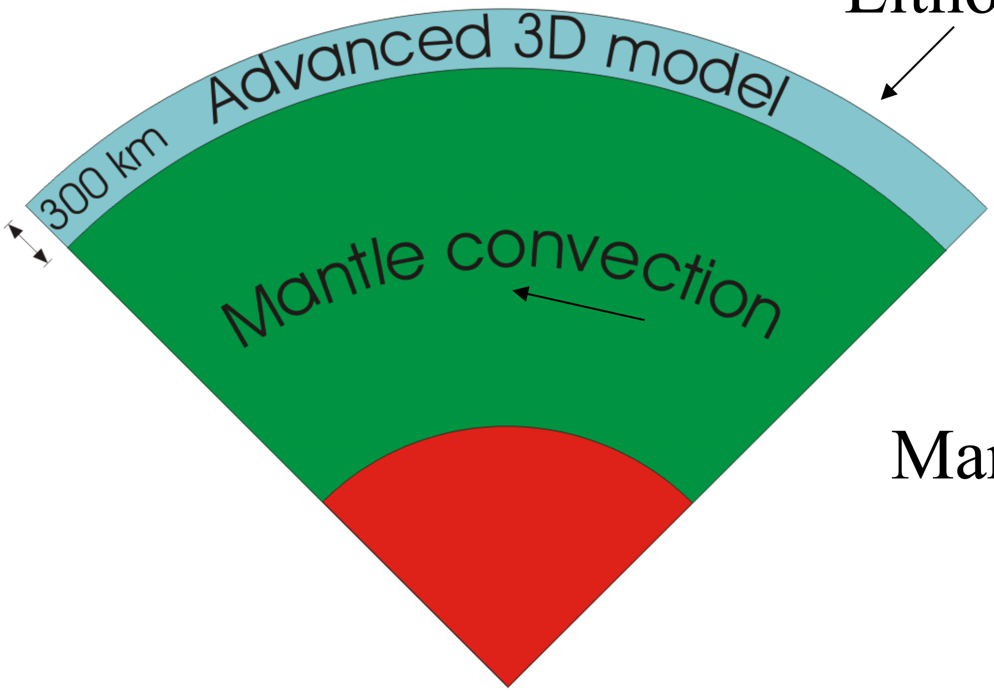


Mantle code (spectral)

Mantle and lithospheric codes are coupled through continuity of velocities and tractions at 300 km.

Sobolev, Popov and Steinberger, in preparation

# Self-generated plate boundaries

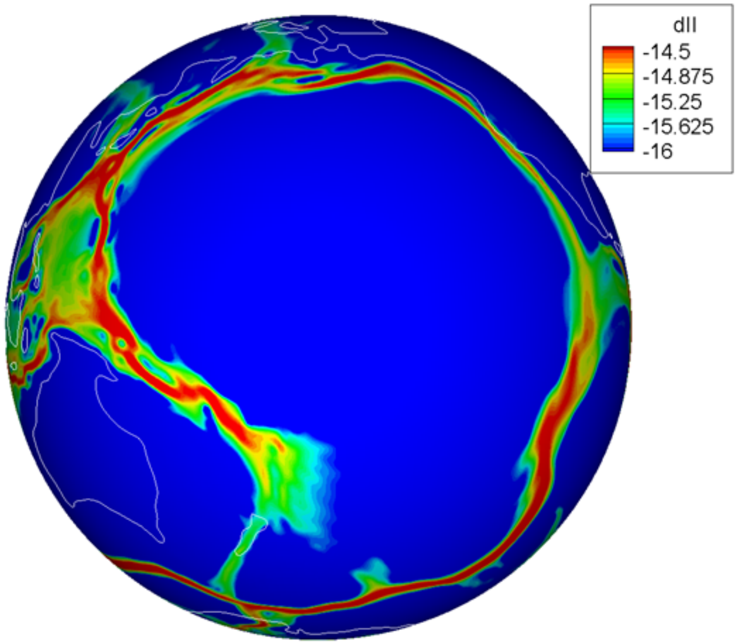


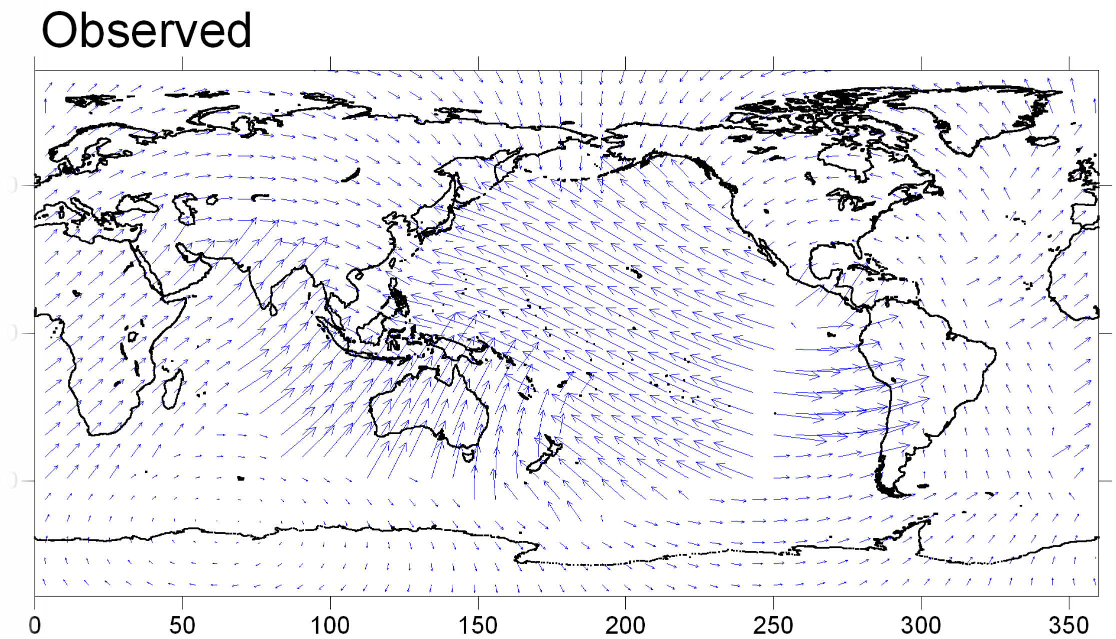


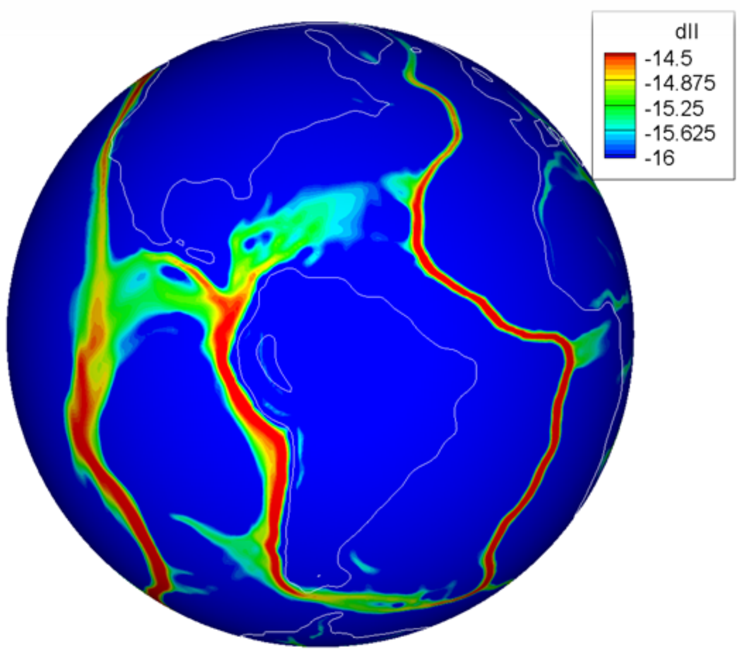


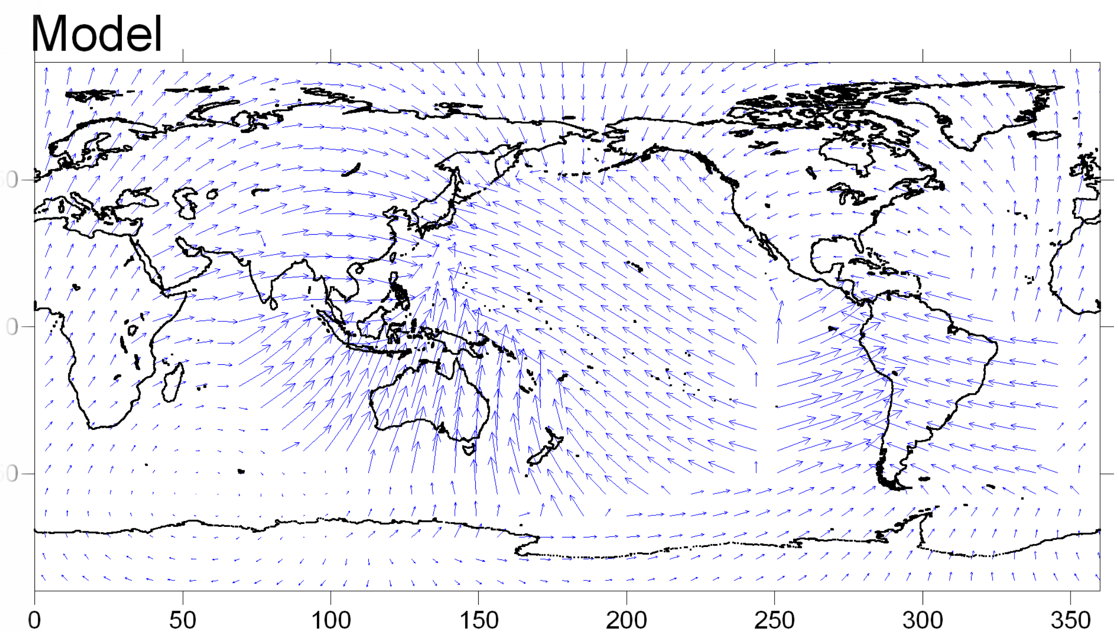


Sobolev, Popov and Steinberger, in preparation

# Modelling uplift rates

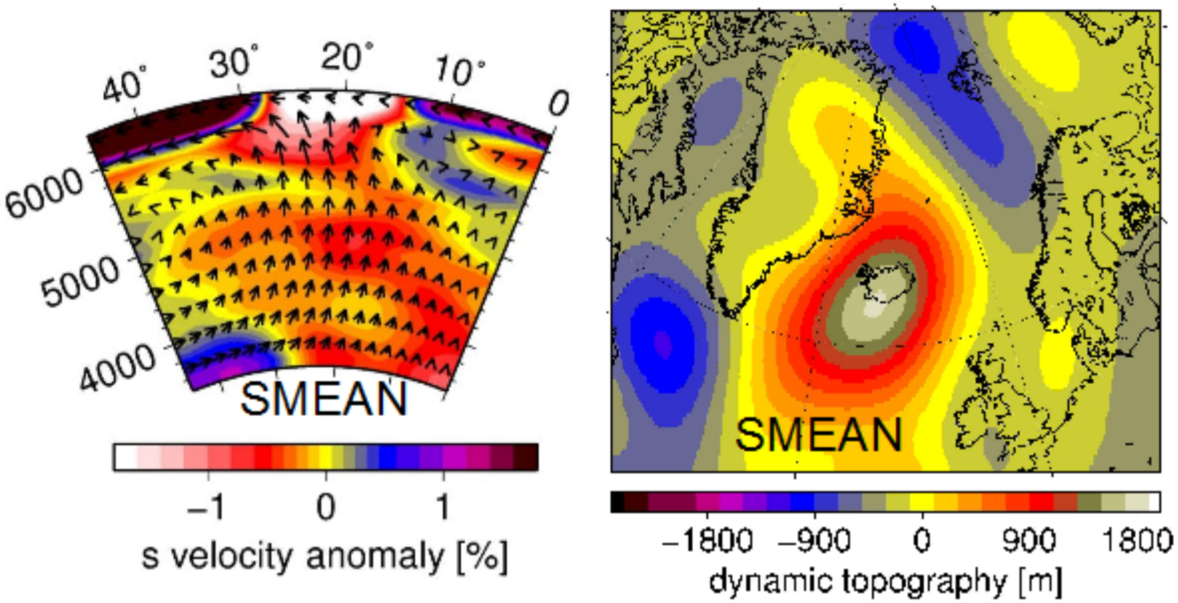


Gurnis, Mitrovica, Ritsema and van Heijst (G-Cubed, 2000) "conclude that uplift rate, when combined with estimates of present-day dynamic topography, provides a powerful tool to constrain the properties of the deep mantle"

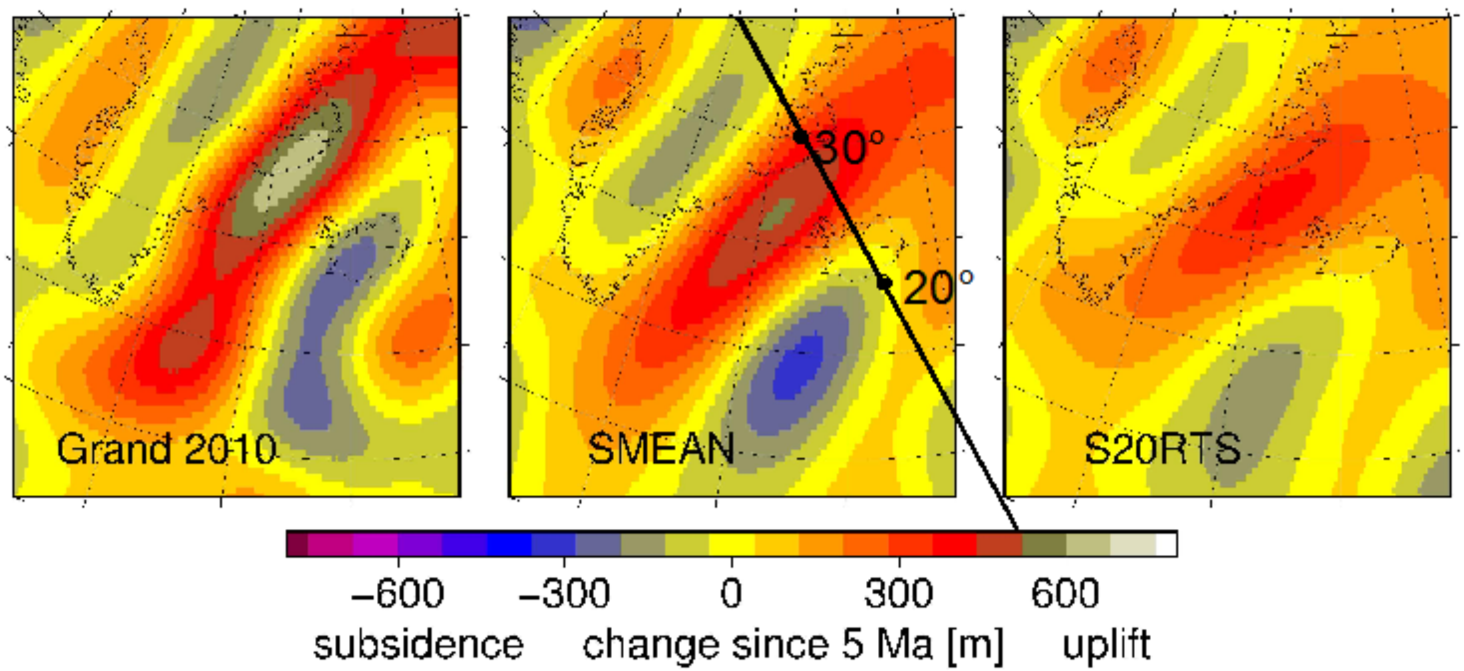


Example Iceland/ Greenland (Steinberger et al., in preparation)

**How is past dynamic topography computed from mantle flow models?**

Backward-advection of density heterogeneities in the flow field

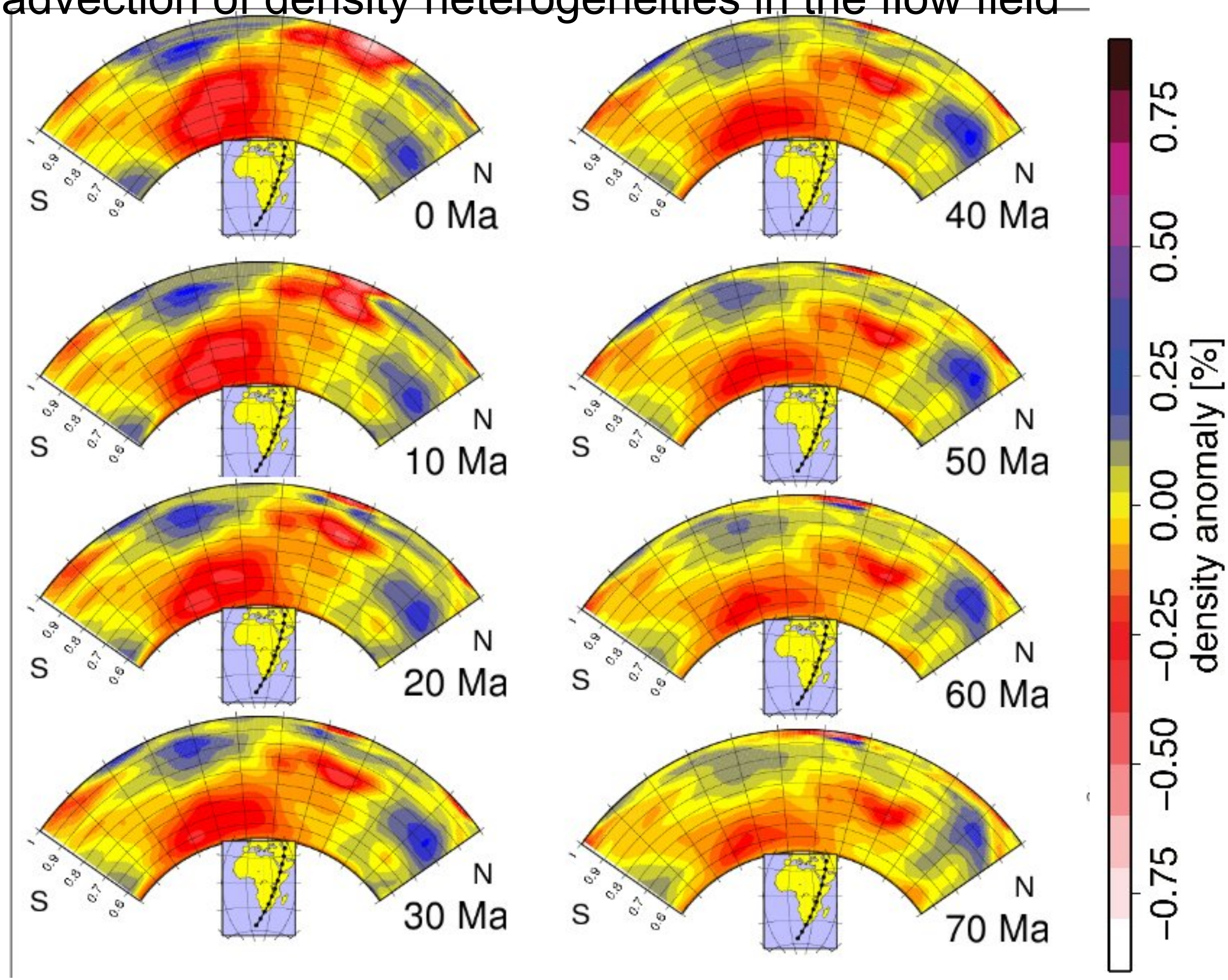

# Example 1: Recent uplift of southern Africa

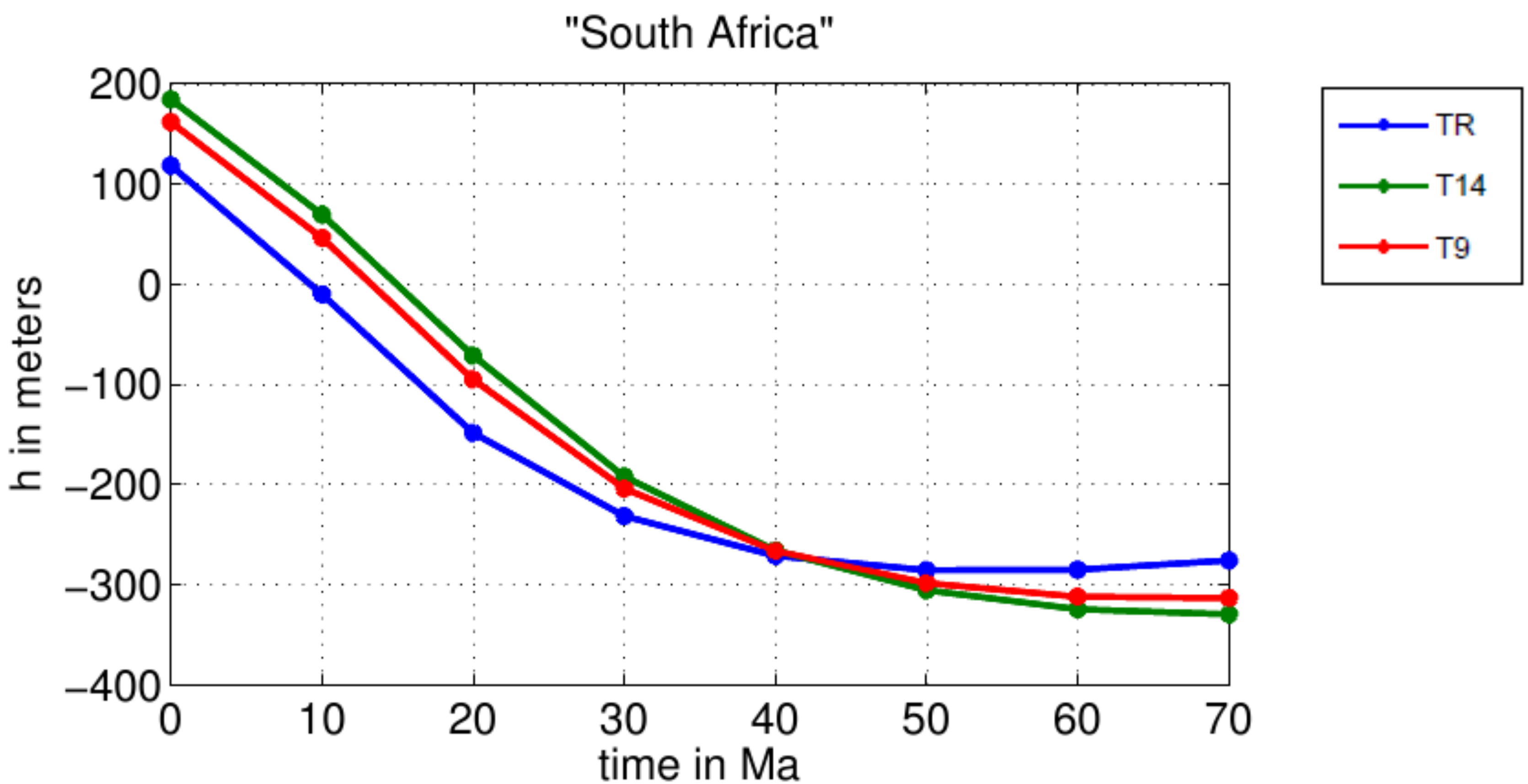


Dependence on lateral viscosity variations

$$\eta = \eta(r) \cdot e^{-E\cdot(T'-0.5)}$$

B.Sc Thesis Robert Herrendörfer, 2011; Calculations with CitcomS

Combined with plate reconstructions to compute uplift/subsidence in reference frame of moving plate

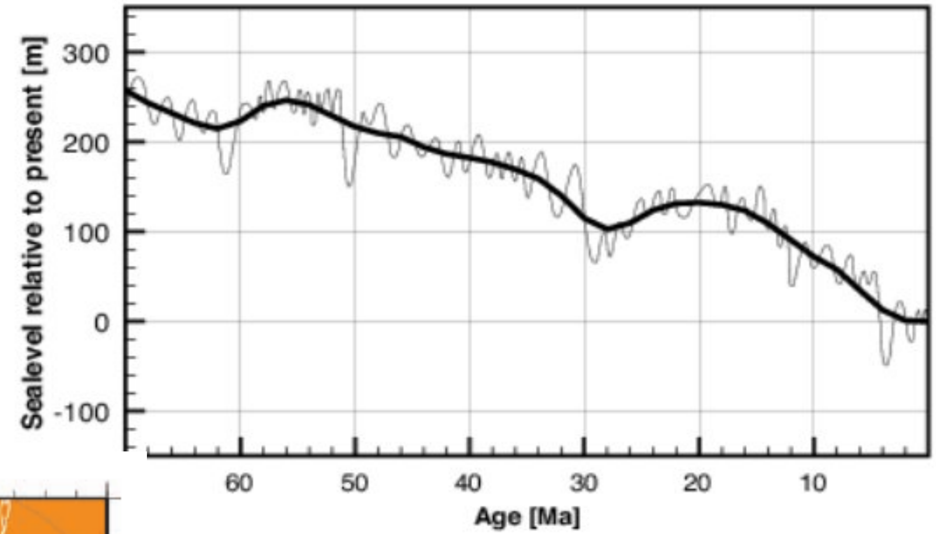


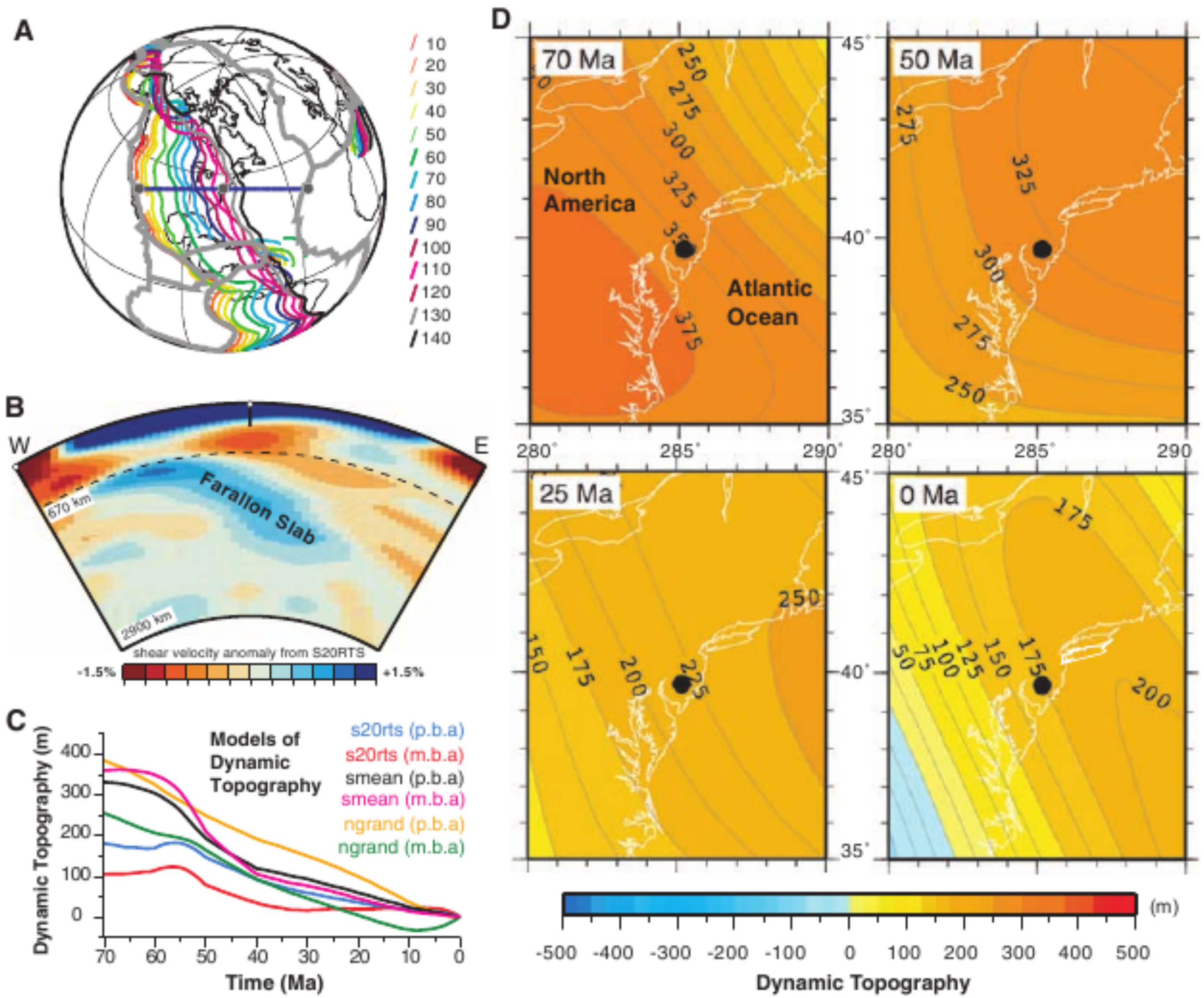


Example 2: Explaining Sea Level Curves on the East Coast of North America (Müller et al., 2008) Use “pure backward advection” vs. “modified backward advection” in which negative density anomalies in upwellings are continued upward to 220 km, and positive density Anomalies in downwellings are Removed from uppwermost 220 km.

# Example 3: Explaining marine inundations in Australia (Heine et al., 2009)

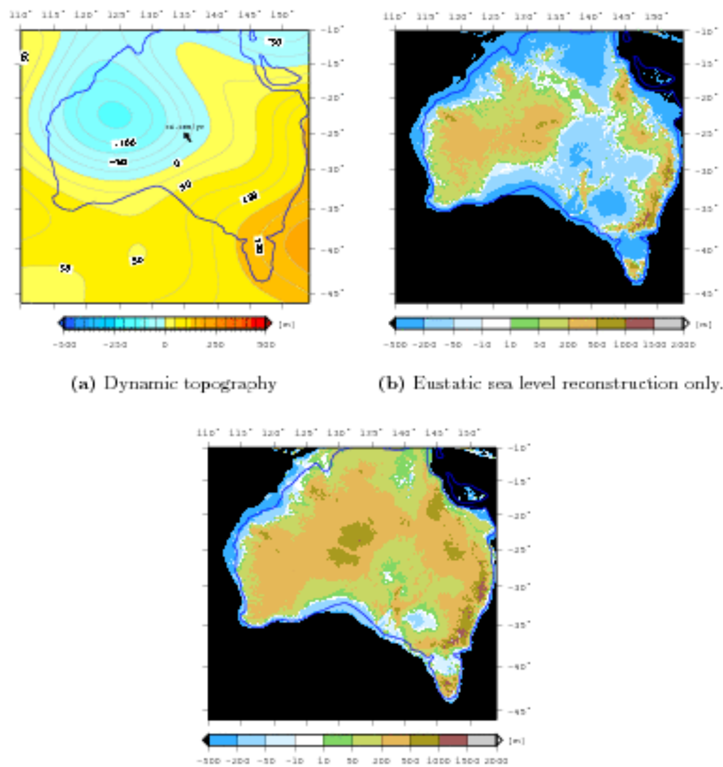

(a) Dynamic topography

(b) Eustatic sea level reconstruction only.

(c) Dynamic topography combined with eustatic sea level.

**Figure 5:** Topographic reconstructions for Australia at ≈64 Ma (Early Paleocene) using the interpreted environment for the Cenozoic 1 timeslice of Langford et al. [1995]. a) Isostatically corrected dynamic topography model. Plate motion indicated by vector at 25° S/135° W; b) Reconstruction using eustatic sea level only; c) Combined dynamic topography and eustatic sea level reconstruction with backstripped sediments in Eucla and Murray Basins; d) Differential topography relative to the present day.

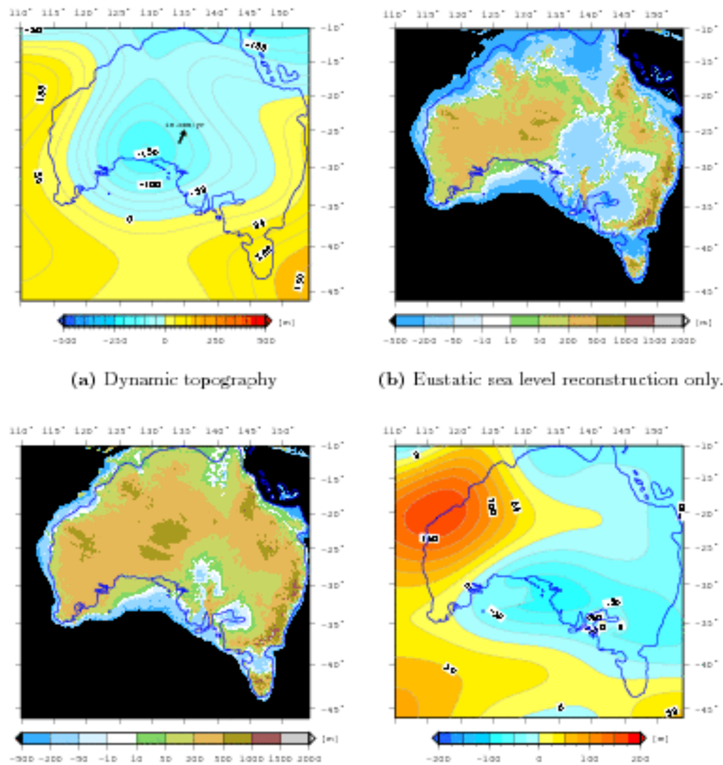

(a) Dynamic topography

(b) Eustatic sea level reconstruction only.

(c) Dynamic topography combined with eustatic sea level.

(d) Differential topography

**Figure 6:** Topographic reconstructions for Australia at ≈ 41 Ma (Mid-Eocene) using the interpreted environment for the Cenozoic 2 timeslice of Langford et al. [1995]. a) Isostatically corrected dynamic topography model. Plate motion indicated by vector at 25° S/135° W; b) Reconstruction using eustatic sea level only; c) Combined dynamic topography (scaled by a factor of 0.3) and eustatic sea level reconstruction with backstripped sediments in Eucla and Murray Basins; d) Differential topography relative to the previous timestep (64 Ma).

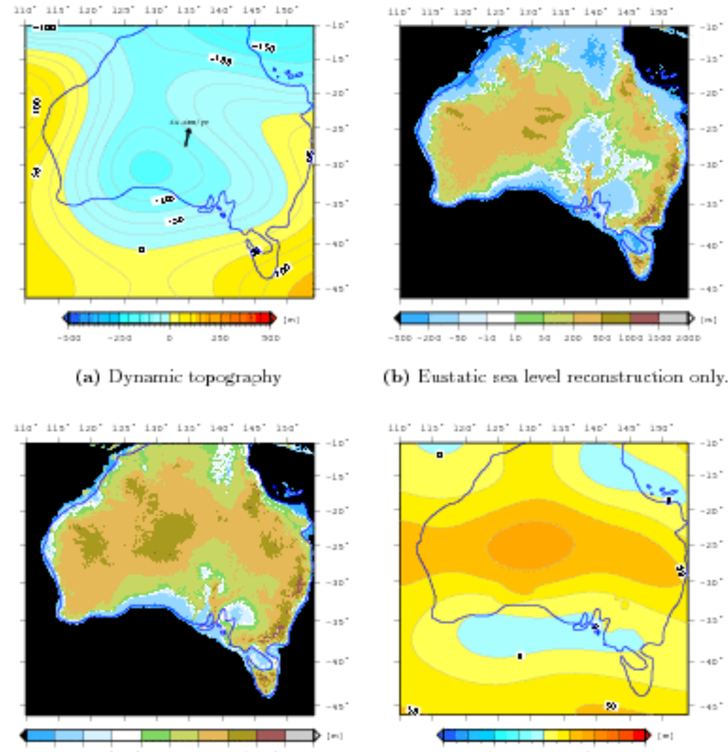

**(a)** Dynamic topography

**(b)** Eustatic sea level reconstruction only.

**(c)** Dynamic topography combined with eustatic sea level.

**(d)** Differential topography

**Figure 7:** Topographic reconstructions for Australia at ≈ 31 Ma (Early/Mid-Oligocene) using the interpreted environment for the Cenozoic 3 timeslice of Langford et al. [1995]. a) Isostatically corrected dynamic topography model. Plate motion indicated by vector at 25° S/135° W; b) Reconstruction using eustatic sea level only; c) Combined dynamic topography (scaled by a factor of 0.3) and eustatic sea level reconstruction with backstripped sediments in Eucla and Murray Basins; d) Differential topography relative to the previous timestep (41 Ma).

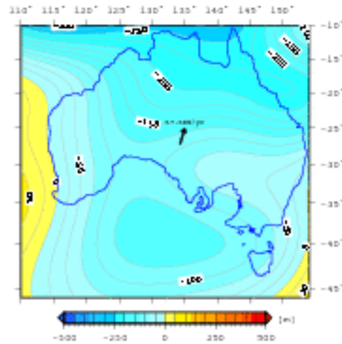

**(a)** Dynamic topography

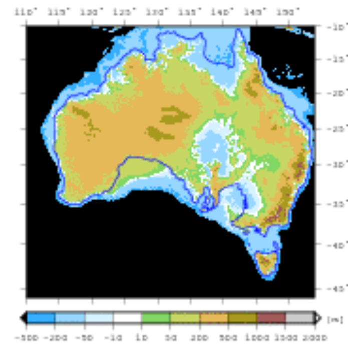

**(b)** Eustatic sea level reconstruction only.

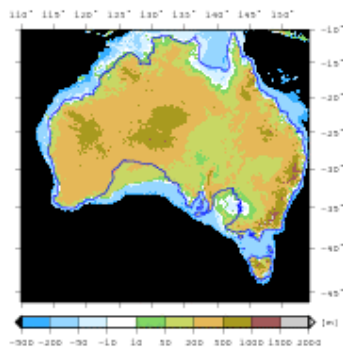

**(c)** Dynamic topography combined with eustatic sea level.

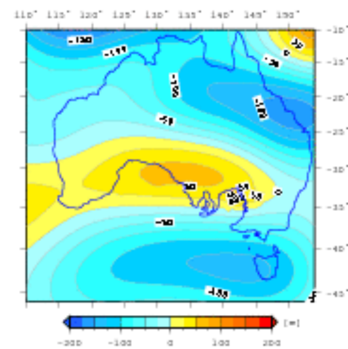

**(d)** Differential topography

**Figure 8:** Topographic reconstructions for Australia at ≈ 13 Ma (Early/Mid-Miocene) using the interpreted environment for the Cenozoic 4 timeslice of Langford et al. [1995]. a) Isostatically corrected dynamic topography model. Plate motion indicated by vector at 25° S/135° W; b) Reconstruction using eustatic sea level only; c) Combined dynamic topography (scaled by a factor of 0.3) and eustatic sea level reconstruction with backstripped sediments in Eucla and Murray Basins; d) Differential topography relative to the previous timestep (31 Ma).

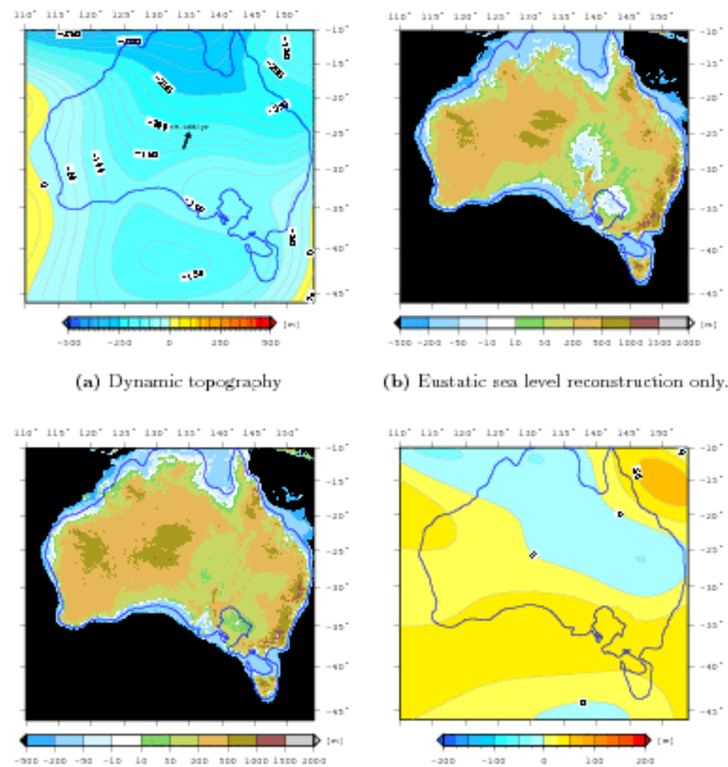

(a) Dynamic topography

(b) Eustatic sea level reconstruction only.

(c) Dynamic topography combined with eustatic sea level.

(d) Differential topography

**Figure 9:** Topographic reconstructions for Australia at $\approx$ 8 Ma (Late Miocene) using the interpreted environment for the Cenozoic 5 timeslice of Langford et al. [1995]. a) Isostatically corrected dynamic topography model. Plate motion indicated by vector at 25° S/135° W; b) Reconstruction using eustatic sea level only; c) Combined dynamic topography (scaled by a factor of 0.3) and eustatic sea level reconstruction with backstripped sediments in Eucla and Murray Basins; d) Differential topography relative to the previous timestep (13 Ma).

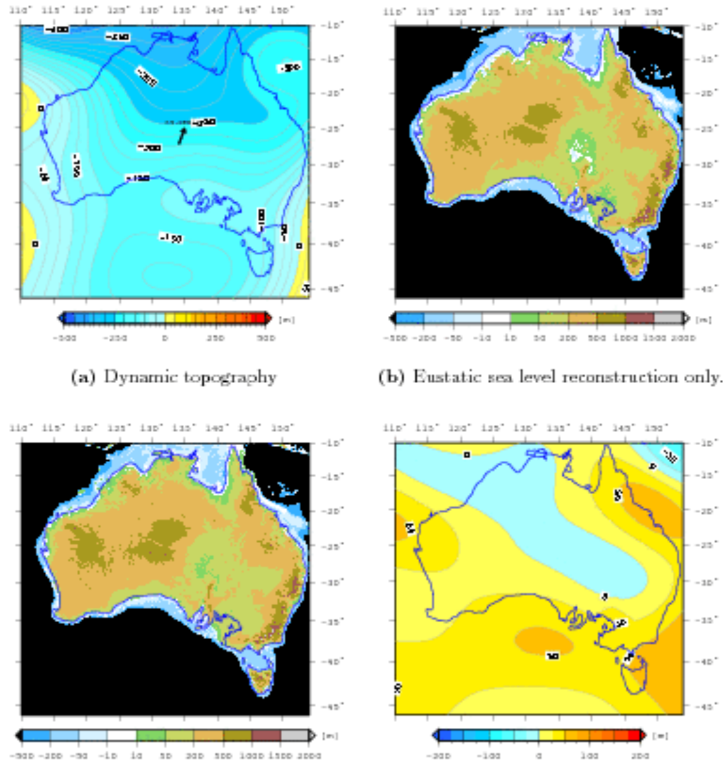

(a) Dynamic topography

(b) Eustatic sea level reconstruction only.

(c) Dynamic topography combined with eustatic sea level.

(d) Differential topography

**Figure 10:** Topographic reconstructions for Australia at ≈ 3 Ma (Pliocene) using the interpreted environment for the Cenozoic 6 timeslice of Langford et al. [1995]. a) Isostatically corrected dynamic topography model. Plate motion indicated by vector at 25° S/135° W; b) Reconstruction using eustatic sea level only; c) Combined dynamic topography (scaled by a factor of 0.3) and eustatic sea level reconstruction with backstripped sediments in Eucla and Murray Basins; d) Differential topography relative to the previous timestep (8 Ma).

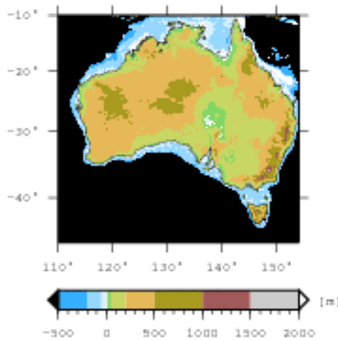


**(a)** ETOPO2 topography

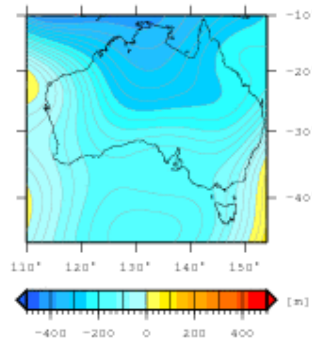


**(b)** scaled dynamic topography

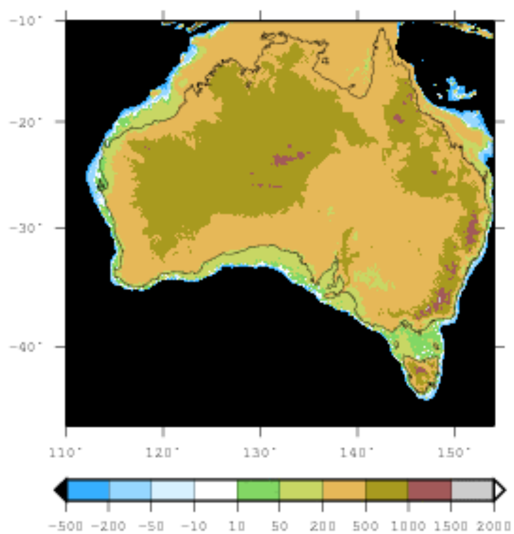


**(c)** ETOPO2 topography with dynamic topography subtracted

**Figure 4:** Present-day Australian topography, dynamic topography and difference topography. The topography with the dynamic component subtracted (Fig 4c) is used as base grid for topography reconstructions. (a) ETOPO2 present-day surface topography; (b) Scaled and isostatically corrected dynamic topography; (c) ETOPO2 topography with dynamic topography component subtracted. Thin, black line is present-day coastline, figures (a) and (c) have the same colourscale.

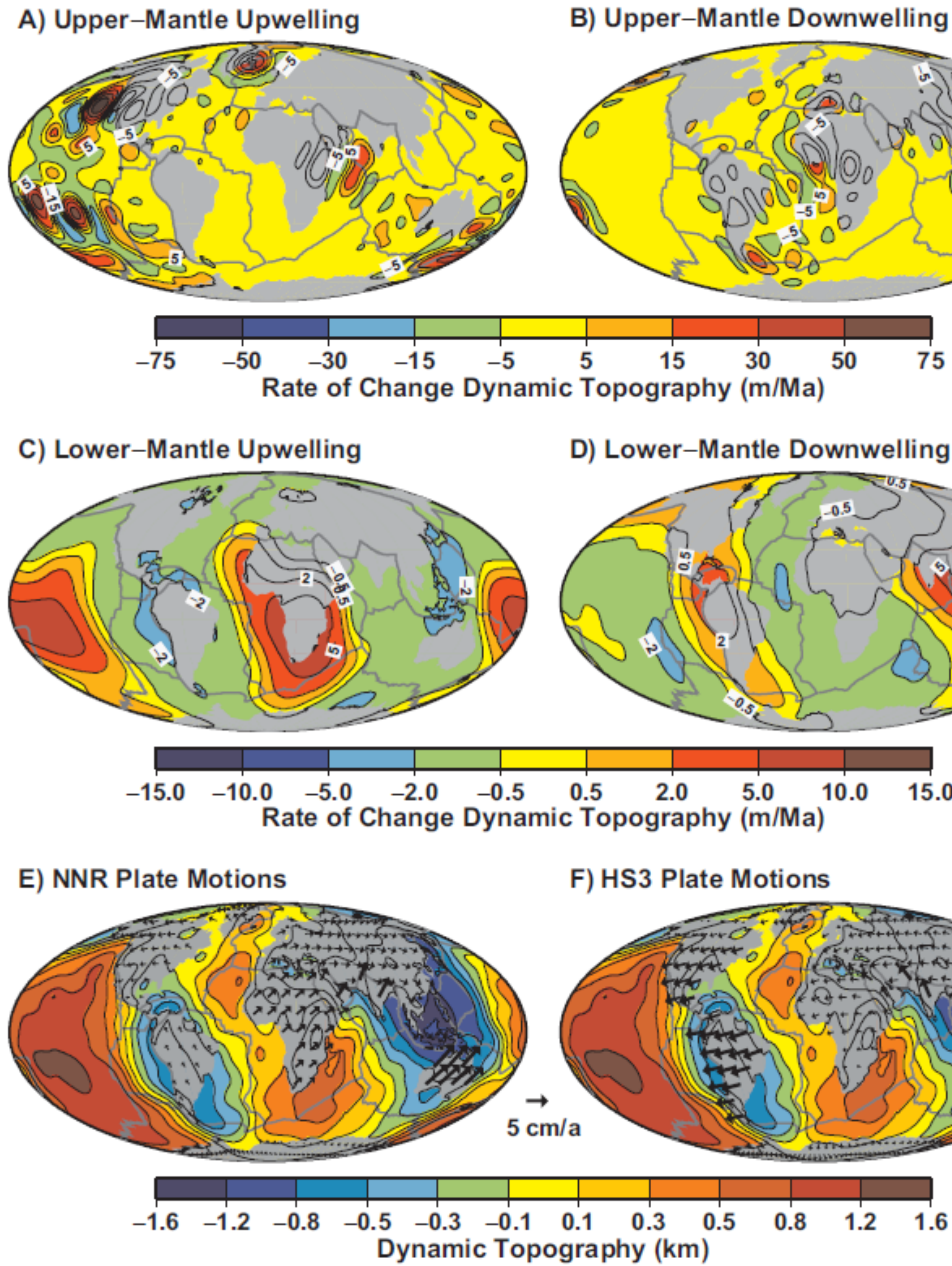


Example 4: Effect on Sea Level (Conrad and Husson, Lithosphere, 2009)

"continents preferentially conceal depressed topography associated with mantle downwelling, leading to net seafl oor uplift and ~90 ± 20 m of positive sea-level offset. Upwelling mantle flow is currently amplifying positive dynamic topography and causing up to 1.0 m/Ma of sea-level rise, depending on mantle viscosity."

# Minimum Global Sea Level @ 250 Ma when Pangea was over Tuzo: Continents moving laterally toward regions of anomalously low topography will moves the average dynamic deflection of the seafloor toward more positive values (Sea Level Rise)

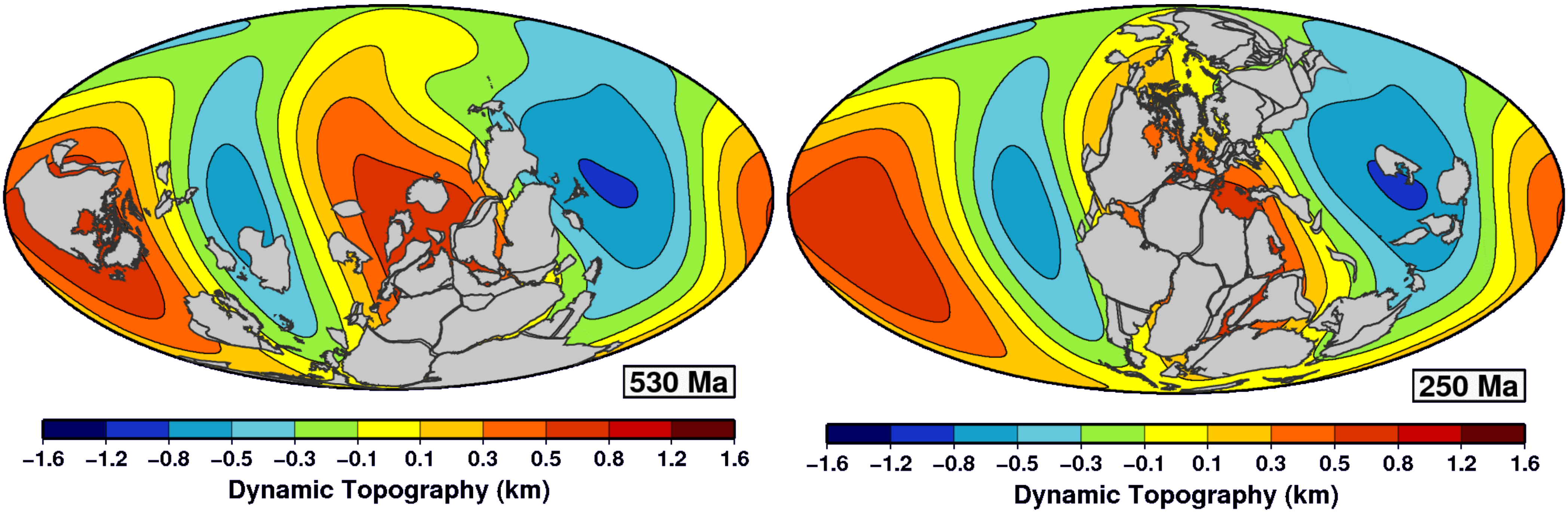


Old Palaeozoic Modell

Not longitude calibrated or corrected for TPW

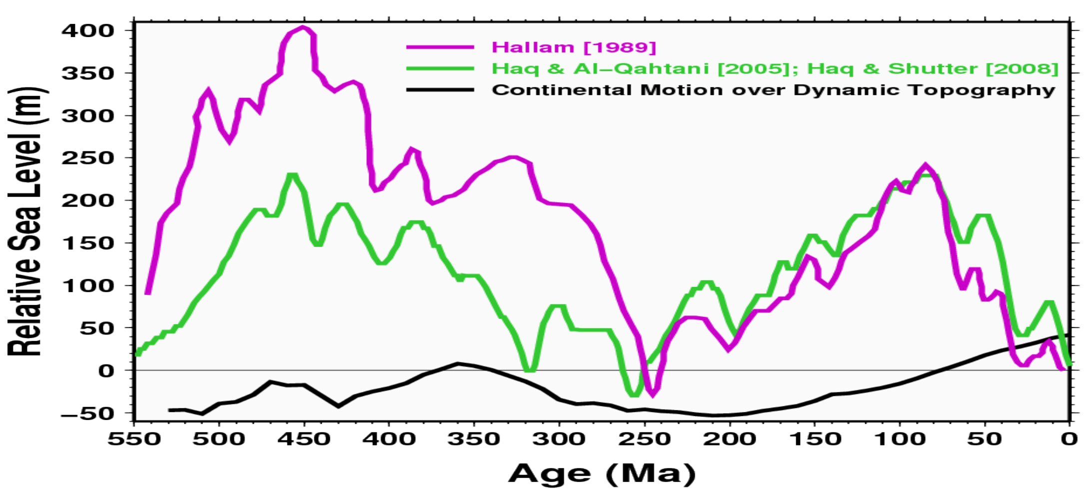


Hybrid TPW modell 0-250 Ma:

(Torsvik et al. 2008; Steinberger & Torsvik 2008)

*Calculations by C. Conrad (2012)*

In reference frame of moving
plate, e.g. high heat flow along ridges leads to subsidence as plate moves away,

Backward advection does not consider diffusion –
Possibly correct based on lateral heat flow variations:

$dh/dt = \alpha / (\rho\, C_p) \cdot$ Heat flow

With $\alpha = 4 \cdot 10^{-5}$ / K, $\rho$ = 3300 kg/m$^3$, $C_p$ = 1250 J/kg/K

a heat flow difference of 100 mW/m$^3$ corresponds to
a relative difference in uplift (subsidence) of 30 m / Myr

**Global Heat Flow *(Degree 12 Spherical Harmonic)***
***From Pollack et al. (1993)***

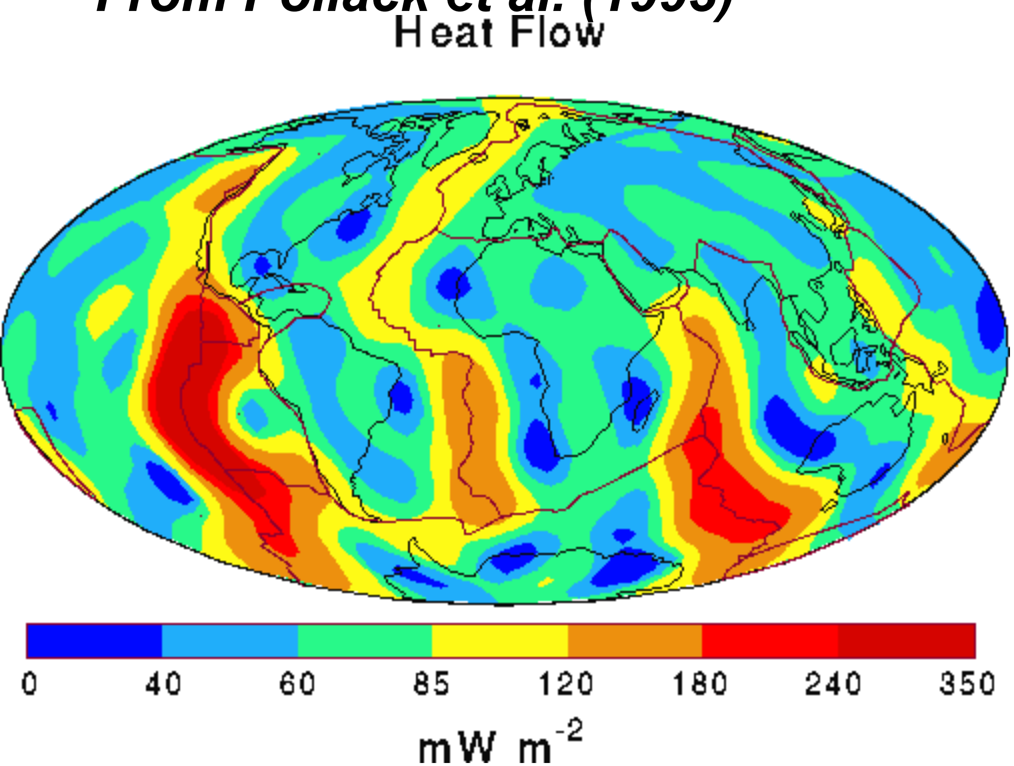


***From Davies and Davies (2010)***

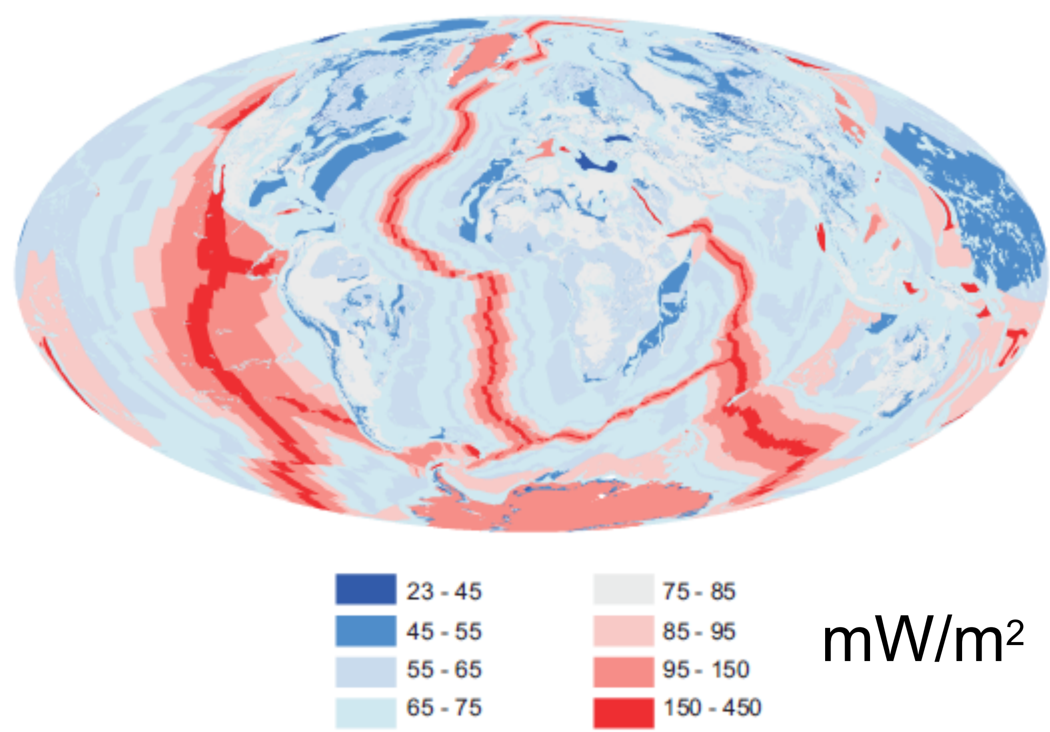

Comparison of computed changes of normal stress $T_{rr}$ (possibly after correction for heat flow variations) to observations, taking erosion into account:
Distinguish rock uplift $v_r$ and surface uplift $v_s$;
$v_r - v_s$ = erosion rate

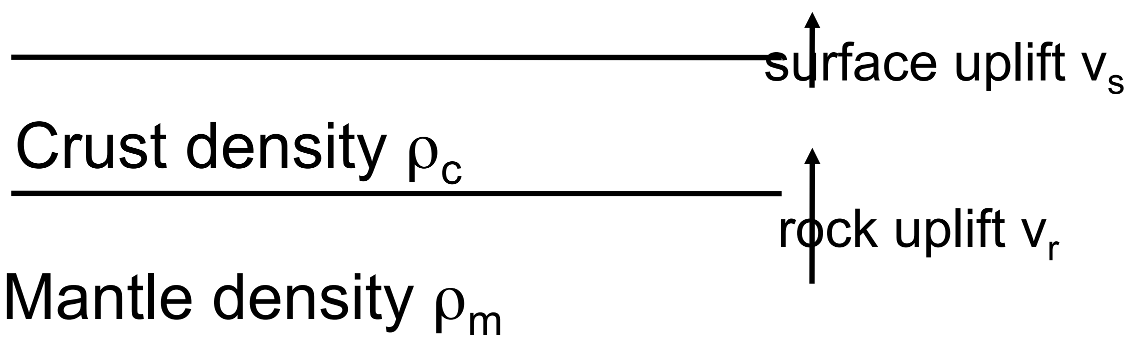


$$dT_{rr}/dt = g\,(\rho_m \cdot v_r - \rho_c \cdot (v_r - v_s))$$

$$\partial T_{rr}/\partial t + v_x\, \partial T_{rr}/\partial x + v_y\, \partial T_{rr}/\partial y$$

in reference frame of moving plate

# Forward models based on subduction history

Example 1: Gurnis, Nature, 364, 1993



# Phanerozoic marine inundation of continents driven by dynamic topography above subducting slabs

**Michael Gurnis**

Department of Geological Sciences, University of Michigan, Ann Arbor, Michigan 48109-1063, USA

**A spherical model of mantle flow constrained by the locations of trenches can be used to predict the dynamic topography of the Earth's surface, and hence the marine inundation of continents. For past periods of high sea level, the predicted geographical pattern of flooding correlates well with the geological record. The high spatial correlation may result from increased plate velocities at these times, leading to increased rates of subduction, subsidence and inundation at convergent margins.**

# Forward models based on subduction history

Example 2: Gurnis, Müller and Moresi, Science, 279, 1998

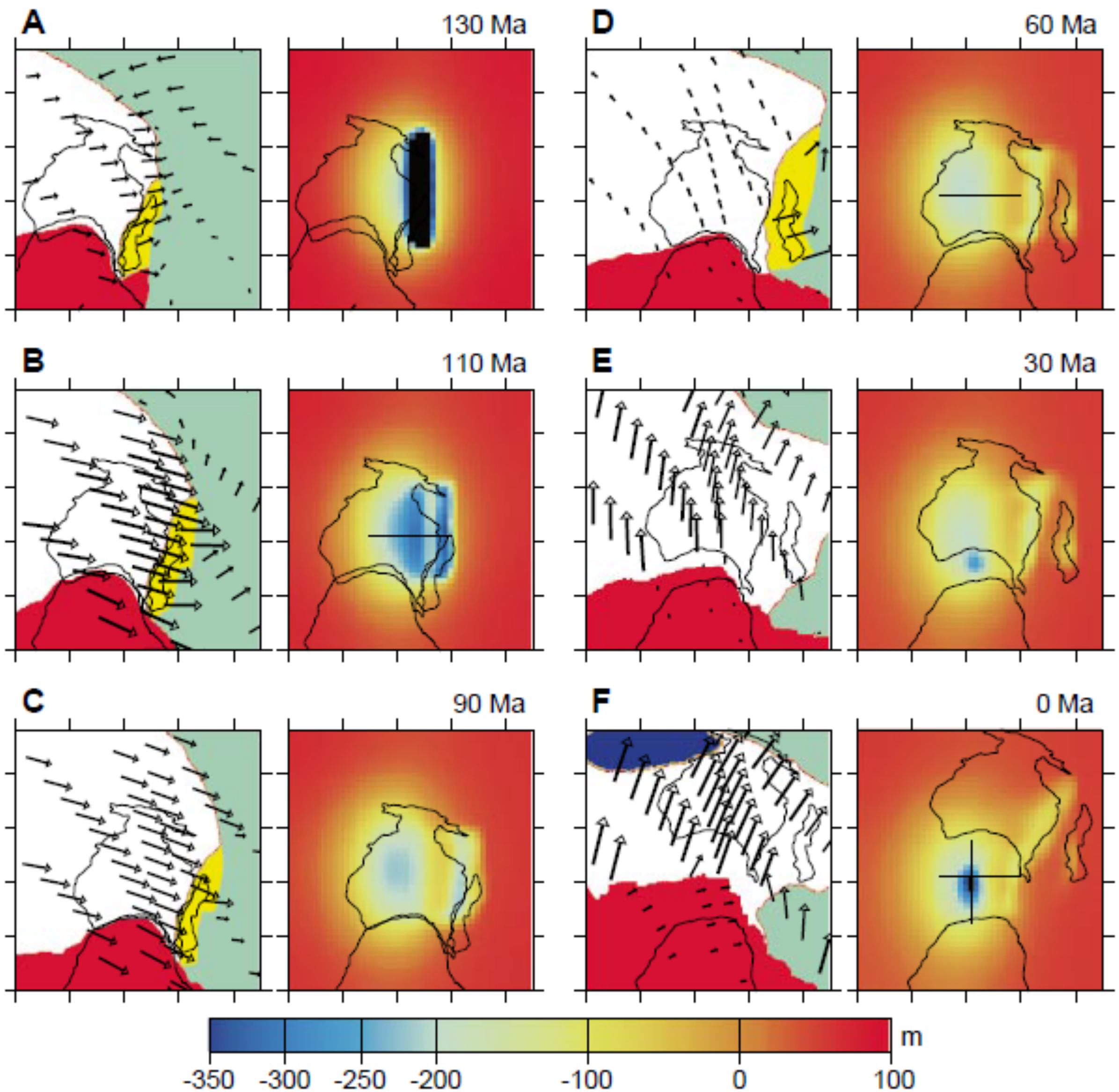


"The dynamic models infer that a subducted slab associated with the long-lived Gondwanaland-Pacific converging margin passed beneath Australia during the Cretaceous, partially stagnated in the mantle transition zone, and is presently being drawn up by the Southeast Indian Ridge."

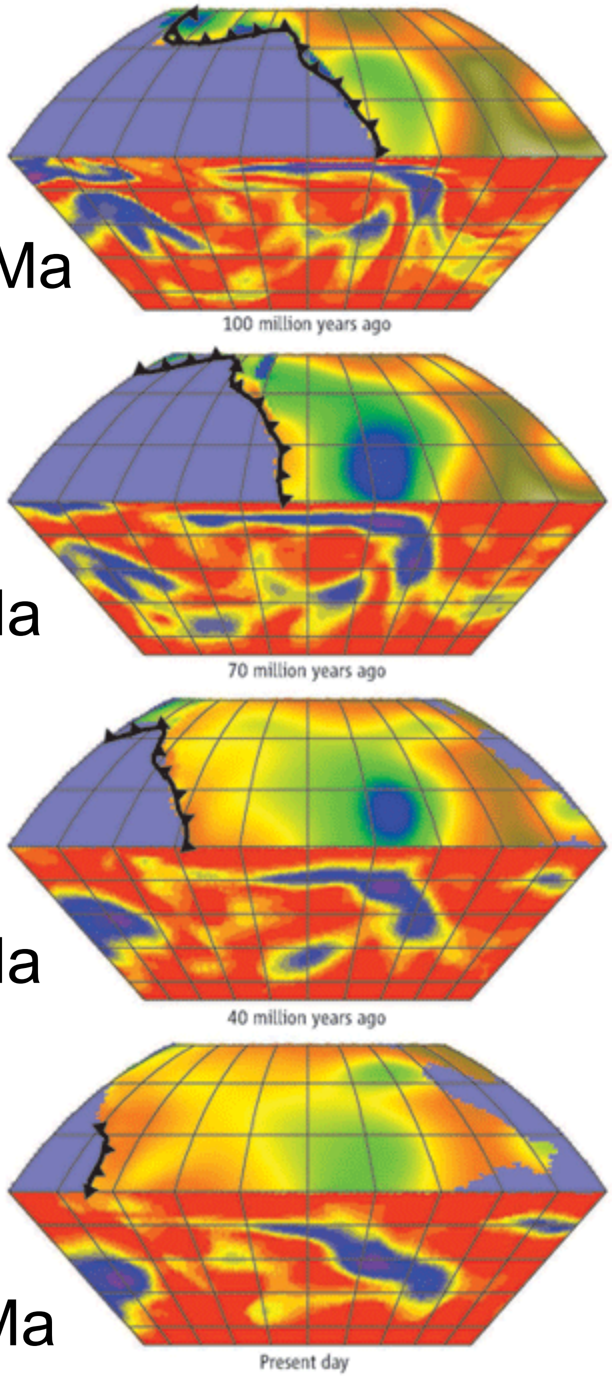


100 Ma

70 Ma

40 Ma

0 Ma

## Adjoint models:

Finding the initial model that matches present-day structure (inferred from tomography) with surface plate motion boundary conditions through time.

Example: Model of Liu, Spasojević and Gurnis (Science, 2008)

TABLE 2. STRENGTHS AND LIMITATIONS OF DYNAMIC TOPOGRAPHY MODELS

| Strengths | Limitations |
|---|---|
| *Forward models* | |
| Computationally relatively cheap | Dependent on synthetic initial condition |
| Can achieve large dimensional time | Kinematically driven |
| Can achieve high resolution | May result in unrealistic slab advection |
| Can be compared to mantle tomography | Upwelling is usually passive |
| *Backward advection* | |
| Computationally relatively cheap | Thermal diffusivity is neglected |
| Can achieve high resolution | Limited to a few tens of millions of years |
| Consistent with the present-day density structure of the mantle | Thermal boundary layers require special treatment |
| | Usually kinematically driven |
| *Adjoint models* | |
| Consistent with the present-day density structure of the mantle | Computationally expensive |
| Thermal diffusivity is accounted for | Usually kinematically driven |

From Flament, Gurnis and Mueller, Invited Review in *Lithosphere*, **5**, 2013.

# Models of topography and equipotential surface on other planets

## Computation of mantle flow field, boundary deformations and geoid

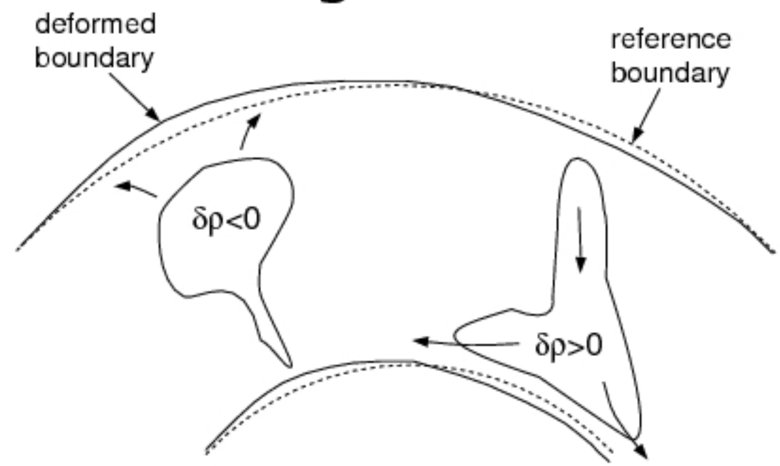


- Density anomalies (inferred from tomography models) drive flow, computed with spectral method (Hager and O'Connell, 1981)
- Flow deforms boundaries
- Density anomalies and deformed boundaries contribute to geoid anomalies

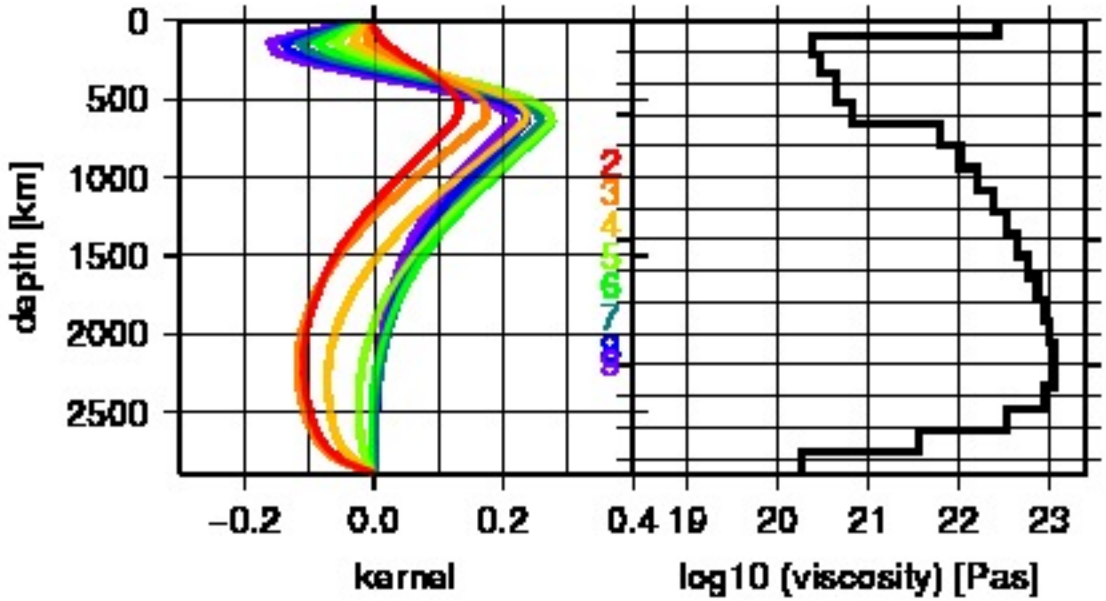


Geoid kernels $K_l(r)$ describe effect of density anomalies at spherical harmonic degree *l* and radius *r* on geoid

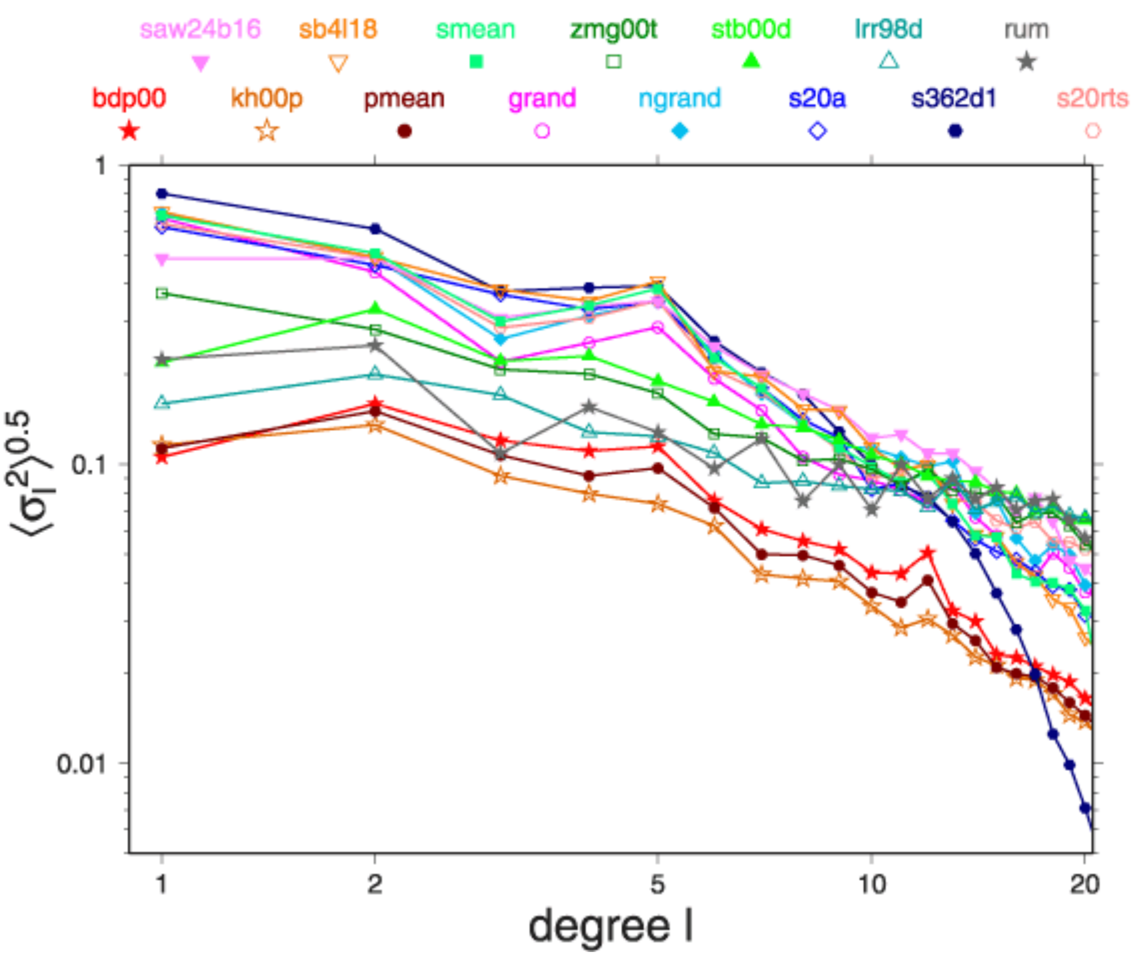


Compute expected gravity power vs. *l*

Assume radial correlation ~1/*l*

Power spectrum of tomography models (depth averaged)

$$\sigma_{1,l} \cong \sigma_0 / \sqrt{(l+1)(2l+1)}$$

(Becker and Boschi, 2002)

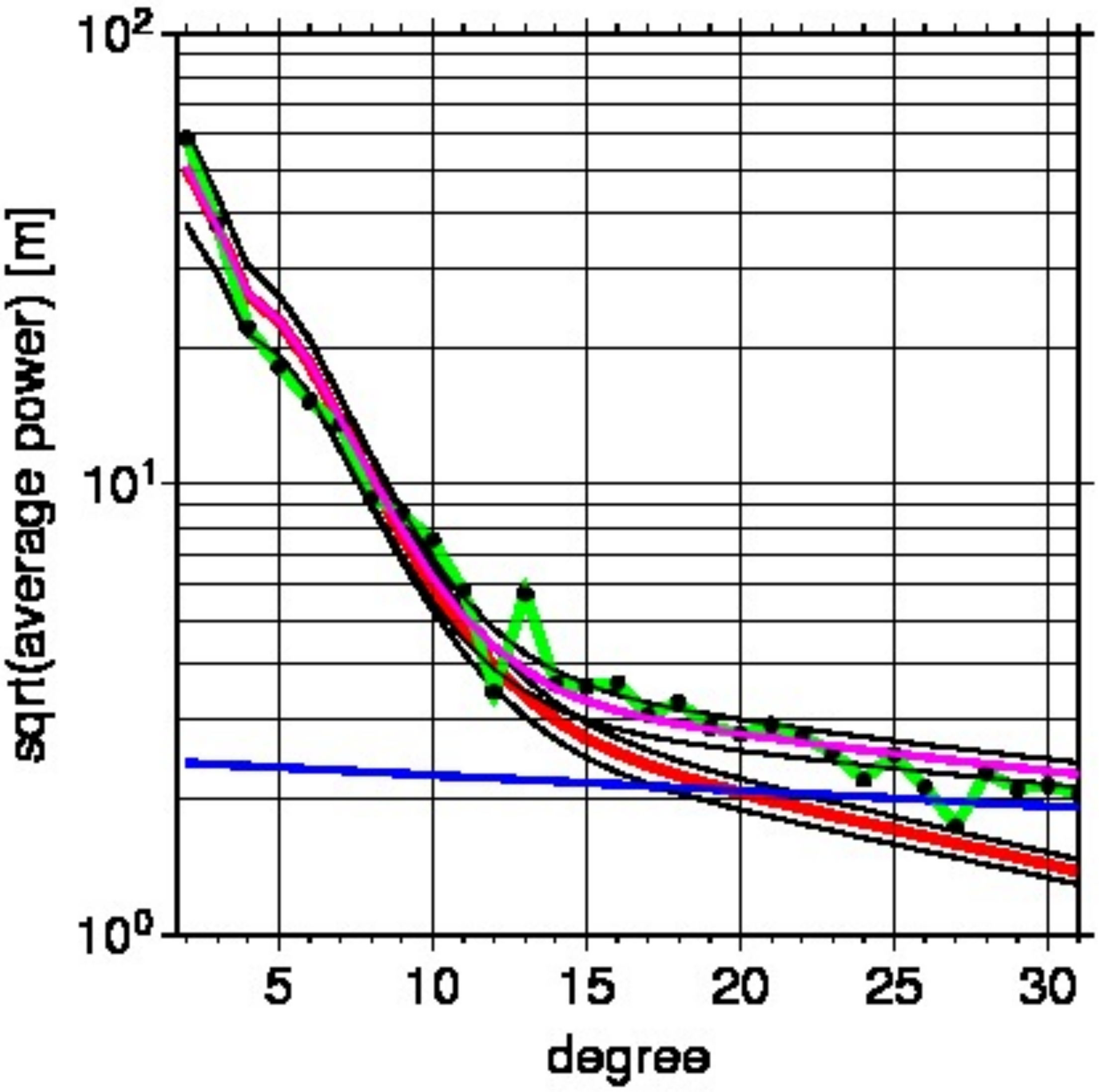


Earth observed – modelled
mantle / lithosphere / total
contribution

(Steinberger and Holme, GRL, 2002)

→ Sublithospheric mantle contribution important up to ~ degree 25-30

→ Lithosphere contribution with “white” power spectrum; observation-based magnitude

Pressure and temperature, and hence viscosity
Increase less strongly with depth in other planets

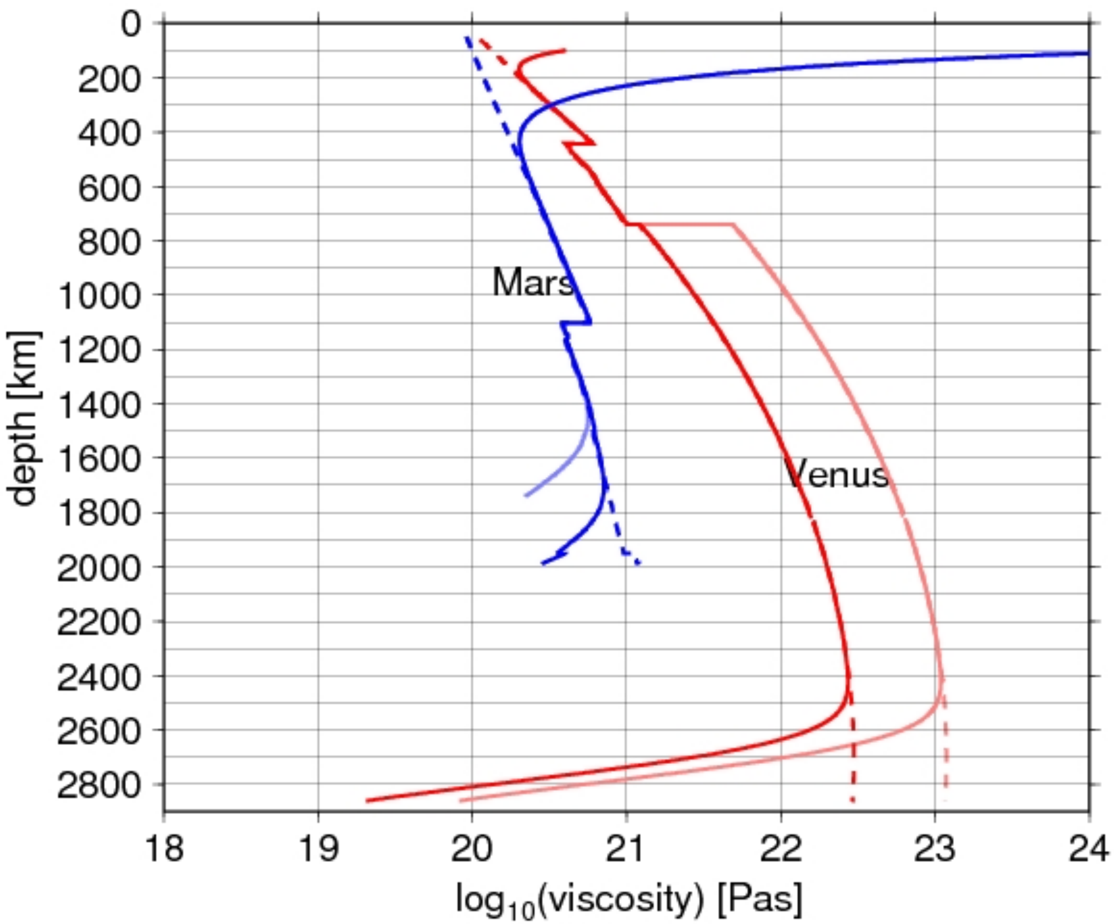

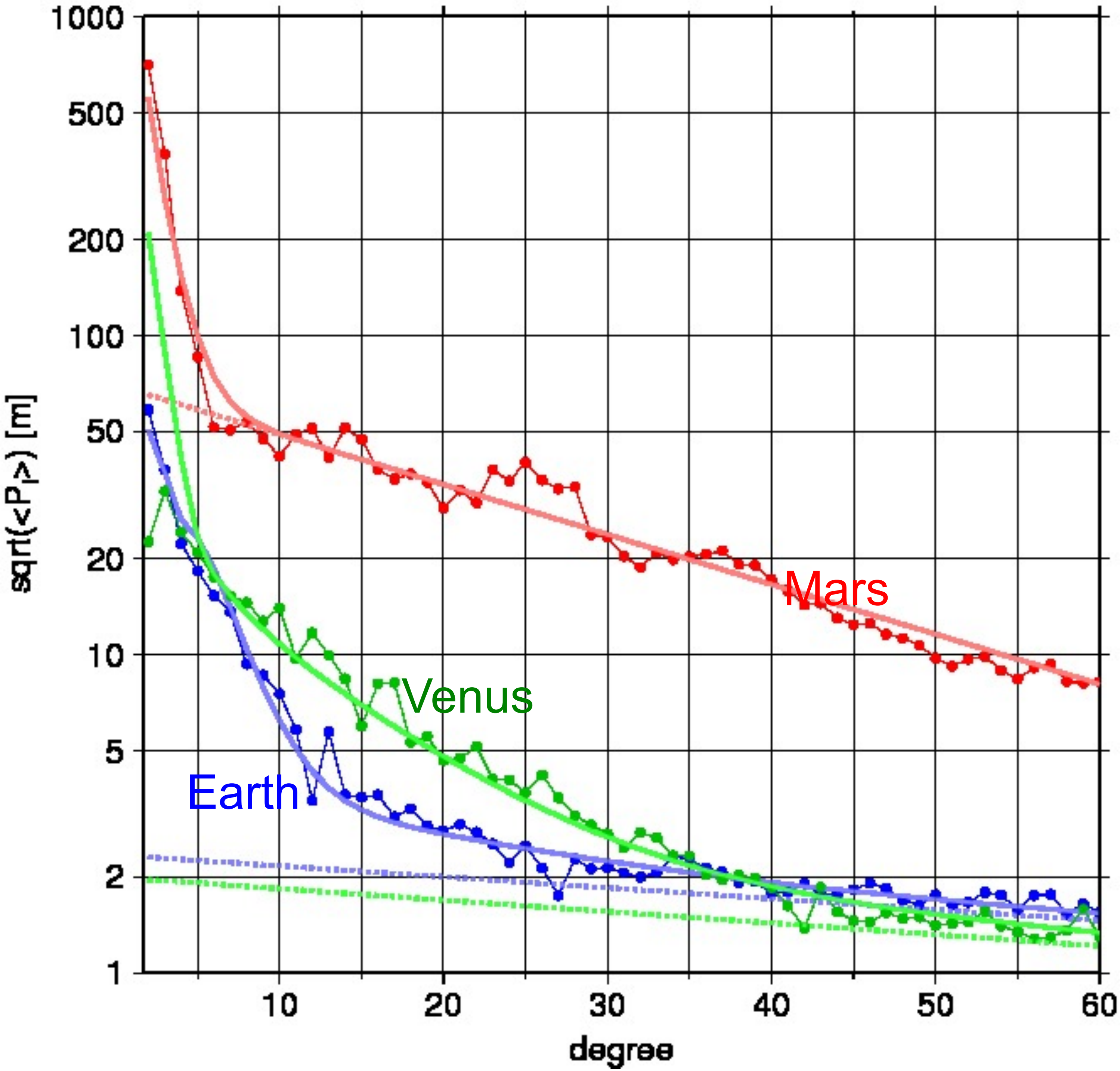


→ With suitable modifications (viscosity profile from temperature and pressure vs. depth; elastic lithosphere) match spectra for Venus and Mars (Steinberger, Werner and Torsvik, Icarus, 2010)

→ For mantle-dominated part can infer depth averaged mantle density (and compare with distribution of volcanics)

Venus observed – modelled
mantle / lithosphere / total
contribution

In contrast to Earth and Mars our model also fits the topography spectrum for Venus for degrees >~5 –
Venus topography appears to be largely dynamically supported

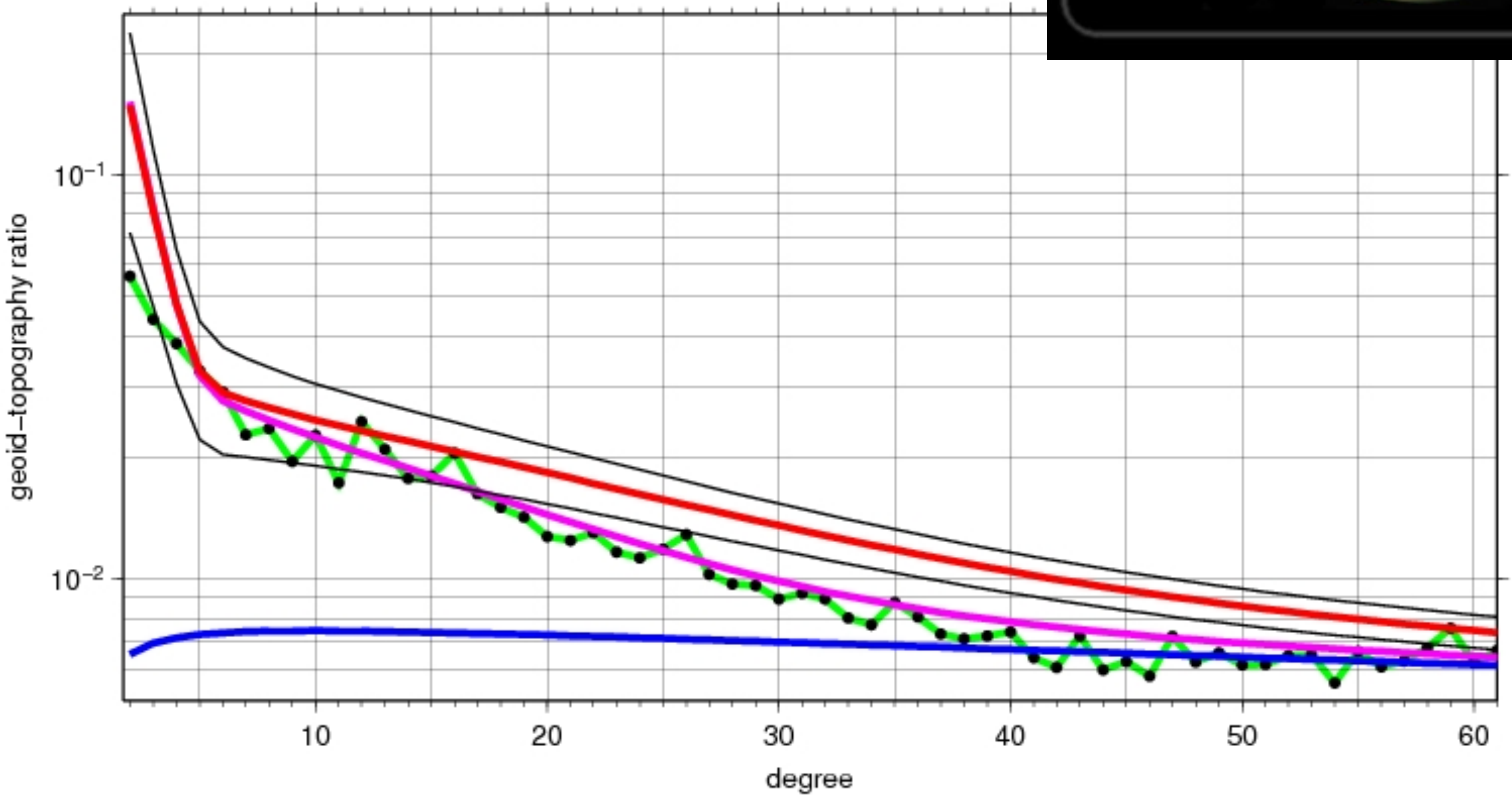

# Venus

## inferred upper mantle density variation

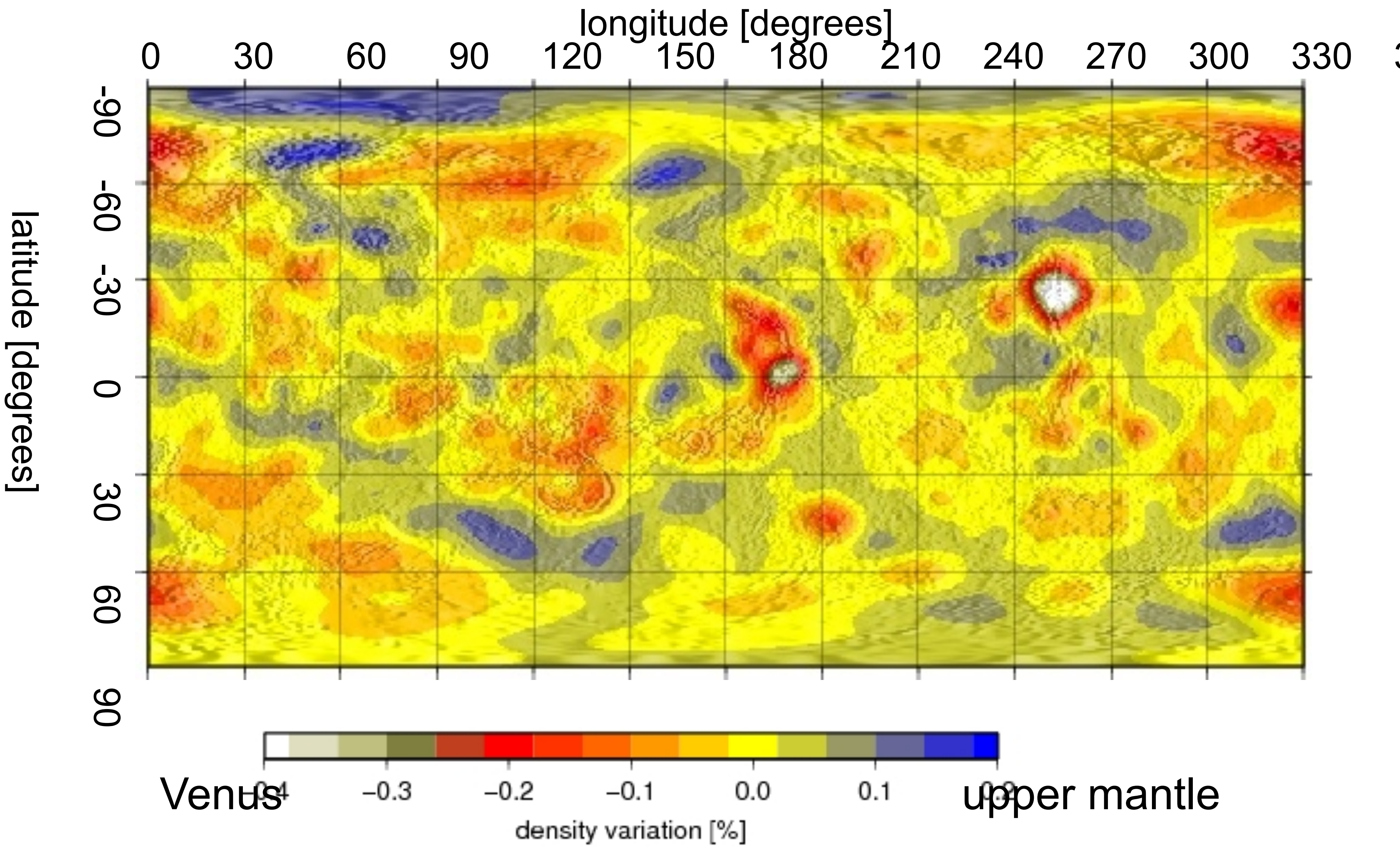

# Venus

inferred upper mantle density variation
distribution of rift zones (in black)
and lobate plains (Ivanov, 2008)

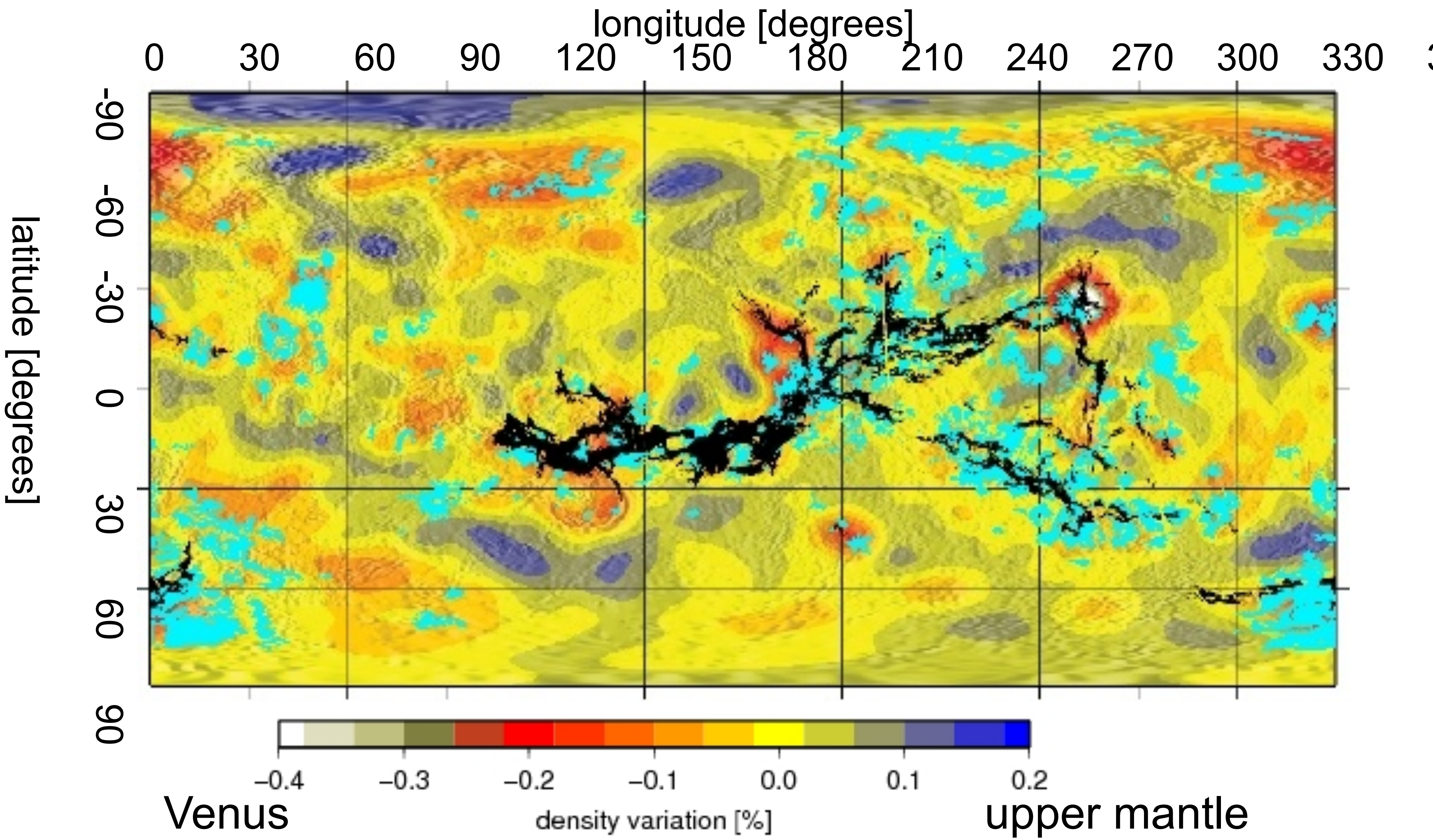


Venus upper mantle

But:

Assumption that density spectrum is same as on Earth not necessarily correct. Therefore also evaluate results from forward convection model (here: Mercury)

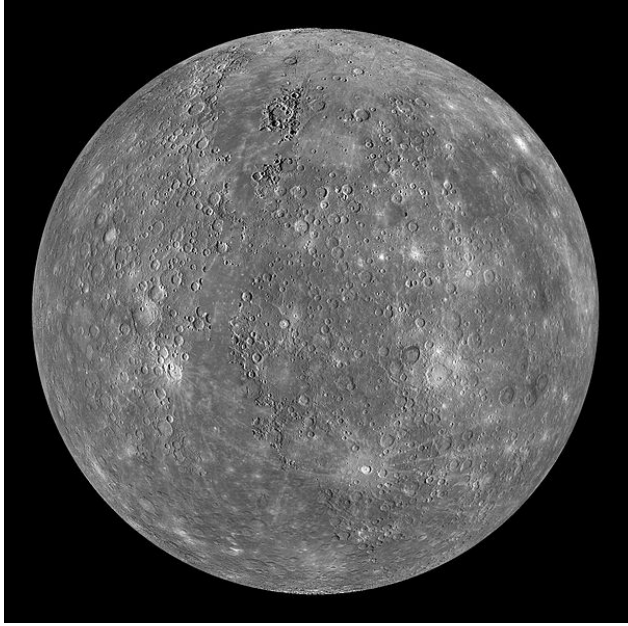

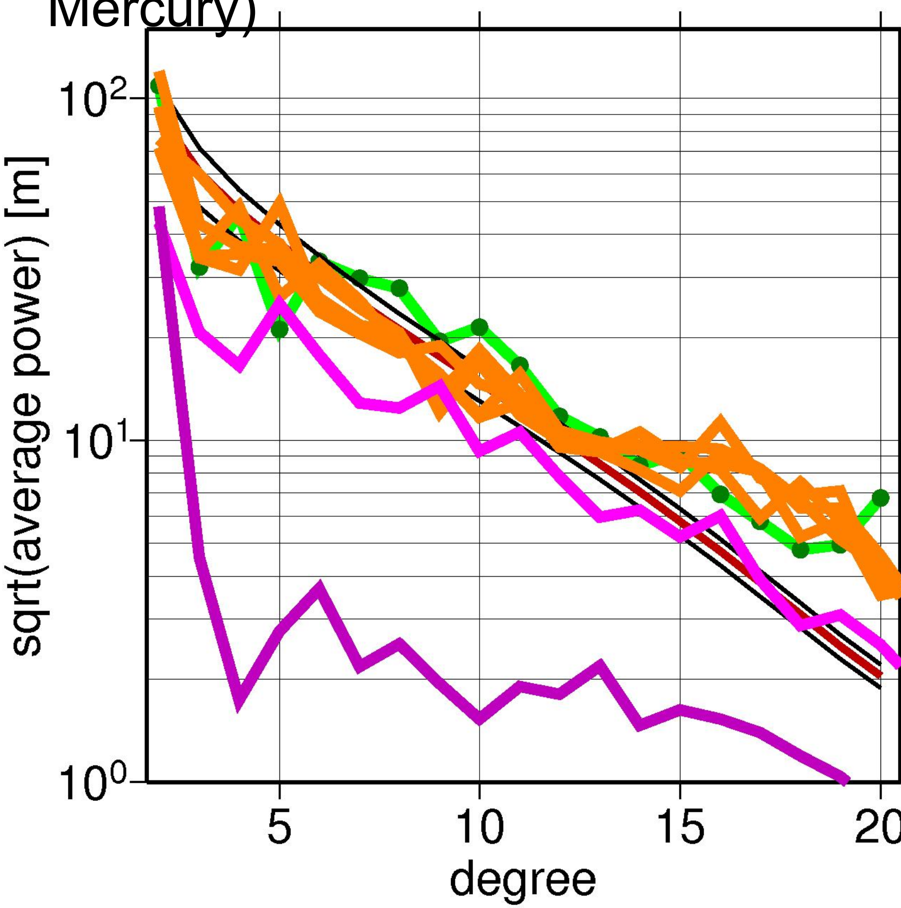


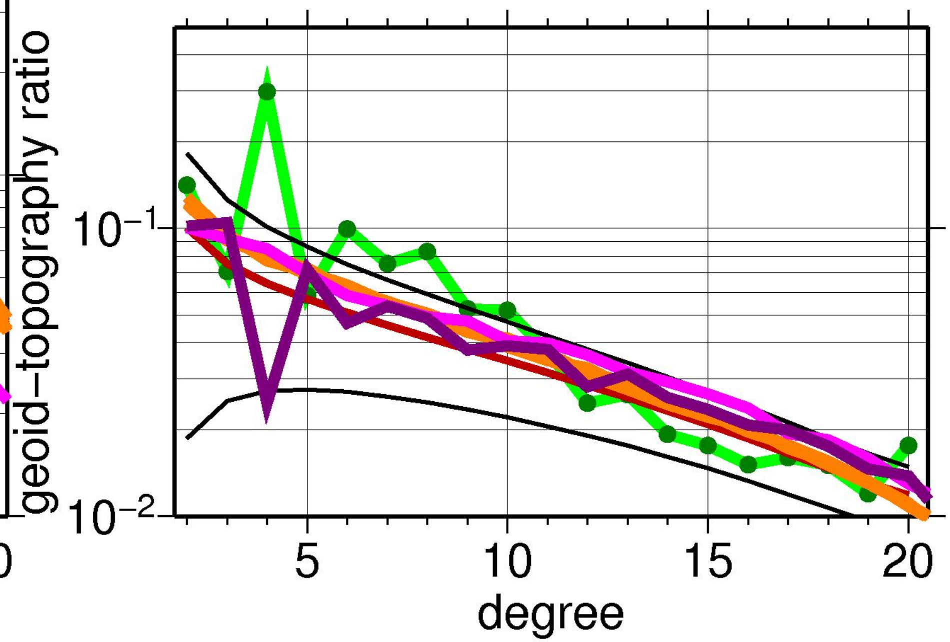


Red lines: Assuming same density spectrum as Earth

Green lines: Observed

Orange / light purple / dark purple: Forward convection models, degrees 31, 63, 127

No-slip;
viscous rheology

No-slip;
elastic lithosphere
174 km thickness;
membrane stresses
not considered

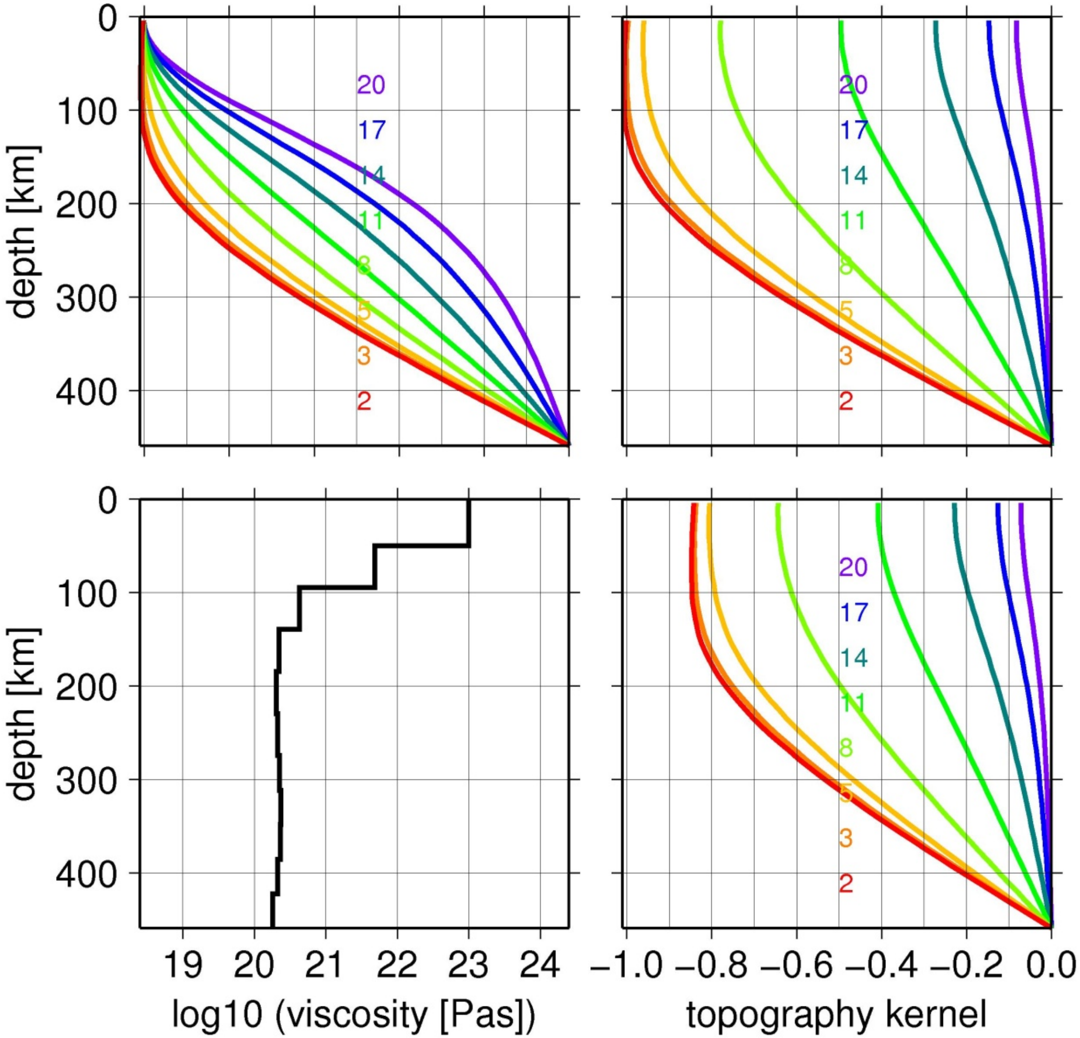


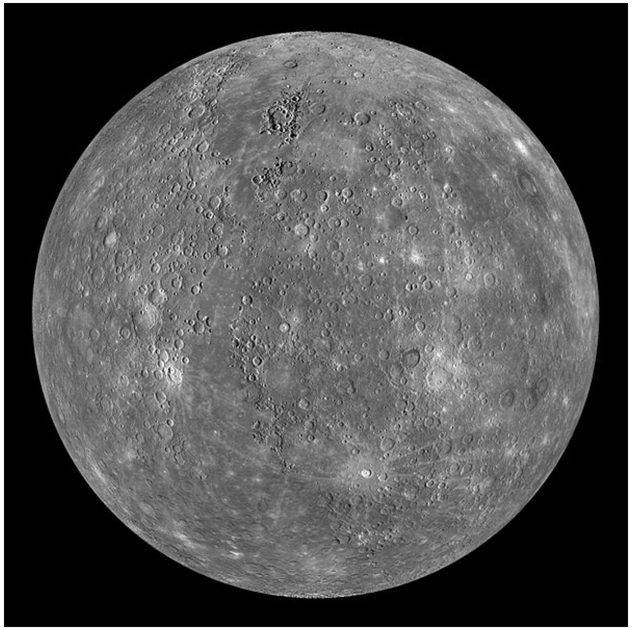

No-slip; elastic lithosphere 174 km thickness;
membrane stresses considered
(Turcotte et al., JGR 86, 3951-59, 1981)

$$p = g[\rho_c h - \rho_m h_g - (\rho_m - \cancel{\rho_c})w] \quad (3)$$

In writing the term $-(\rho_m - \rho_c)w$ it is implicitly assumed that crust with density $\rho_c$ fills the region between 0 and $w$. The

(modified; we do not consider crustal fill)


Thank you for your attention